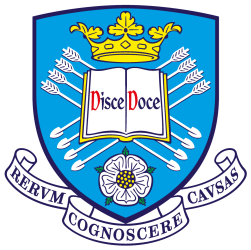

The University Of Sheffield.

Simultaneous Wireless Information and Power Transfer Based on Generalized Triangular Decomposition

By

Ahmed Al-Baidhani

A doctoral thesis submitted in fulfillment of the requirements for the award of

Doctor of Philosophy

The University of Sheffield

Department of Electronic and Electrical Engineering

December 2019

Simultaneous Wireless Information and Power Transfer Based on Generalized Triangular Decomposition

Ahmed Al-Baidhani

PhD Thesis

Communications Group

Department of Electronic and Electrical Engineering

The University of Sheffield

2019

Acknowledgements

I would like to express my sincere gratitude to my supervisor Dr. Mohammed Benaissa for his encouragement and support throughout my study. Completing this work would have been impossible without his guidance and insightful comments.

I would like to take this opportunity to express my deep gratitude to Dr. Mikko Vehkapera for his valuable advice and many insightful discussions. Dr. Vehkapera's suggestions were instrumental in helping me to develop the results in this thesis.

I am grateful to all my colleagues within the Communications Research Group for the wonderful years that I spent with them. Special thanks go to my friend Mohammad R. Eissa for the time that he spent with me to revise some parts in this thesis.

From the bottom of my heart come out my deep gratitude and thankfulness to my father, mother, brothers, and sisters for their continues love and support. Also, I'm very grateful to my wonderful wife, Sarah, who stood by me through the difficult times. Not to forget my lovely children, Abdullah, Mohammed, and Narjis who always filled me with joy and happiness.

Last but not least, I'm grateful to my sponsor (The Higher Committee for Education Development in Iraq) for their moral and financial support.

In memory of my father...

I hope that I have done you proud.

Abstract

The rapidly growing number of wireless devices has raised the need for designing self-sustained wireless systems. Simultaneous wireless information and power transfer (SWIPT) has been advocated as a promising solution. Various approaches have emerged to design wireless systems that enable SWIPT. In this thesis, we propose a novel approach for spatial switching (SS) based SWIPT using the generalized triangular decomposition (GTD) for point-to-point multiple-input-multiple-output (MIMO) systems. The GTD structure allows the transmitter to use the highest gain subchannels jointly for energy and information transmissions and these joint transmissions can be separated at the receiver. We first derive the optimal GTD structure to attain optimal performance in SS based SWIPT systems. This structure is then extended to design three novel transceivers where each transceiver achieves a certain objective and meets specific constraints. The first transceiver focuses on minimizing the total transmitted power while satisfying the energy harvesting and data rate constraints at the receiver. The second transceiver targets the data rate maximization while meeting a certain amount of energy at the receiver. The third transceiver considers the energy harvesting maximization and guarantees to satisfy the required data rate constraint. The proposed transceivers are designed assuming two transmitted power constraints at the transmitter; the instantaneous total transmit power and the limited transmit power per subchannel. For each designed transceiver, optimal and/or suboptimal solutions are developed to obtain joint power allocation and subchannel assignment under a linear energy harvesting model. Additionally, a novel extension to the SS based SWIPT system is proposed considering a non-linear energy harvesting model. Thereafter, the case of maximizing the energy harvesting for a given data rate and instantaneous total transmitted power constraints is studied. A solution is developed that obtains jointly the optimal power allocation and the subchannel assignment alongside the optimal and/or suboptimal split ratios at the energy harvesters. The theoretical and simulation results show that our novel proposed GTD designs for both linear and non-linear energy harvesting models outperform the state-of-the-art singular value decomposition (SVD) based SWIPT designs.

Contents

List of Figures

List of Abbreviations

AF	Amplify-and-Forward.
AS	Antenna-Switching.
AWGN	Additive White Gaussian Noise.
BS	Base Station.
CR	Cognitive Radio.
CSI	Channel State Information.
DC	Direct Current.
DF	Decode-and-Forward.
EE	Energy Efficiency.
EH	Energy Harvesting.
FD	Full-Duplex.
GMC	Geometric Mean Constraint.
GTD	Generalized Triangular Decomposition.
i.i.d	Independent and Identically Distributed.
IoT	Internet-of-Things.

MILP Mixed-Integer Linear Programming.

MIMO Multiple-Input Multiple-Output.

MISO Multiple-Input Single-Output.

MISOCP Mixed-Integer Second Order Cone Programming.

MRT Maximum Ratio Transmission.

MSE Mean-Square-Error.

NOMA Non-Orthogonal Multiple Access.

OFDM Orthogonal Frequency Division Multiplexing.

OFDMA Orthogonal Frequency Division Multiplexing Access.

PR Primary Receiver.

PS Power-Splitting.

PT Primary Transmitter.

QoS Quality of Service.

RZF Regularized Zero-Forcing.

SISO Single-Input Single-Output.

SNR Signal-to-Noise Ratio.

SORC Second Order Rotated Conic.

SR Secondary Receiver.

SS Spatial Switching.

ST Secondary Transmitter.

SVD Singular Value Decomposition.

SWIPT Simultaneous Wireless Information and Power Transfer.

TS Time-Switching.

WPCN Wireless Powered Communication Network.

WSNs Wireless Sensors Networks.

ZF Zero-Forcing.

Notations

$\mathbf{a}$	Vector
$\mathbf{A}$	Matrix
$\mathbf{A}_{(i:k,j:l)}$	Submatrix with elements taken from the i-th row to the k-th row and from the j-th column to l-th column of the matrix $\mathbf{A}$.
$(.)^T$	Transpose operator
$(.)^H$	Hermitian transpose operator
$tr(.)$	Trace operator
$\mathbf{I}_N$	N-by-N identity matrix
$\mathbf{0}_N$	N-by-N zeros matrix
$\mathbb{R}$	The set of real numbers
$\mathbb{C}$	The set of complex numbers
$\mathcal{A}$	Set of defined elements
$\in$	An element in a set
$\bigcap$	Sets intersection process
$\bigcup$	Sets union process
$\setminus$	Sets difference process
$\emptyset$	Empty set
$\mathbb{E}(.)$	Expectation process
$\prod(.)$	Product of elements

$\sum(.)$	Sum of elements
$\arg\min$	Argument minimum value
$\arg\max$	Argument maximum value
$\log_2(.)$	Logarithmic function to base 2
$\preceq$	Multiplication majorization process
$\approx$	Approximately equal to
$\|.\|$	Absolute value
$\|\mathcal{A}\|$	Cardinality of set $\mathcal{A}$

Chapter 1

Introduction

1.1 Overview

The demand for wireless applications is growing rapidly, especially with the deployment of wireless sensor networks (WSN) and the emerging Internet of Things (IoT) devices. To sustain this growth, the provision of an automated source of energy becomes increasingly important for these devices as they are often characterized by stringent resource constraints and varying environments. Therefore, multiple renewable energy sources such as wind, solar, thermo-electric and vibrations have been considered to power the wireless networks [1]. However, these types of sources are characterized by their intermittence, instability and unreliability [2]. Hence, it is risky to rely on the aforementioned sources to deliver sufficient energy to the wireless networks when the quality of service (QoS) is an essential priority [2]. Furthermore, the nature of these sources requires modifications in the hardware design of the wireless nodes and the architecture of the wireless network in order to properly scavenge the energy [3].

To overcome the limitations above, electromagnetic waves of the wireless signals are considered a promising solution for energy harvesting [4]. The energy content in electromagnetic waves can be converted to a DC voltage by using specific rectenna circuits [5, 6]. This field has attracted various research directions such as development of highly efficient rectenna circuits [7, 8] or designs that can harvest energy from multiple frequency bands [9, 10]. Instead of hardware design, however, the focus of the present work is in

the signal processing and communications aspects of wireless energy transfer when the network needs to convey information to the nodes as well. In fact, combining wireless energy transfer simultaneously with information transfer is a concept known as simultaneous wireless information and power transfer (SWIPT) [11, 12]. The early studies of SWIPT [11, 12] focused on developing theoretical bounds such as the trade-off between the information rate and the harvested energy. However, these studies suggested that the receiver is able to decode data and harvest energy from the same signal, an approach which is practically infeasible. To address this problem, the received signal has to be split into two parts, one part for information decoding and the other part for energy harvesting. In fact, the received signal can be separated in different domains such as time domain, power domain, space domain [13] or spatial domain[14]. More details regarding the received signal separation techniques can be found in Chapter 2. The research outlined in this thesis focuses on developing a new approach for SWIPT where the received signal is separated in the spatial domain. This separation technique is also referred to as spatial switching (SS) [14].

1.2 Research Motivation and Aims

Recently, SWIPT has been considered a promising solution to design a perpetual lifetime wireless communications system. To enable SWIPT in such a system, the received RF signal has to be split into two parts, one part used for information decoding and the other used for energy harvesting as mentioned in the previous section. One of the techniques used to enable SWIPT is spatial switching (SS), which is applicable to the MIMO systems. The SS technique exploits the degrees of freedom of the MIMO channel to enable SWIPT. Basically, singular value decomposition (SVD) is used to transform the MIMO link to parallel subchannels where each subchannel is used either for information decoding or energy harvesting [14–16]. This process leads to design a point-to-point MIMO SS SWIPT system based on the SVD architecture, termed an SVD- based SWIPT system.

The symmetric setup of the SVD results in a binary allocation to the subchannels. This allocation is considered to be a significant disadvantage in the SVD based SWIPT

system because the highest gain subchannels are beneficial for transferring information and energy signals. This issue gives motivation for developing a SWIPT system that can transmit information and energy signals jointly over the highest gain subchannels and at the same time complies with the SS technique's main requirement, which is that each of the received streams should be used either for information decoding or energy harvesting.

The SVD based SWIPT system use is limited only to the point-to-point MIMO case due to the structure of the SVD. Therefore, this study is also motivated by the interest to develop a new SS SWIPT system that could be extended to different wireless network configurations, such as multi-user MIMO networks and relay networks.

1.3 Thesis Key Contributions

This thesis focuses on developing a novel SWIPT system based on SS technique that efficiently exploits the degrees of freedom of the MIMO channel. The main contributions of the thesis are summarized as follows:

- Proposing a novel approach for SS SWIPT, in point-to-point MIMO systems, based on GTD.

- Derivation of the optimal structure of the GTD that serves as a framework to design GTD based SWIPT transceivers. The theoretical developments of the GTD show that the proposed approach well outperforms the SVD based SWIPT approach (see Chapter 3).

- Development of three GTD based SWIPT transceivers where each one is set to achieve a specific target and requirements. The first transceiver is designed to minimize the total transmitted power and satisfy the data rate and energy harvesting constraints. The second transceiver is used to maximize the data rate and meets the required energy harvesting constraint. The last transceiver considers maximizing the harvested energy while guaranteeing that the data rate constraint is met. All the transceivers are characterized by either limited instantaneous total transmit power (see Chapter 3) or maximum transmit power per subchannel (see Chapter 4). Optimal and suboptimal solutions that jointly obtain the power allocation and

the subchannel assignment for all of the proposed transceivers are developed.

- The above development is derived for the linear energy harvesting model. An extension of both GTD and SVD based SWIPT systems is developed for the non-linear energy harvesting model proposed in [17]. A simplified structure based on attaching one subchannel at the receiver to multiple energy harvesters is developed for the GTD and SVD based SWIPT systems. With the focus on maximizing the harvested energy, an optimization problem is formulated to jointly obtain the optimal power allocation and subchannel assignment alongside the optimal/suboptimal split ratios at the energy harvesters while ensuring that the required data constraint is met.

  The work in this thesis studies the GTD based SWIPT only theoretically and the practical realization is beyond the scope of this thesis. Therefore, the parameters that are used for the simulations of the proposed GTD based SWIPT approach in the upcoming chapters are not selected based on any of real-world applications such as 5G and IoT systems. In fact, the study in this thesis presents theoretical foundations for the GTD based SWIPT approach that serves as a basis for any future investigations regarding the practical implementation of the GTD based SWIPT.

1.4 Thesis Outlines

The thesis is organized in six chapters. Details of the topics that are covered in each chapter are briefly introduced below:

- **Chapter 1** introduces the research topic of this thesis and sheds light on the requirement for a sustainable solution to face the growth in energy demand in the wireless networks. The motivation and aim of this research are presented, followed by the key contributions. The structure of the thesis and the published works are presented at the end of the chapter.

- **Chapter 2** provides a review of the techniques that enable SWIPT in various network configurations and setups. Because the focus in this thesis is on designing a novel SS based SWIPT system, two fundamental mathematical tools that are essential to design such system are introduced. In particular, the SVD and GTD

are studied. Afterwards, the point-to-point MIMO SVD and GTD based SWIPT systems models, which are used in the designs during the rest of this thesis, are presented in this chapter.

- **Chapter 3** begins with an important theoretical development that addresses the reasons for the superior performance of the proposed GTD based SWIPT system over the state-of-the art SVD based SWIPT system. Exploiting this development, GTD based SWIPT transceiver designs are proposed where each design is set to achieve a particular objective, that is, transmit power minimization, data rate maximization and energy harvesting maximization. An optimization problem is formulated to describe the objective of each particular design. The optimization problems are characterized by instantaneous total transmit power constraint. algorithms that jointly find the optimal power allocation and subchannel assignment for each optimization problem are developed. For comparison purposes, three SVD based SWIPT transceivers that are designed to achieve the same objectives above are studied. To compare the performance of the proposed GTD designs against the state-of-the-art SVD designs, numerical results are introduced in this chapter.

- **Chapter 4** restudies the designs proposed in the previous chapter, considering per subchannel transmit power constraint instead of the instantaneous total transmit power constraint. The effect of adjusting the transmit power constraint on the proposed designs is highlighted. Optimal and suboptimal solutions are developed to obtain the power allocation and subchannel assignment that are required to design the GTD and SVD based SWIPT transceivers. Numerical results are presented in this chapter to highlight the difference in the performance between the proposed GTD based designs and their counterpart SVD designs.

- **Chapter 5** studies the GTD and the SVD based SWIPT systems assuming a non-linear energy harvesting model instead of the linear model used in Chapters 4 and 5. The case of designing energy harvesting maximization transceivers based on GTD and SVD are considered in this chapter. The impact of using the non-linear energy harvesting model on the proposed design is investigated where the design limita-

tions and possible solutions are highlighted. Optimal and suboptimal solutions are developed to meet the GTD and SVD transceivers' design requirements. Simulation results are introduced to characterize the performance of the proposed designs.

- **Chapter 6** concludes the thesis and remarks on the research outcomes. Moreover, possible future directions of this work are also envisioned.

1.5 Publications

Part of the work in this thesis has appeared in the following publications:

1. A. Al-Baidhani, M. Vehkapera, and M. Benaissa, "Simultaneous wireless information and power transfer based on generalized triangular decomposition," *IEEE Transactions on Green Communications and Networking*, pp. 1-1, 2019.

2. A. Al-Baidhani, M. Benaissa, and M. Vehkapera, "Wireless information and power transfer based on generalized triangular decomposition," in *IEEE Global Communications Conference (GLOBECOM)*, Dec 2018, pp. 1-7.

3. A. Al-Baidhani, M. Benaissa, and M. Vehkapera, "Transceiver design for data rate maximization of MIMO SWIPT system based on generalized triangular decomposition," in *10th international conference on Wireless Communications and Signal Processing (WCSP)*, Oct 2018, pp. 1-5.

The following work is also under preparation for a possible publication in the future:

- A. Al-Baidhani, M. Benaissa, and M. Vehkapera, "A Novel spatial switching approach for simultaneous wireless information and power transfer,"(**to be submitted**) in *IEEE Transactions on Green Communications and Networking*.

Chapter 2

Background

2.1 Introduction

Recent interest in energy harvesting from ambient radio frequency (RF) signals has prompted researchers to review the design of the conventional wireless communication systems. These systems are not only used to decode information reliably but also to harvest energy from the RF signals. RF signals can be harvested and converted to electrical energy using rectenna circuits. Historically, this technology is associated with the first experiment of wireless power transfer that was conducted by Nicola Tesla in 1890 [18]. Although Tesla's experiment failed, the idea of wireless energy transfer using RF signals was established. The first successful attempt for wireless energy transfer using RF signals was reported in 1964 when William C. Brown succeeded in transmission of power by RF signals to a thirty foot high tethered helicopter [18]. Despite this success, the developed system size and cost were inconvenient to implement such technology for commercial applications [19].

The wide deployment of various wireless networks has made RF signals a ubiquitous power source. Moreover, recent advances in electronic circuit design have resulted in manufacturing micro-size circuits that can be easily integrated into small-size wireless devices. For example, the Powercast PCC114 Powerharvester receiver has a size of (1×0.6× 0.3) mm [20], which allows it to easily fit in small-size devices. These developments have again placed significant attention on RF energy harvesting technology, which has become

a more attractive choice for designing self-powered wireless networks. The methods by which RF energy harvesting is achieved can be categorized into two types; non-direct RF energy harvesting and direct energy harvesting.

The non-direct RF energy harvesting method refers to harvesting the ambient RF signals that are not intended for energy transfer. These RF signals are normally transmitted from different types of wireless networks such as public broadcasting networks, mobile cellular networks and wireless local area networks (WLAN) [21]. Most of the works that considered this method have focused on the circuit design levels for highly efficient multi-band energy harvesting systems; for more details, see [22–26] and the references therein. However, the energy harvested by this method is unstable and has fluctuating levels because the harvested RF signals are not primarily transmitted for energy scavenging.

The direct RF energy harvesting method denotes to harvesting RF signals that are originally transmitted for energy transfer. Essentially, the RF signals could be used to transfer information and energy simultaneously [2]. This type of transmission is known as simultaneous information and power transfer (SWIPT) and requires special transceivers design in order to retrieve the information and the energy properly at the receiver. The next section provides a comprehensive review on the techniques that enable SWIPT in wireless communications systems.

This chapter gives the essential preliminaries that are required for the developments in the next chapters of this thesis. In Section 2.2, a comprehensive review on the techniques that enable SWIPT in wireless communications systems is introduced. Section 2.3 presents the mathematical tools required to design spatial switching (SS) based SWIPT systems, which are the topic of interest in this thesis. Two SS based SWIPT system models that serve as a basis to the transceiver designs in next chapters are presented in Section 2.4. The first system model is the well known SVD based SWIPT that is proposed in [14–16]. The second system model is the GTD based SWIPT, which is the key contribution in this work. Finally, this chapter is summarized in Section 2.5.

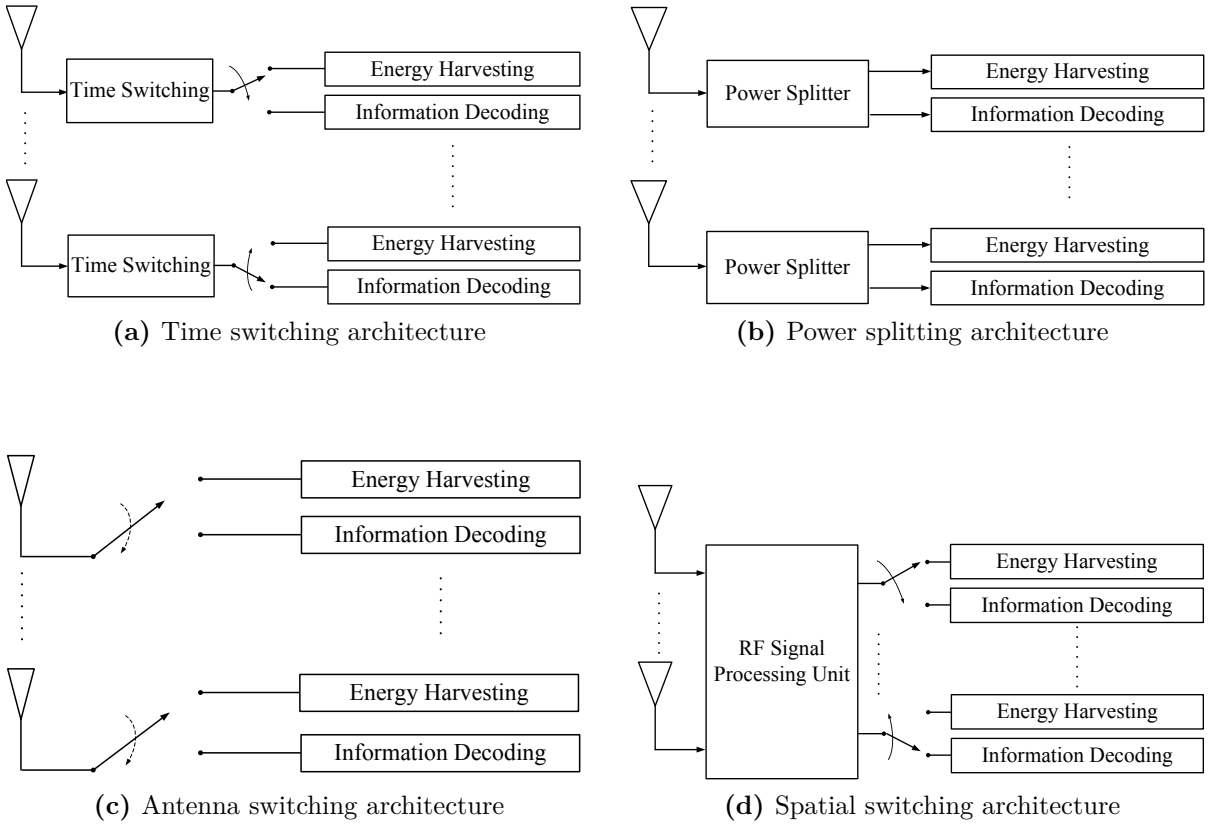

(a) Time switching architecture

(b) Power splitting architecture

(c) Antenna switching architecture

(d) Spatial switching architecture

Figure 2.1: Receiver architecture designs for SWIPT.

2.2 SWIPT

The first information-theoretic study that considered simultaneous information transmission and energy harvesting was conducted by Varshney [11]. The trade-off between the maximum achievable information rate and the harvested energy, also referred to as the rate-energy (R-E) region, for a single-input single-output (SISO) setup in binary discrete and additive white Gaussian noise (AWGN) channels was studied. This study was extended to a frequency-selective channel with AWGN in [12]. Both studies assumed that the receiver is able to decode the information and harvest the energy from the same signal, which was a practical limitation. To overcome this limitation, three receiver architectures were proposed in [13]: time-switching (TS), power-splitting (PS) and antenna-switching (AS). In TS, the receiver has the ability to switch between decoding information and harvesting energy, as illustrated by Figure 2.1a while in PS, the receiver has the ability to split the received signal into two parts, one for decoding information and one for

harvesting energy, as shown in Figure 2.1b; further, in the AS architecture, the receiver switches between the antennas so that each antenna has either an energy signal to be harvested or an information signal to be decoded, as shown in Figure 2.1b. The work in [13] studied the achievable R-E regions for the both schemes, TS and PS, for point-to-point MIMO systems. A different receiver architecture that exploits the spatial domain of the MIMO channel instead of time switching, power splitting or antenna switching was proposed in [15]. Using singular value decomposition (SVD), the point-to-point MIMO channel was transformed into orthogonal subchannels carrying either information or energy, as illustrated by Figure 2.1d. The work in [15] studied the case of minimizing the transmitted power subject to information rate and energy harvesting constraints. Since then, the aforementioned techniques have been widely investigated in different network configurations and scenarios. In the following sections, an overview is presented for the aforementioned receiver architectures that practically enable SWIPT.

Note that Figure 2.1 simply shows a schematic representation of SWIPT techniques and each of these techniques has its own circuit designs and architectures. For example, implementing TS in Figure 2.1a requires using synchronization circuits so the receiver can perfectly switch in time between harvesting energy and information decoding [13]. In Figure 2.1b, PS can be implemented by using different technologies such as Wilkinson power divider [27] divider, varactor diodes [28] and CMOS technology [29–31] to split the received RF signals into energy signals and information signals. For AS technique in Figure 2.1c, a number of switches that is equal to the number of the antenna at the receiver can be used to select between energy harvesting or information decoding from the received RF signals at each particular antenna. Implementing SS technique, whose its schematic representation appears in Figure 2.1d, requires using some elements that have a capability to perform signal processing at the RF band in order to switch spatially between energy harvesting and information decoding [14].

2.2.1 Time Switching Receiver

The TS receiver architecture has been widely studied and considered to enable SWIPT in different network configurations. In [32], the optimal switching time was derived for a point-to-point SISO system to achieve a desired trade-off between information trans-

fer and energy harvesting when the channel state information (CSI) was available or unavailable at the transmitter. The work in [33] studied the TS technique in a SISO amplify-and-forward (AF) wireless relaying network where the relay uses the harvested energy to forward the transmitted signal to the destination. The proposed system in [33] was evaluated by determining the rate achieved at the final destination assuming both delay-limited and - tolerated transmissions. The work in [34] considered TS in decode-and-forward (DF) relay networks where the ergodic capacity of network was derived in the presence of an energy harvesting constraint at the relay node. In [35], the problem of maximizing the transmission rate was studied in multi-hop DF relay networks where the relay node used the TS technique to recharge its own battery. In [36], the system outage probability was studied in two-hop DF relay where the TS protocol is assumed to power the relay node in order to forward the transmitted signal to the destination. In [37], TS was considered for a SISO amplify-and-forward (AF) and decode-and-forward (DF) wireless relaying network where the relay uses the harvested energy to forward the transmitted signal to the receiver. Two transmissions mode were assumed in this study; in the first mode, for each transmission block the relay nodes switches in time to harvest energy and process the information from the received signal while the other mode assumes that the received signal at each transmission block is used either for energy harvesting or information processing. For each mode, the achievable rate was obtained to evaluate the proposed system. The work in [38] studied TS in wireless sensor networks where the problem of joint power allocation and time switching under long-term power consumption and heterogeneous QoS requirements of different types of traffics was investigated. The authors in [39] studied TS in a full duplex AF relay network where the problem of maximizing the data rate at a specific receiver under the relay energy constraint was considered. The authors of [40] adopted the TS technique for a MIMO DF relay broadcast channel (BC), where the goal being to maximize the energy harvested at the relays.

Besides relay networks, the work in [41] investigated TS in an ad-hoc network that consists of multiple transmitters each equipped with multiple antennas and a single antenna receiver. The outage probability for maximum ratio transmissions (MRT) of the proposed ad hoc network was derived in this work. In [42], TS was used to enable SWIPT

in a dense heterogeneous network that consists of multiple tiers of base stations and a single antenna receiver. In this study, a closed-form solution was derived for the average harvested energy, the average information rate and the average transmitted power where the energy-information switching time is fixed at the receiver.

Furthermore, the TS technique has been considered in multi-carrier systems in different scenarios. For example, the authors [43] studied the optimal power allocation and the optimal time-switching that maximizes the sum-rate for a multiuser orthogonal frequency division multiplexing (OFDM) based downlink SWIPT system with TS reception. This study assumed that each single antenna user is able to harvest energy and decode information from a multiple-antenna fixed access point. In [44], TS was studied in a SISO multicarrier DF relay network. The authors in [44] developed a solution that jointly obtains the optimal power allocation and the time-switching ratio at each of the source and the relay nodes to maximizes the end-to-end achievable rate of the DF relay network.

In addition to the network configurations mentioned above, the TS technique has also been investigated for multi-user systems. In [45], the TS technique was applied to a multi-user multiple-input single-output (MISO) network that consists of multiple access points, each equipped with multiple antenna serving single antenna multi receivers. The optimal power allocation at the transmitters and the optimal time-switching at the receivers that maximizes the data rate while maintaining a specific amount of energy at each receiver were derived in this work. The work in [46] considered a full duplex multicell multiuser MIMO network where an efficient design is developed for the precoding matrices for a sum-throughput maximization given quality of service (QoS) and energy harvesting constraints where the TS technique is applied; the problem of maximizing the energy harvesting given throughput constraints with the TS technique was also considered in this paper. In [47], the authors studied TS in MISO multi-user system where the case of jointly optimizing the transmit covariance matrices and the TS ratio at the transmitter was analyzed in order to obtain the boundary points of the rate-energy region at the receiver. The work in [48] investigated the case of maximizing the sum-rate in multi-user MISO where each user adopts TS in order to harvest a required amount of energy.

The works mentioned above showed that TS technique have been widely investigated

in different wireless networks assuming various scenarios. In general, TS technique has two main drawbacks. Firstly, the TS technique is limited to the applications where the delay can be tolerated since part of the symbol time is used for energy harvesting instead of information decoding. Secondly, the TS technique requires accurate information/energy scheduling and time synchronization because any mismatch in the information/energy scheduling time leads to information loss at the receiver [49].

2.2.2 Power Splitting Receiver

Power splitting has been widely investigated in the literature as a technique used to enable SWIPT in multiple scenarios and different network structures. In addition to the TS technique, the works [33–35] have also investigated PS in relay networks, as discussed in Section 2.2.1. Also, the study in [43] considered PS for OFDM systems, and the work of [46] investigated PS in a full duplex multicell multiuser MIMO network, as described in the previous section.

In addition to the research mentioned above, the PS technique has been extensively studied in various wireless network configurations. The works in [50–56] applied PS in a multiuser system. The study in [50] considered PS for MISO multi-user assuming one multiple antenna base station (BS) serving multiple mobile receivers, each one equipped with a single antenna. The problem of minimizing the total transmitted power at the BS while achieving specific amounts of data rate and harvested energy at each mobile was analyzed. A similar scenario was considered in [51] but with the case of imperfect CSI at the transmitter. In [52], PS was proposed for MISO multi-user networks that consists of an equivalent number of transmitters and receivers. Transmitters have an identical number of antennas and each receiver has a single antenna. In this work, the optimal beamforming design and the power splitting ratio were obtained to minimize the transmitted power that meets certain QoS and energy requirements at each receiver. In addition to the optimal beamforming design, well-known beamforming such as zero-forcing (ZF), regularized zero-forcing (RZF) and MRT were also investigated in [52] to obtain the optimal power allocation and the splitting ratio that minimize the transmitted power required to maintain specific amounts of data rate and energy at each receiver. The study in [53] applied PS in multi-user MISO systems where the interference is exploited to improve

data decoding and energy harvesting at the receivers. The work in [54] considered PS in K-user MISO networks where each multiple antenna transmitter serves single antenna receivers. Assuming imperfect CSI, the authors in [54] at the transmitter, a suboptimal transceiver design was developed to minimize the transmitted power that satisfies minimum requirements of data rate and energy harvesting for each end-user. Zong *et al.* in [55] studied PS in K-user MIMO networks where each multiple antenna transmitter communicates with multiple antennas receivers. In this study, joint design of transmit precoding matrices, power splitters and receive filters to minimize the transmitted power subject to both information decoding and energy harvesting constraints was investigated. In [56], PS was applied in multi-user MIMO systems where multiple antenna transmitter transfers data and energy to multiple antenna receivers. Assuming that the receivers are powered by the harvested energy only, the case of maximizing the sum rate of both downlink and uplink was studied in this paper.

Additionally, PS has been studied in full-duplex (FD) systems as well. For example, the work in [57] applied PS in an FD SISO DF relay network that consists of a single antenna source, single antenna relay and single antenna destination. This work studied the problem of maximizing the data rate at the receiver subject to limited transmit power at the source and a specific amount of energy harvested at the relay node. The work of [58] considered PS in point-to-point FD MIMO systems where the problem of the weighted sum transmit power minimization subject to energy harvesting, data rate and limited transmit power constraints was studied. The work in [59] used PS to enable SWIPT in multi-user FD systems. This paper studied the joint design of the transmit-receive beamforming vectors and the receive power splitting ratio to minimize the total transmitted power subject to data rate and energy harvesting constraint at each node. Zhao *et al.* in [60] applied PS in K-pair FD MIMO networks where the FD transceiver nodes were equipped with multiple antennas. This work studied two optimization problems; the first one is the sum power minimization subject to data rate and energy harvesting constraints, and the second problem is the sum rate maximization subject to limited transmitted power and energy harvesting constraints. In [61], PS in full duplex AF MIMO networks was considered where a multiple antenna transmitter wants to send a message to a multiple

antennas receiver via a multiple antennas relay. This work studied the optimal joint design of the transmitter and relay beamformers and the power splitting ratio that minimizes the mean-square-error (MSE) at the receiver.

In cognitive radio (CR) networks, the PS technique has captured some interest in the literature as well. For instance, the works in [62–64] have used PS to harvest energy from the received signals in cognitive radio networks. Zheng *et al.* [62] study the joint information and energy cooperation in CR networks where the primary networks consists of single antenna primary transmitter (PT) and primary receiver (PR) while the secondary network has a multiple antenna secondary transmitter (ST) and a single antenna secondary receiver (SR). In this work, the PT uses the ST to forward massages to the PT and in the meantime the ST also benefits from the PT transmitted signal to harvest energy. The problem of maximizing the data rate in the secondary network by optimizing the beamforming vectors and power splitting ratio at the ST was studied in this work. In [63], PS was applied in SISO CR networks where the PT attempts to send information to its own PR while the ST communicates its own information with an energy harvesting enabled SR. This work studied the case of maximizing the ergodic capacity while meeting a specific ergodic capacity at the PR and a specific amount of energy harvesting at the SR under limited transmit power at each of PT and ST. The work in [64] studied downlink beamforming for SWIPT in multi-user MISO underlay CR networks. In this work, a multi antennas PR communicates with single antenna PRs while a multiple antenna SR transfers data and energy to single antenna SRs. The authors in this work studied the case of optimizing the downlink beamformers and the power splitting ratio that minimizes the total transmitted power required to satisfy energy harvesting and data rate constraints at SRs and PRs.

Power splitting has been used to enable users to harvest energy from the received signals in multiple access systems [65–67]. Chou *et al.* in [65] considered a multi-objective optimization problem that targets data rate and energy harvesting maximization in multi-user MISO orthogonal frequency division multiple access (OFDMA) systems. The work in [66] applied PS in a cooperative MISO non-orthogonal multiple access (NOMA) system that consists of a multiple antenna BS and two users. The user with a strong channel

condition has the ability to harvest energy via PS in order to forward information to the other user which suffers from poor channel condition. In this study, the problem of maximizing the data rate at the strong user while achieving QoS requirement at the weak user was solved by jointly optimizing the PS ratio at the strong user and the beamforming vector at the BS. Maximizing the energy harvesting in SISO NOMA system was studied in [67].

The PS technique has been extensively studied to enable SWIPT in different types of wireless networks, however, there are concerns regarding applying this technique [49]. The main concern in applying the PS technique is its need to a dynamic split ratio approach in order to achieve the optimal performance. The split ratio, in general, is associated with the wireless channel state information which has a time-varying nature and therefore, applying a dynamic split ratio requires developing sophisticated circuits and this increases the power consumption as well as the system complexity [49].

2.2.3 Antenna Switching Receiver

An antenna switching (AS) technique was proposed in [13] where the antennas at the receiver are divided into two subsets; one subset is used for information decoding while the other subset is used to harvest energy. In fact, the AS technique is considered to be a special case of the PS technique [13]. However, AS is characterized by its low complexity from a practical implementation view point because it does not require additional circuits for power splitting or time switching as in PS and TS architectures [21, 68]. This section presents some works that have considered the AS technique for energy harvesting in different network configurations.

Krikidis *et al.* in [69] employed AS in a DF relay network where a single antenna source sends messages to a single antenna destination via an energy harvesting enabled multiple antenna relay. The optimal antenna selection at the relay that minimizes the outage probability in the network was investigated in this work. This research was restudied in [70] assuming Nakagami-m fading channels where closed-form expressions for the probability density function and the cumulative distribution function of the signal-to-noise ratio at the destination and the optimal antenna selection at the relay were derived. In [71], AS was considered in a MIMO DF relay network where a multiple antenna relay

employs the harvested energy to forward a multiple antenna source message to a multiple antenna destination. The optimal beamforming at the source and the relay with optimal antenna assignment at the relay were jointly obtained to maximize the data rate at the destination.

The works in [72, 73] considered the AS technique in CR networks. In [72], AS was applied in a CR network that consists of single antenna PT, ST and SR with a multiple antenna PR that has energy harvesting capability. This study investigated the outage probability at both the primary network and the secondary network where the outage probability at the primary network is defined as an event when the PR fails to achieve a certain amount of data rate and energy, whereas the outage probability at the secondary network is defined as an event when the data rate requirement at the SR is not satisfied. The study in [73] considered CR networks where a multiple antenna SR adopting AS to harvest energy from signals transmitted by a single antenna PT and ST. Based on MRC, the authors in this work proposed an antenna selection scheme at SR that chooses antennas for information decoding in order to guarantee that the received power from the ST is above a certain predefined threshold.

Although the AS technique is characterized by its low complexity which makes this technique appealing for practical SWIPT implementation, this technique has some disadvantages. The main disadvantage of the AS technique is that it is not optimal in comparison with the PS technique and for some scenarios the the transmit power that is used to meet amount of the energy and the data at the receiver is relatively high in comparison with the transmit power used in PS or TS techniques [13]. These scenarios usually occur when the subsets of the antenna that are used for energy/information reception are fixed. Therefore, a dynamic antenna subsets allocation can be used to improve the performance of the AS technique but this rises the complexity of the system [68].

2.2.4 Spatial Switching Receiver

The spatial switching technique was proposed for the first time in [15] to enable SWIPT in point-point MIMO systems. This technique is still in its early stages and has only so far been studied in point-to-point MIMO systems [14–16, 74–76]. In all of these works, SVD was used to transform the MIMO channel into parallel subchannels where each single

subchannel is used at the receiver either to decode information or to harvest energy. In this section, a detailed overview is presented to highlight the developments in the aforementioned works.

The problem of minimizing the transmitted power subject to information rate and energy harvesting constraints was studied in [15] assuming imperfect CSI at both the transmitter and receiver. Since there are multiple subchannels available and each one could be used for information exchange or energy transfer, the problem of the transmitted power minimization in [15] is combinatorial and therefore, a joint optimal solution that obtains the optimal subchannel assignment and power allocation is required. However, combinatorial optimization problems are hard to solve in general. To tackle this issue, the authors in [15] suggested to solve the transmitted power minimization problem for each subchannel assignment and choose the assignment that returns the minimum total transmitted power as the optimal subchannel assignment.

The work in [15] was extended in [14, 16] to find jointly the optimal subchannel assignment and the optimal power allocation that minimizes the total transmit power subject to information rate, energy harvesting and instantaneous per subchannel power constraints. Two exponentially complex optimal and near-optimal solutions based on integer programming were proposed given either perfect or imperfect CSI knowledge. In the first solution, the problem of minimizing the transmit power was formulated as mixed-integer second order cone programming (MISOCP) where the optimal subchannel assignment and the power allocation were jointly obtained using Gurobi software package [77]. In the second solution, the authors proposed a method used to linearize the logarithmic function of the data rate constraint and hence, the optimization problem can be formulated as mixed-integer linear programming (MILP). The MILP formulation has a sub-optimal solution, but the complexity is less than the solution in the MISOCP formulation. However, both solutions have exponential complexity resulted from the integer variables that are imposed in the optimization problem in order to identify the optimal subchannel assignment associated with optimal power allocation. To overcome the complexity problem, the authors developed a sub-optimal heuristic solution where the power allocation is obtained optimally for a selected number of subchannel assignments. The process of the subchannel

assignments selection is based on the data rate and energy harvesting constraint where the subchannels that have the highest gains are selected either to satisfy the data rate constraint or the energy harvesting constraint. The power allocation is obtained optimally in each assignment by using a water-filling-like algorithm. In addition to these solutions, a polynomial complexity algorithm was developed to find the optimal solution for the problem of minimizing the transmitted power when the instantaneous transmit power was not constrained.

The energy efficiency (EE) of the SS based MIMO SWIPT system was investigated in [74, 75], where the energy efficiency is defined as the number of the delivered bits per unit power. The objective in [74, 75] was to maximize the energy efficiency subject to data rate, energy harvesting and limited transmit power constraints. The optimization problem ; *i.e.*, EE maximization that was considered in [74, 75] was fractional combinatorial and non-convex, and the optimal solution is required to jointly obtain the power allocation, subchannels assignment and active receive antenna set selection that all together maximizes EE and meets data rate and energy harvesting requirements under limited transmit power constraints. The authors in [74, 75] proposed a two stages solution to solve the problem of EE maximization. In the first stage, the optimal power allocation is jointly obtained alongside the optimal subchannel assignment, whereas in the second stage the optimal set of the active received antennas is selected.

Mishra *et al.* in [76] studied the problem of maximizing energy harvesting in SS based MIMO SWIPT systems subject to data rate and limited transmit power constraints. The authors in this work developed an optimal solution that jointly obtains the optimal power allocation and the optimal subchannel assignment that maximizes the energy harvesting and satisfies the information rate constraint.

The works mentioned above use SVD to enable SWIPT in the spatial domain. Due to the symmetric setup of SVD, each subchannel is used either for energy harvesting or information decoding and this is considered the main disadvantage since the highest gains subchannels are beneficial for both energy and information transmission. The use of SVD results to a binary assignment of the subchannels and this leads to have a combinatorial transmit power allocation problem which requires in general a high complexity solution.

[14]. Besides, SVD is applicable only to a single matrix and this case is corresponded to the scenario of point-to-point MIMO communication systems where the MIMO channel is represented by a single matrix. Therefore, the SVD based SWIPT approach cannot be extended to more practical scenarios such as multi-user MIMO systems or relay networks. In this study, GTD is used to tackle the above concerns that are raised by the use of SVD. The key advantage of using GTD is its ability that allows the transmitter to assign the highest gains subchannels for joint information and energy transmissions whereas these transmission can be separated at the receiver as will be discovered on the next sections and chapters of this thesis . We address also address that in Chapter 6 that the GTD approach can extended to enable SS based SWIPT systems in the scenarios of MIMO multi-user and relay networks and this is considered another key advantage of using GTD.

2.3 Mathematical Tools

In this section, SVD and GTD which are essential mathematical tools to design SS based SWIPT systems are presented. The SVD is introduced briefly in Subsection 2.3.1 while the GTD is explained in details in Subsection 2.3.2.

2.3.1 Singular Value Decomposition

The singular value decomposition (SVD) is an orthogonal factorization of a matrix. Suppose that $\mathbf{H}$ is an $m \times n$ matrix of rank $K \leqslant \min(m,n)$. Then there exist an $m \times m$ unitary matrix $\mathbf{U}$ and an $n \times n$ unitary matrix $\mathbf{V}$ such that

$$\mathbf{H} = \mathbf{U}\mathbf{\Sigma}\mathbf{V}^H, \tag{2.1}$$

where $\mathbf{\Sigma}$ is an $m \times n$ diagonal matrix whose first K diagonal elements $\sigma_1 \geqslant \sigma_2, \geqslant \ldots, \geqslant \sigma_K$ are the positive singular values of $\mathbf{H}$ [78]. The rest elements of $\mathbf{\Sigma}$ are all zero.

The SVD has been widely used in wireless communications to analyze MIMO channels and determine the degrees-of-freedom that are intrinsic to these channels. Assume that the matrix $\mathbf{H}$ represents the MIMO channel and the dimensions n and m denote to the number of antenna at the transmitter and the receiver, respectively. The entries of the matrix $\mathbf{H}$, in this case, represent the channel coefficients from the n-th transmit antenna to the m-th

receive antenna. Taking the SVD of $\mathbf{H}$ transforms the MIMO channel into K parallel independent subchannels with gains equal to the singular values ; *i.e.*, each particular subchannel has a gain that equals to σ_k, where $k = 1, \ldots, K$. In the context of SWIPT, the SVD has been used as a key tool for SS technique as discussed in Subsection 2.2.4.

2.3.2 Generalized Triangular Decomposition

The generalized triangular decomposition GTD is used to decompose a matrix into three parts: left and right unitary matrices and a matrix in the middle that has an upper triangular block with predefined diagonal elements. In the literature, GTD has been previously employed in point-to-point MIMO systems to create subchannels with predefined information rate [79, 80]. This section presents the GTD algorithm with details.

Let us first recall the definition of multiplicative majorization and then recap [81, Theorem 2.3] that provides the necessary and sufficient conditions for GTD of a given matrix to exist.

Definition 2.1. (Multiplicative majorization [82]) Let $\mathbf{u} = [u_1, \ldots, u_k]^T$ and $\mathbf{v} = [v_1, \ldots, v_k]^T$ be two real-valued vectors with positive elements. Vector $\mathbf{u}$ is multiplicatively majorized by $\mathbf{v}$ if

$$\prod_{i=1}^{k} u_i = \prod_{i=1}^{k} v_i, \tag{2.2}$$

and their descendingly ordered elements satisfy

$$\prod_{i=1}^{n} u_i \leqslant \prod_{i=1}^{n} v_i, \tag{2.3}$$

for all $1 \leqslant n < k$. In the following, the terms multiplicative majorization and majorization are used interchangeably and denoted $\mathbf{u} \preceq \mathbf{v}$ for brevity.

Theorem 2.1 (Generalized triangular decomposition [81])**.** *Consider a matrix* $\mathbf{H} \in \mathbb{C}^{m \times n}$ *that has rank* K *and positive singular values* $\boldsymbol{\sigma} = [\sigma_1, \ldots, \sigma_K]$*. The matrix* $\mathbf{H}$ *can be decomposed as*

$$\mathbf{H} = \mathbf{Q}\mathbf{R}\mathbf{X}^H, \tag{2.4}$$

if and only if the positive diagonal elements of $\boldsymbol{R}$ *are multiplicatively majorized by* $\boldsymbol{\sigma}$*.*

Matrices $\mathbf{Q} \in \mathbb{C}^{m\times m}$ *and* $\mathbf{X} \in \mathbb{C}^{n\times n}$ *are unitary matrices (or real orthogonal matrices if* $\mathbf{H}$ *is real) while* $\mathbf{R} \in \mathbb{R}^{m\times n}$ *is a rectangular matrix whose upper-left corner is a* $K \times K$ *upper triangular matrix and the rest of the elements are zeros.*

The decomposition given in Theorem 2.1 introduces flexibility to define a vector $\mathbf{r} = [r_1, \ldots, r_K]^T$ as the positive diagonal of the matrix $\mathbf{R}$ as long as $\mathbf{r} \preceq \boldsymbol{\sigma}$. In addition, some structure can be forced also on the off-diagonal elements of $\mathbf{R}$, as can be observed from the algorithm below that calculates the decomposition (2.4). More details on GTD can be found in [81].

GTD Algorithm

1. Given the SVD of $\mathbf{H}$ as $\mathbf{H} = \mathbf{U}\boldsymbol{\Sigma}\mathbf{V}^H$ and a prescribed vector $\mathbf{r} = [r_1, \ldots, r_K]^T \in \mathbb{R}^K$ that satisfies $\mathbf{r} \preceq \boldsymbol{\sigma}$, iteration $k = 1$ is initialized by setting $\mathbf{Q} = \mathbf{U}$, $\mathbf{X} = \mathbf{V}$, and $\mathbf{R} = \boldsymbol{\Sigma}$.

2. Indices p and q are defined as

$$p = \underset{k\leqslant i\leqslant K}{\arg\min} \{R_{ii} : R_{ii} \geqslant r_k\}, \tag{2.5a}$$

$$q = \underset{k\leqslant i\leqslant K}{\arg\max} \{R_{ii} : R_{ii} \leqslant r_k \wedge i \neq q\}, \tag{2.5b}$$

where R_{ij} denotes the (i,j)th elements of $\mathbf{R}$. Let $\psi_k = R_{pp}$ and $\omega_k = R_{qq}$ for future convenience and perform the following permutations on the matrices $\mathbf{R}$, $\mathbf{X}$ and $\mathbf{Q}$:

$$(R_{kk}, R_{k+1k+1}) \leftrightarrow \left(R_{pp}, R_{qq}\right), \tag{2.6a}$$

$$\left(\mathbf{R}_{(1:k-1,k)}, \mathbf{R}_{(1:k-1,k+1)}\right) \leftrightarrow \left(\mathbf{R}_{(1:k-1,p)}, \mathbf{R}_{(1:k-1,q)}\right), \tag{2.6b}$$

$$\left(\mathbf{X}_{(:,k)}, \mathbf{X}_{(:,k+1)}\right) \leftrightarrow \left(\mathbf{X}_{(:,p)}, \mathbf{X}_{(:,q)}\right), \tag{2.6c}$$

$$\left(\mathbf{Q}_{(:,k)}, \mathbf{Q}_{(:,k+1)}\right) \leftrightarrow \left(\mathbf{Q}_{(:,p)}, \mathbf{Q}_{(:,q)}\right). \tag{2.6d}$$

The permutations in (2.6a) and (2.6b) can also be written in matrix form

$$\tilde{\mathbf{R}} = \boldsymbol{\Pi}_2^T \mathbf{R} \boldsymbol{\Pi}_1, \tag{2.7}$$

while the expressions (2.6c) and (2.6d) are equivalent to

$$\tilde{\mathbf{X}} = \mathbf{X}\mathbf{\Pi}_1 \quad \text{and} \quad \tilde{\mathbf{Q}} = \mathbf{Q}\mathbf{\Pi}_2, \tag{2.8}$$

respectively, where $\mathbf{\Pi}_1 \in \mathbb{R}^{n\times n}$ and $\mathbf{\Pi}_2 \in \mathbb{R}^{m\times m}$ are appropriate permutation matrices.

3. Construct two matrices, $\mathbf{G}_1$ and $\mathbf{G}_2$, as follows

$$\mathbf{G}_1 = \begin{bmatrix} c & -s \\ s & c \end{bmatrix}, \qquad \mathbf{G}_2 = \frac{1}{r_k}\begin{bmatrix} c\psi_k & -s\omega_k \\ s\omega_k & c\psi_k \end{bmatrix}. \tag{2.9}$$

The variables s and c are given by $s = 0$ and $c = 1$ if $\psi_k = \omega_k = r_k$ and

$$c = \sqrt{\frac{r_k^2 - \omega_k^2}{\psi_k^2 - \omega_k^2}}, \qquad s = \sqrt{1 - c^2}, \tag{2.10}$$

otherwise. Note that the matrices $\mathbf{G}_1$ and $\mathbf{G}_2$ are orthogonal. Then, let $\mathbf{B}_1 = \mathbf{I}_n$ and $\mathbf{B}_2 = \mathbf{I}_m$ and update the elements of $\mathbf{B}_1$ and $\mathbf{B}_2$ as

$$\mathbf{B}_{1(k:k+1,k:k+1)} = \mathbf{G}_1, \qquad \mathbf{B}_{2(k:k+1,k:k+1)} = \mathbf{G}_2. \tag{2.11}$$

The matrices $\tilde{\mathbf{R}}$, $\tilde{\mathbf{X}}$ and $\tilde{\mathbf{Q}}$ are then updated to $\hat{\mathbf{R}}$, $\hat{\mathbf{X}}$ and $\hat{\mathbf{Q}}$ as follows

$$\hat{\mathbf{R}} = \mathbf{B}_2^H \tilde{\mathbf{R}} \mathbf{B}_1, \tag{2.12a}$$

$$\hat{\mathbf{X}} = \tilde{\mathbf{X}}\mathbf{B}_1, \qquad \hat{\mathbf{Q}} = \tilde{\mathbf{Q}}\mathbf{B}_2. \tag{2.12b}$$

Note that (2.12a) ensures that the element $\hat{R}_{kk}$ is updated to r_k. For future convenience, we also remark that according to (2.12a), the elements $\hat{R}_{kk+1}$ and $\hat{R}_{k+1k+1}$ are given by

$$\hat{R}_{kk+1} = \frac{sc(\psi_k^2 - \omega_k^2)}{r_k}, \tag{2.13a}$$

$$\hat{R}_{k+1k+1} = \frac{\psi_k \omega_k}{r_k}. \tag{2.13b}$$

4. While $k < K$, set $\mathbf{R} = \hat{\mathbf{R}}$, $\mathbf{X} = \hat{\mathbf{X}}$ and $\mathbf{Q} = \hat{\mathbf{Q}}$ and then replace k by $k+1$. Go to Step 2).

5. If $k = K$, replace R_{KK} by r_K and $\mathbf{H}$ is decomposed into $\mathbf{QRX}^H$ based on $\mathbf{r}$.

We denote the outcome of this algorithm as $[\mathbf{Q}, \mathbf{R}, \mathbf{X}] \leftarrow \text{GTD}(\mathbf{H}, \mathbf{r})$ in the following sections.

Remark 2.1. The GTD provided by the above algorithm is related to the SVD as [81]

$$\mathbf{H} = \overbrace{\underbrace{\mathbf{U}\left(\mathbf{Q}_1 \cdots \mathbf{Q}_{K-1}\right)}_{\mathbf{Q}} \mathbf{R} \underbrace{\left(\mathbf{X}_{K-1}^H \cdots \mathbf{X}_1^H\right)}_{\mathbf{X}^H} \mathbf{V}^H}^{\mathbf{\Sigma}}, \tag{2.14a}$$

$$\mathbf{R} = \left(\mathbf{Q}_{K-1}^H \cdots \mathbf{Q}_1^H\right)\mathbf{\Sigma}\left(\mathbf{X}_1 \cdots \mathbf{X}_{K-1}\right), \tag{2.14b}$$

where $\mathbf{Q}_k$ and $\mathbf{X}_k$ are the matrices created in Step 4) during iteration $k = 1, \ldots, K-1$. The direct implication of (2.14) is that the matrix $\mathbf{R}$ is obtained from $\mathbf{\Sigma}$ through a series of rotations by unitary matrices so that the energy $\text{tr}(\mathbf{\Sigma\Sigma}^H) = \text{tr}(\mathbf{RR}^H)$ is conserved.

2.4 System Models

Consider a point-to-point MIMO system where the source and the destination are equipped with N_t and N_r antennas, respectively. The transmitter uses a linear precoder to transmit information and energy simultaneously and the destination applies a linear filter on the received signal to harvest energy and to decode information in spatial domain. Narrowband transmission over a flat fading MIMO channel represented by a complex matrix $\mathbf{H} \in \mathbb{C}^{N_r \times N_t}$ is assumed. The channel remains constant for each transmission time-slot and changes independently from one slot to another. Uncorrelated Rayleigh fading is assumed so that the elements of $\mathbf{H}$ are independent and identically distributed (i.i.d) zero-mean circularly symmetric complex Gaussian (ZMCSCG) random variables with variance σ_h^2. The channel is assumed perfectly known at both the transmitter and the receiver.

The signal model for the system under consideration is given as

$$\mathbf{y} = \mathbf{HFs} + \mathbf{n}, \tag{2.15}$$

where $\mathbf{y} \in \mathbb{C}^{N_r \times 1}$ is the received signal vector and $\mathbf{n} \in \mathbb{C}^{N_r \times 1}$ denotes the additive noise vector whose elements are independent ZMCSCG random variables with variance σ^2. The transmitted signal vector $\mathbf{s} \in \mathbb{C}^{N_t \times 1}$ is precoded using the matrix $\mathbf{F} \in \mathbb{C}^{N_t \times N_t}$ that in general depends on the instantaneous channel realization $\mathbf{H}$. Transmitter employes Gaussian signaling so that $\mathbf{s} \in \mathbb{C}^{N_t \times 1}$ is a ZMCSCG random vector with covariance $\mathbb{E}[\mathbf{s}\mathbf{s}^H] = \mathbf{I}_{N_t}$. It should be noted that even though the vector $\mathbf{s}$ has nominally N_t degrees-of-freedom, the maximum number of streams after precoding will always be $K = \min\{N_t, N_r\}$.

In the following, we describe two specific precoder designs applicable to spatial domain SWIPT, the first based on SVD and the second based on GTD.

2.4.1 SVD Based Precoding

Recall that the SVD of the channel $\mathbf{H}$ is given by $\mathbf{H} = \mathbf{U}\mathbf{\Sigma}\mathbf{V}^H$, where $\mathbf{\Sigma} \in \mathbb{C}^{N_t \times N_r}$ is a rectangular diagonal matrix whose elements $\boldsymbol{\sigma}$ represent the singular values of $\mathbf{H}$ and both $\mathbf{U} \in \mathbb{C}^{N_r \times N_r}$ and $\mathbf{V} \in \mathbb{C}^{N_t \times N_t}$ are unitary matrices. For simplicity, the singular values are assumed to be positive and ordered descendingly, that is, $\sigma_1 \geqslant \sigma_2 \geqslant \cdots \geqslant \sigma_K > 0$.

The precoder in (2.15) for the SVD based SWIPT can be written as

$$\mathbf{F} = \mathbf{V}\mathbf{P}^{1/2}, \tag{2.16}$$

where $\mathbf{P}$ is a square diagonal matrix that has transmit-side power allocation $(p_1, p_2, \ldots, p_{N_t})$ on the diagonal. Using linear filter $\mathbf{U}^H$ at the receiver and omitting subchannels that carry only noise parallelizes the MIMO channel into K parallel Gaussian channels with signal-to-noise ratios (SNRs) $p_1\sigma_1^2/\sigma^2, \ldots, p_K\sigma_K^2/\sigma^2$, so that the achievable rate and the harvested energy of the SVD based SWIPT are given by

$$C = \sum_{i \in \mathcal{I}_{\mathrm{SVD}}} \log_2\left(1 + \frac{p_i\sigma_i^2}{\sigma^2}\right), \tag{2.17a}$$

$$EH = \sum_{e \in \mathcal{E}} \eta p_e \sigma_e^2, \tag{2.17b}$$

respectively. The index sets $\mathcal{E} \subseteq \{1, 2, \ldots, K\}$ and $\mathcal{I}_{\mathrm{SVD}} \subseteq \{1, 2, \ldots, K\} \setminus \mathcal{E}$ represent the subchannels assigned for energy harvesting and information exchange, respectively, and

$\eta \in (0,1]$ is the energy conversion efficiency of the energy harvesting circuit; *i.e.*, the rectifier. Note that the conversion efficiency is assumed to be independent of the rectifier input signal. Extension to a different energy harvesting model where the conversion efficiency η is a function of the rectifier input power [17] is presented in Chapter 5. Clearly the information rate or the harvested energy of a specific subchannel for SVD based SWIPT is determined only by the corresponding singular value of the channel and the amount of power allocated to it. While this structure is optimal for information transmission when combined with power allocation through the water filling algorithm, it is suboptimal when both energy and information need to be transmitted simultaneously in spatial domain, as shown later in this study.

2.4.2 GTD Based Precoding

Let's start by recalling the SVD of the channel $\mathbf{H} = \mathbf{U}\mathbf{\Sigma}\mathbf{V}^H$ and multiplying the precoder given in (2.16) by an orthogonal matrix $\mathbf{X} \in \mathbb{R}^{N_t \times N_t}$ that is designed based on the decomposition $[\mathbf{Q}, \mathbf{R}, \mathbf{X}] \leftarrow \text{GTD}(\mathbf{\Sigma}\mathbf{P}^{1/2}, \mathbf{r})$. As discussed in Subsection 2.3.2, the positive vector $\mathbf{r}$ needs to satisfy the majorization condition $\mathbf{r} \preceq \boldsymbol{\lambda}$, where $\boldsymbol{\lambda}$ contains the non-zero diagonal elements of $\mathbf{\Sigma}(\mathbf{P}^\star)^{1/2}$ in descending order. Substituting the modified precoder

$$\mathbf{F} = \mathbf{V}\mathbf{P}^{1/2}\mathbf{X}, \tag{2.18}$$

with identities $\mathbf{H} = \mathbf{U}\mathbf{\Sigma}\mathbf{V}^H$ and $\mathbf{Q}\mathbf{R}\mathbf{X}^T = \mathbf{\Sigma}\mathbf{P}^{1/2}$ into the signal model (2.15) gives

$$\begin{aligned}
\mathbf{y} &= \mathbf{H}\mathbf{F}\mathbf{s} + \mathbf{n}, && \text{(2.19a)}\\
&= \mathbf{U}\mathbf{\Sigma}\mathbf{V}^H\mathbf{V}\mathbf{P}^{1/2}\mathbf{X}\mathbf{s} + \mathbf{n}, && \text{(2.19b)}\\
&= \mathbf{U}\mathbf{Q}\mathbf{R}\mathbf{X}^T\mathbf{X}\mathbf{s} + \mathbf{n}, && \text{(2.19c)}\\
&= \mathbf{U}\mathbf{Q}\mathbf{R}\mathbf{s} + \mathbf{n}. && \text{(2.19d)}
\end{aligned}$$

Applying linear filter $\mathbf{W}^H = \mathbf{Q}^T\mathbf{U}^H$ on the received vector $\mathbf{y}$ as depicted in Figure 2.2, leads to an end-to-end signal model for GTD based SWIPT as

$$\tilde{\mathbf{y}} = \mathbf{W}^H\mathbf{y} = \mathbf{R}\mathbf{s} + \tilde{\mathbf{n}}, \tag{2.20}$$

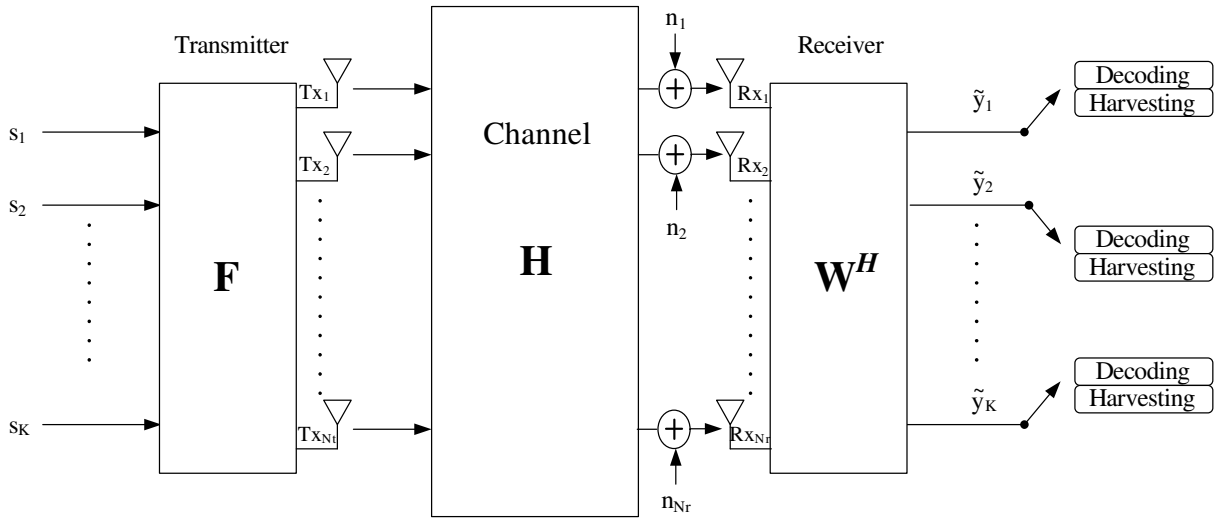

Figure 2.2: System model for GTD based SWIPT with per-stream decoding at the receiver.

where $\tilde{\mathbf{n}} = \mathbf{Q}^T\mathbf{U}^H\mathbf{n}$ has the same distribution as $\mathbf{n}$ in (2.15). According to equation (2.14b), the equivalent channel $\mathbf{R}$ after precoding and receive-side filtering is related to the singular values $\mathbf{\Sigma}$ of the fading channel $\mathbf{H}$ through rotations by orthogonal matrices. Since the matrix $\mathbf{R}$ is not in general diagonal, the received signal at a specific subchannel may now contain interference. While this interference is useful for increasing the amount of energy that can be harvested at the receiver, it degrades total information rate if such subchannel is assigned for information exchange and per-stream decoding without interference cancellation is used at the receiver. For the rest of the study we therefore focus on GTD based designs that create interference-free subchannels for information exchange; *i.e.*, the subchannels used for information decoding at the receive-side correspond to the rows of $\mathbf{R}$ that have only diagonal elements. This allows for per-stream decoding, similar to the case of SVD-based SWIPT, to be used at the receiver as depicted in Figure 2.2. The achievable rate and the harvested energy for the GTD based SWIPT system described above are given by

$$C = \sum_{i \in \mathcal{I}_{\mathrm{GTD}}} \log_2\left(1 + \frac{R_{ii}^2}{\sigma^2}\right), \tag{2.21a}$$

$$EH = \sum_{j \in \mathcal{J}} \sum_{l=j}^{K} \eta R_{jl}^2, \tag{2.21b}$$

respectively, where R_{ij} denotes the (i,j)th elements of $\mathbf{R}$ and $\mathcal{I}_{\text{GTD}}$ and $\mathcal{J}$ are disjoint sets, related to the subchannels that are used for information exchange and energy harvesting at the receive-side, respectively. Note that the effect of power allocation matrix $\mathbf{P}$ is embedded in $\mathbf{R}$ due to the decomposition of $\mathbf{\Sigma}\mathbf{P}^{1/2}$.

2.5 Summary

This chapter introduced a general review of techniques that are frequently used to design SWIPT systems. Since the focus in this thesis is on designing a novel SS based SWIPT system, two fundamental mathematical tools that are essential to design such system were presented. In particular, the SVD and the GTD were studied. The GTD was introduced with details in this chapter and the relation between the GTD and the SVD was also highlighted. The SVD based SWIPT and the GTD based system models were also presented in this chapter. The mathematical expressions of the achievable rate and the harvested energy for each system model were introduced. The effect of the decomposition structure on the system models was discussed briefly.

Chapter 3

Transceiver Design for SS Based MIMO SWIPT With Instantaneous Total Transmit Power Constraint

3.1 Introduction

The RF energy harvesting technology resulted in modification of transceiver designs in wireless devices. Besides information transmission/decoding, wireless systems require to facilitate energy transmission/harvesting. Therefore, most state of the art wireless communication systems and networks such as MIMO systems, relay networks, and cognitive networks have been restudied to accommodate the RF energy harvesting requirement as discussed in Chapter 2.

This chapter is structured in seven main sections. Section 3.2 identifies the difference between the SVD and GTD based SWIPT systems where the optimal structure that is essential design the GTD based MIMO SWIPT transceivers are developed. Section 3.3 presents GTD and SVD transceiver designs that minimize the transmit power and meet specific data rate and energy constraints. Section 3.4 focuses on maximizing the data rate in GTD and SVD based SWIPT transceivers. In Section 3.5, energy harvesting maximization transceiver for GTD and SVD based SWIPT are studied. In these three sections, solutions that obtain jointly the optimal power allocation and subchannel assignment for

the GTD based SWIPT transceivers are developed. Section 3.6 introduces simulation results to compare the proposed GTD designs with state-of-art SVD designs. Finally, Section 3.7 summarizes this chapter.

3.2 SVD and GTD based SWIPT With Unlimited Instantaneous Transmit Power Constraint

In this subsection we provide a simplified example that highlights the main differences between the SVD and GTD based systems. We also show that the latter provides superior performance in most scenarios and present preliminary results that will be used in the latter parts of the study. The channel is assumed to be perfectly known at the transmitter and receiver. For simplicity, no instantaneous power constraint is enforced; *i.e.*, $P_t = +\infty$ here.

3.2.1 SVD Based SWIPT

Consider the problem of minimizing the total transmit power $\mathrm{tr}(\mathbf{P})$ with information rate constraint C_{SVD} and energy harvesting constraint EH_{SVD} in the SVD based system introduced in Subsection 2.4.1. The information rate and harvested energy for a given channel realization and subchannel assignment $\mathcal{E} \subseteq \{1, 2, \ldots, K\}$ and $\mathcal{I}_{\mathrm{SVD}} \subseteq \{1, 2, \ldots, K\} \setminus \mathcal{E}$ are given as in expression (2.17). The goal is to find the subchannel assignment (sets $\mathcal{E}$ and $\mathcal{I}_{\mathrm{SVD}}$) and power allocation $\mathbf{P}$, that jointly satisfy the constraints and minimize the total transmitted power. The power allocation problem for the SVD based SWIPT reads then

$$\underset{\mathbf{P},\, \mathcal{I}_{\mathrm{SVD}},\, \mathcal{E}}{\text{minimize}} \quad \mathrm{tr}(\mathbf{F}\mathbf{F}^H), \tag{3.1a}$$

$$\text{s.t.} \quad \sum_{i \in \mathcal{I}_{\mathrm{SVD}}} \log_2\left(1 + \frac{p_i \sigma_i^2}{\sigma^2}\right) \geqslant C_{\mathrm{SVD}}, \tag{3.1b}$$

$$\sum_{e \in \mathcal{E}} \eta p_e \sigma_e^2 \geqslant EH_{\mathrm{SVD}}, \tag{3.1c}$$

where $\mathbf{F}$ is given by equation (2.16), $\mathcal{I}_{\mathrm{SVD}} \subseteq \{1, \ldots, K\} \setminus \mathcal{E}$ are the subchannels assigned for information exchange and $\mathcal{E} \subseteq \{1, \ldots, K\}$ denotes to the subchannels that are assigned for

energy harvesting. As shown in [14, 16], when there is no instantaneous power constraint, it is optimal to choose only one subchannel for energy harvesting, that is, $\mathcal{E} = \{e\}$ for SVD based SWIPT. The optimal value of e can be found numerically by solving problem (3.1) for all K possible subchannel assignments; *i.e.*, $e = 1, 2, \ldots, K$, and choosing the one that satisfies the energy harvesting and rate constraints with the least transmitted power. For each subchannel assignment, power is first allocated to satisfy the energy harvesting constraint. Then a water filling type algorithm developed in [76] is used for the information bearing subchannels to obtain power allocation that meets the rate constraint with minimum total transmit power, namely,

$$p_i = \begin{cases} p_w + \sigma^2 \left(\frac{1}{\sigma_w^2} - \frac{1}{\sigma_i^2} \right), & i \leqslant w \quad \text{and} \quad i \neq e, \\ 0, & w < i \leqslant K \quad \text{and} \quad i \neq e, \end{cases} \tag{3.2}$$

where the subchannel index w is given by

$$w = \max \left\{ k \,\middle|\, 2^{C_{\mathrm{SVD}}} > \prod_{i=1}^{k} \frac{\sigma_i^2}{\sigma_k^2} \ \wedge \ k \in \{1, 2, \ldots K\} \setminus \{e\} \right\}, \tag{3.3}$$

and p_w is defined as

$$p_w = \sigma^2 \left(\frac{2^{\frac{C_{\mathrm{SVD}}}{L-1}}}{\left(\prod_{i=1, i \neq e}^{w} \sigma_i^2 \right)^{\frac{1}{L-1}}} - \frac{1}{\sigma_w^2} \right), \tag{3.4}$$

where L is the number of subchannels that have nonzero power. Note that for given subchannel gains $\sigma_1^2 \geqslant \cdots \geqslant \sigma_K^2$ and energy harvesting assignment, the water filling algorithm may allocate power to only some of the strongest subchannels in its use. Therefore, the optimal subchannel assignment for problem (3.1) in general has the first $L \leqslant K$ subchannels active so that $e^\star \in \{1, 2, \ldots, L\}$ and $\mathcal{I}_{\mathrm{SVD}}^\star = \{1, 2, \ldots, L\} \setminus \{e^\star\}$. The power allocation matrix that jointly minimizes the transmitted power with the optimal subchannel assignment $\left(e^\star, \mathcal{I}_{\mathrm{SVD}}^\star\right)$ for SVD based SWIPT is denoted $\mathbf{P}^\star$.

3.2.2 GTD based SWIPT

Consider now the design of the GTD based precoder equation (2.18) when the power allocation matrix $\mathbf{P}^\star$ optimized for the SVD based SWIPT is used also by the GTD based precoder. Clearly this may not be the optimal choice for GTD. However, it turns out that the structure of GTD provides enough flexibility to achieve superior information rate compared to SVD most of the time, even when the power allocation is suboptimal.

According to expression (2.21), it is required to select two disjoint index sets, denoted for the GTD based system $\mathcal{I}_{\text{GTD}}$ and $\mathcal{J}$, that can be different from the index sets $\mathcal{I}_{\text{SVD}}$ and $\mathcal{E}$ used for the SVD based SWIPT. As with SVD, using using one subchannel for energy harvesting at the receiver is optimal, so that $\mathcal{J} = \{j\}, j \in \{1, 2, \ldots, L\}$, and we can define an optimization problem

$$\underset{\mathbf{r} \preceq \boldsymbol{\lambda},\, \mathcal{I}_{\text{GTD}},\, j}{\text{maximize}} \quad C_{\text{GTD}} = \sum_{i \in \mathcal{I}_{\text{GTD}}} \log_2\left(1 + \frac{R_{ii}^2}{\sigma^2}\right), \tag{3.5a}$$

$$\text{s.t.} \qquad \sum_{l=j}^{L} \eta R_{jl}^2 \geqslant EH_{\text{GTD}}, \tag{3.5b}$$

where $\mathcal{I}_{\text{GTD}} = \{1, \ldots, L\} \setminus \{j\}$ is the set of subchannels that used for information decoding at the receive-side. Matrix $\mathbf{R}$ is designed to guarantee interference-free information subchannels and satisfy the majorization condition $\mathbf{r} \preceq \boldsymbol{\lambda}$, where $\boldsymbol{\lambda} = [\lambda_1, \lambda_2, \ldots, \lambda_L]^T$ contains the non-zero diagonal elements of $\mathbf{\Sigma}(\mathbf{P}^\star)^{1/2}$ in descending order, as explained in Subsection 3.2.1.

The following theorem shows that with appropriate selection of $\mathcal{I}_{\text{GTD}}$ and $\mathcal{J}$, the solution to the optimization problem (3.5) provides a GTD based design that achieves an information rate that is better, or at least as good as, than that obtained with SVD, even when the power allocation is specifically designed to optimize the SVD based system.

Theorem 3.1. *Consider the SVD based precoder given in* (2.16). *Let* $e^\star \in \{1, \ldots, L\}$ *with* $L \leqslant K$ *be the optimal subchannel index for energy harvesting and* $\mathbf{P}^\star$ *the optimal power allocation that solve the SVD based design problem* (3.1) *for the given rate and energy constraints* C_{SVD} *and* EH_{SVD}, *respectively. Given the power allocation* $\mathbf{P}^\star$, *if* $e^\star \in \{1, L\}$, *the optimal GTD precoder* (2.18) *reduces to the SVD based precoder and both systems have*

the same performance. When $e^\star \notin \{1, L\}$*, selecting the diagonal elements* $\mathbf{r} = [r_1, \ldots, r_L]^T$ *of* $\mathbf{R}$ *as*

$$\begin{bmatrix} r_1 \\ r_2 \\ \vdots \\ r_{L-2} \\ r_{L-1} \\ r_L \end{bmatrix} = \begin{bmatrix} \lambda_2 \\ \lambda_3 \\ \vdots \\ \lambda_{L-1} \\ \frac{\lambda_1 \lambda_L}{\sqrt{\lambda_1^2 + \lambda_L^2 - \frac{EH_{\mathrm{SVD}}}{\eta}}} \\ \sqrt{\lambda_1^2 + \lambda_L^2 - \frac{EH_{\mathrm{SVD}}}{\eta}} \end{bmatrix}, \tag{3.6}$$

and choosing $\mathcal{I}_{\mathrm{GTD}} = \{1, 2, \ldots, L-2, L\}$*,* $\mathcal{J} = \{L-1\}$*, guarantees that the harvested energy satisfies* $EH_{\mathrm{GTD}} = EH_{\mathrm{SVD}}$ *and the information rate* $C_{\mathrm{GTD}} > C_{\mathrm{SVD}}$ *of the GTD based system is maximized.*

Proof: See Appendix B. ■

Theorem 3.1 can be divided into two cases: 1) When the information rates are equal ($C_{\mathrm{GTD}} = C_{\mathrm{SVD}}$); and 2) when GTD achieves a higher rate than SVD ($C_{\mathrm{GTD}} > C_{\mathrm{SVD}}$). The first case occurs when the transmit power for the SVD based precoder is minimized by associating the strongest or the weakest eigenmode of $\mathbf{\Sigma}(\mathbf{P}^\star)^{1/2}$; *i.e.*, λ_1 or λ_L, with energy harvesting. This corresponds to a scenario where either the energy harvesting or the information rate requirement dominates the constraints, respectively, and no additional benefit can be achieved by the GTD based system.

The case $C_{\mathrm{GTD}} > C_{\mathrm{SVD}}$ occurs when the energy harvesting constraint (3.1c) for SVD is satisfied through any subchannel but the best or the worst; *i.e.*, $\mathcal{E} = \{e\}, e \notin \{1, L\}$. In this case, $\mathbf{R}$ is obtained via the GTD according to Theorem 2.1, $[\mathbf{Q}, \mathbf{R}, \mathbf{X}] \leftarrow \mathrm{GTD}\big(\mathbf{\Sigma}(\mathbf{P}^\star)^{1/2}, \mathbf{r}\big)$, where $\mathbf{r}$ is given in expression (3.6). The only non-zero off-diagonal element of $\mathbf{R}$ is at the $(L-1)$-th row and reads

$$R_{L-1L} = \frac{1}{r_{L-1}} \sqrt{\big(\lambda_1^2 - r_{L-1}^2\big)\big(r_{L-1}^2 - \lambda_L^2\big)}, \tag{3.7}$$

which is non-zero when $e \notin \{1, L\}$. By recalling that $\lambda_k = \sqrt{p_k}\sigma_k, k = 1, 2, \ldots, L$, it is straightforward to verify that matrix $\mathbf{R}$ constructed as in expressions (3.6) and (3.7) satisfies $EH_{\mathrm{SVD}} = EH_{\mathrm{GTD}}$ and $r_{L-1} < \lambda_e$. Together with Remark 2.1 this implies that

more energy is received in the information bearing subchannels of the GTD based system and higher rate can be achieved.

The key difference between the SVD based design and the GTD based system described above is that in the GTD based system the transmitter has the ability to use the subchannel associated with the highest singular value to transmit both information and energy signals while the receiver is able to separate that particular transmission into two different streams; one is used for information and the other is used for energy harvesting. This is in contrast with SVD based system where each subchannel can carry either information or energy signals [14, 15]. As a result, more transmit power can be used in information bearing subchannels since subchannel with highest singular value is used to transfer information and energy as well.

3.3 Transmit Power Minimization With Energy Harvesting and Data Rate Constraints

In this section, two SS based MIMO SWIPT transceivers are presented. The first transceiver is developed based on GTD while the second transceiver is designed based on SVD. The objectives of transceivers are set to minimize the total transmitted power and guaranteeing that the required data rate and energy harvesting constraints at the receiver are met.

3.3.1 Transmit Power Minimization for GTD Based SWIPT

As discussed in Subsection 3.2.2, the received signal at the k-th subchannel contains interference if the k-th row in $\mathbf{R}$ has off-diagonal elements. Since interference is detrimental for achievable rate, we concentrate here on designing GTD based precoder and receive-side filter that guarantee interference-free subchannels for information transfer. However, the interference is useful for increasing the amount of energy available for harvesting at the receive-side and, thus, saves transmit power for satisfying the rate constraint. Based on the above discussion, the following optimization problem can be formulated

$$\underset{\mathbf{P},\, \mathbf{r} \preceq \boldsymbol{\lambda},\, \mathcal{I},\, \mathcal{J}}{\text{minimize}} \quad \text{tr}(\mathbf{F}\mathbf{F}^H), \tag{3.8a}$$

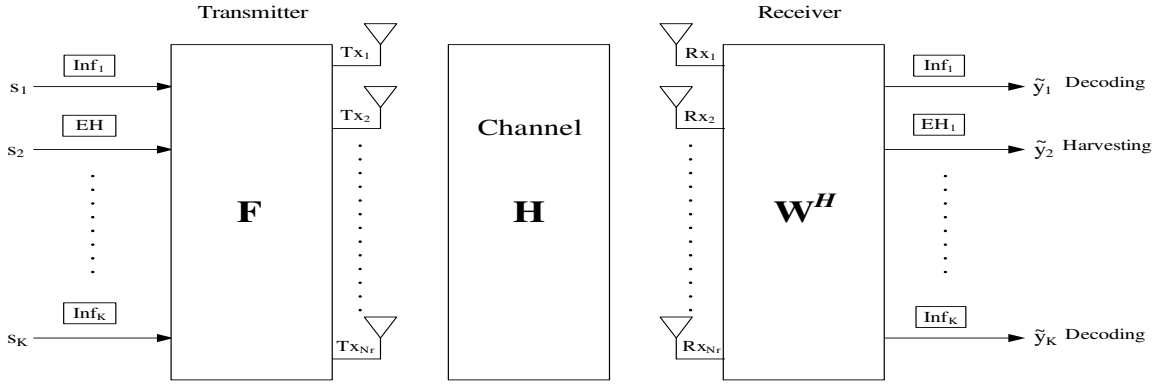

(a) SVD based SWIPT

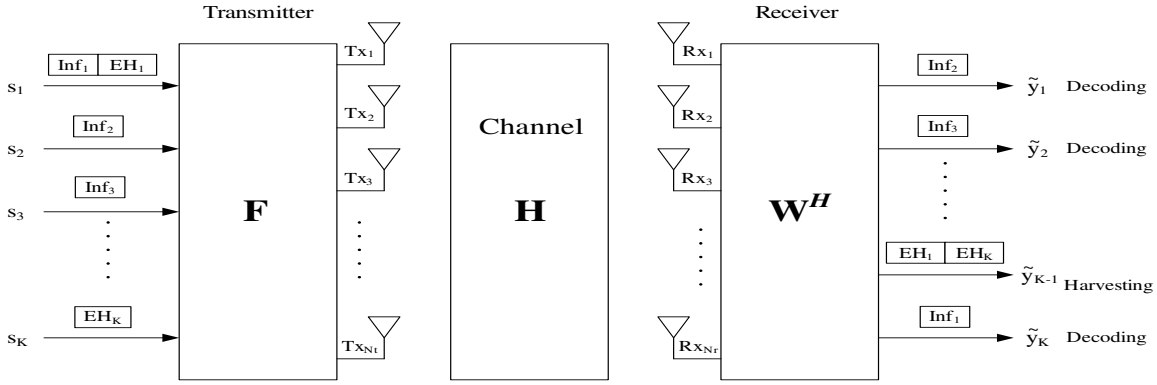

(b) GTD based SWIPT

Figure 3.1: Comparison between SVD and GTD based SWIPT. The GTD system can use any subchannel for joint energy and information transmission where that particular transmission can be separated at the receiver.

$$\text{s.t.} \quad \sum_{i\in\mathcal{I}} \log_2\left(1+\frac{R_{ii}^2}{\sigma^2}\right) \geqslant C, \tag{3.8b}$$

$$\sum_{j\in\mathcal{J}}\sum_{l=j}^{K} \eta R_{jl}^2 \geqslant EH, \tag{3.8c}$$

$$\sum_{k\in\mathcal{K}} p_k \leqslant P_t, \tag{3.8d}$$

where the precoder matrix $\mathbf{F}$ is given by equation (2.18), $\boldsymbol{\lambda}$ represents the positive diagonal elements of $\mathbf{\Sigma P}^{1/2}$ and $\mathcal{K}$ denotes the set of the total available subchannels while $\mathcal{I} \subseteq \mathcal{K}$ and $\mathcal{J} \subseteq \mathcal{K}\backslash\mathcal{I}$ are the sets of subchannels from which the receiver decodes the information and harvests the energy, respectively. In addition to finding power allocation matrix $\mathbf{P}$, optimal solution requires also to identify which subchannels are used for information and energy transfer, and construction of the precoding and the receive-side matrices $\mathbf{F}$ and

W, respectively.

In the following we show that while the SVD based transceiver design allows a particular subchannel to carry only one type of signal, information or energy, the GTD based system can be designed so that a particular transmitted stream separates at the receiver into two parts; one stream that is used for decoding information and another stream from which energy is harvested, as illustrated in Figure 3.1. This is the key difference between the two approaches and is the main reason why the GTD based SWIPT outperforms its SVD counterpart. It should be noted, however, that the same receive-side stream cannot be used to both harvest energy and decode information in the GTD based system either, rather, the subchannel "re-use" happens at the transmit-side.

To solve problem (3.8), a two-stage process is proposed that consists of first finding the power allocation matrix $\mathbf{P}^\star$ and then using GTD to construct the precoding and the receive-side matrices **F** and **W**, respectively. The power allocation for information transmission is carried out according to the singular values $\mathbf{\Sigma}$ of the MIMO channel matrix **H** using the water filling algorithm that is developed in [76], and then power necessary for satisfying the energy harvesting constraint is added to it. After obtaining the complete power allocation $\mathbf{P}^\star$, GTD is used to decompose the matrix $\mathbf{\Sigma}(\mathbf{P}^\star)^{1/2}$ as $[\mathbf{Q}, \mathbf{R}, \mathbf{X}] \leftarrow \text{GTD}\big(\mathbf{\Sigma}(\mathbf{P}^\star)^{1/2}, \mathbf{r}\big)$ to arrive at the input-output relation (2.20). The following subsections explains the above process.

A. Optimal Power Allocation

To follow the above process, we need to show that the power allocation matrix can be optimized based on the singular values of $\mathbf{\Sigma}$ so that the constraints (3.8b) and (3.8c) are both satisfied if the diagonal elements **r** of **R** in the GTD are chosen appropriately. This design rule relies on the fact that it is optimal to allocate all power that is used for energy harvesting to the strongest singular value σ_1 [14, 16], see Appendix A for the details. Specifically, the aim is to prove that information rate C and harvested energy EH given as

$$C = \sum_{k=1}^{K-1} \log_2\left(1 + \frac{\alpha_k \sigma_k^2}{\sigma^2}\right), \tag{3.9a}$$

$$EH = \eta\left(\beta_1 \sigma_1^2 + p_K \sigma_K^2\right), \tag{3.9b}$$

can be achieved in GTD based SWIPT. Note that α and β are the powers that are allocated by the transmitter for information exchange and energy transfer, respectively. In equation (3.9a), the powers $(\alpha_1, \alpha_2, \ldots, \alpha_{K-1})$ are obtained by applying the waterfilling algorithm that is proposed in [76] on the parallel Gaussian subchannels that have the gains $\sigma_1^2, \sigma_2^2, \ldots \sigma_{K-1}^2$ as follows

$$\alpha_k = \begin{cases} \alpha_w + \sigma^2 \left(\frac{1}{\sigma_w^2} - \frac{1}{\sigma_k^2} \right), & k \leqslant w \\ 0, & w < k \leqslant K-1 \end{cases} \tag{3.10}$$

where w is given by

$$w = \max \left\{ j \middle| 2^C > \prod_{k=1}^{j} \frac{\sigma_k^2}{\sigma_j^2}, \quad j = 1, 2, \ldots K-1 \right\}, \tag{3.11}$$

and α_w is defined as

$$\alpha_w = \sigma^2 \left(\frac{2^{\frac{C}{w}}}{\left(\prod_{k=1}^{w} \sigma_k^2 \right)^{\frac{1}{w}}} - \frac{1}{\sigma_w^2} \right). \tag{3.12}$$

Note that a similar strategy was used for the SVD based system in Section 3.2.1, but now σ_1 is associated with both information and energy, which is not allowed in the SVD based SWIPT.

For notations simplicity, we consider first the case when the water filling algorithm returns $(\alpha_1, \alpha_2, \ldots, \alpha_{K-1})$ that are all non-zero ; *i.e.*, $w = K-1$. The power $p_K > 0$ is set to be as small as possible while keeping the corresponding subchannel active; therefore, the total number of subchannels that have nonzero power is $L = K$. Given that $p_K \sigma_K^2$ is very low and from equation (3.9b) we see that β_1 is mainly responsible for satisfying the energy harvesting constraint. The reason for the special treatment of p_K will be explained later. From expression (3.9), the power allocation matrix that uses the least power and satisfies both constraints is given by

$$\mathbf{P}^\star = \operatorname{diag}\left(\left[\alpha_1 + \beta_1,\ \alpha_2,\ \ldots,\ \alpha_{K-1},\ p_K \right] \right), \tag{3.13}$$

where $\mathbf{P} = \text{diag}(\mathbf{p})$ constructs a square diagonal matrix with $\mathbf{p}$ on the diagonal. Therefore, problem (3.8) is feasible if

$$\sum_{k=1}^{K-1} \alpha_k + \beta_1 + p_K \leqslant P_t, \tag{3.14}$$

holds and (3.9a)–(3.9b) match (3.8b)–(3.8c) exactly.

B. Precoder and Receiver Filter Design

After obtaining the optimal power allocation $\mathbf{P}^\star$, the GTD is applied to $\mathbf{\Sigma}(\mathbf{P}^\star)^{1/2}$ in order to construct the precoder $\mathbf{F}$ and the receiver-side matrix $\mathbf{W}$. Note that using $\mathbf{F}$ at the transmitter and $\mathbf{W}^H$ at the receiver results $\mathbf{R}$ that satisfies the information rate and energy harvesting constraints given in (3.8b) and (3.8c). As discussed in Subsection 3.2.2, the chosen $\mathbf{r}$ must be multiplicatively majorized by the diagonal elements of $\mathbf{\Sigma}(\mathbf{P}^\star)^{1/2}$, that is, $\mathbf{r} \preceq \boldsymbol{\lambda}$. Using $\mathbf{r}$ given in Theorem 3.1 satisfies this condition and results in a receive-side subchannel assignment where $\mathcal{J} = \{K-1\}$ is used for energy harvesting and $\mathcal{I} = \{1, \ldots, K-2, K\}$ for information decoding.

C. Harvested Energy and Achievable Rate

To show that this GTD structure indeed solves problem (3.8), it is necessary to verify that the resulting $\mathbf{R}$ with $\mathcal{I}$ and $\mathcal{J}$ as given satisfy constraints (3.8b) and (3.8c).

For energy harvesting, we note that R_{K-1K-1} coincides with r_{L-1} given in equation (3.6) and R_{K-1K} matches equation (3.7) if we set $L = K$. From equation (3.6), to have a non-zero $(K-1)$-th receive-side subchannel for energy harvesting, we need $\lambda_K = p_K\sigma_K > 0 \iff p_K > 0$. This is the reason why $p_K > 0$ even though it does not contribute to satisfying the constraints. With the above, substituting $\lambda_1 = \sqrt{\beta_1 + \alpha_1}\sigma_1$ and $\lambda_K = \sqrt{p_K}\sigma_K$ to equation (3.6) and equation (3.7) verifies that $R_{K-1K-1}^2 + R_{K-1K}^2 = \beta_1\sigma_1^2 + p_K\sigma_K^2$, so that constraint (3.8c) and equation (3.9b) are equal, as desired. To guarantee that the information rates in (3.8b) and (3.9a) are equal, we need to have

$$\sum_{k=1}^{K-1} \log_2\left(1 + \frac{\alpha_k\sigma_k^2}{\sigma^2}\right) = \sum_{i\in\mathcal{I}} \log_2\left(1 + \frac{r_i^2}{\sigma^2}\right), \tag{3.15}$$

Algorithm 1 Solution to the problem (3.8)

1: $[\mathbf{U}, \mathbf{\Sigma}, \mathbf{V}] \leftarrow \text{SVD}(\mathbf{H})$
2: Obtain $[\alpha_1, \alpha_2, \ldots, \alpha_{K-1}]$ that satisfy (3.8b) using (3.10), (3.11) and (3.12), given channel gains $\sigma_1^2, \sigma_2^2 \ldots, \sigma_{K-1}^2$.
3: Set minimum transmit power $p_K > 0$, so that the K-th transmit stream is active
4: Set $\beta_1 = (EH - p_K\sigma_K^2)/\eta\sigma_1^2$
5: **if** (3.14) holds **then**
6: Set power allocation $\mathbf{P}^\star$ as in (3.13)
7: Set vector $\mathbf{r}$ as in (3.6)
8: $[\mathbf{Q}, \mathbf{R}, \mathbf{X}] \leftarrow \text{GTD}(\mathbf{\Sigma}(\mathbf{P}^\star)^{1/2}, \mathbf{r})$
9: Transmit using precoder (2.18) and apply filter (2.20) at the receiver
10: Harvest energy from the subchannel $\mathcal{J} = \{K-1\}$
11: Decode information from the subchannels $\mathcal{I} = \{1, \ldots, K\} \setminus \mathcal{J}$
12: **else**
13: Problem (3.8) is infeasible for GTD based SWIPT
14: **End if**

where $R_{ii} = r_i$. As discussed in Subsection 3.2.2, vector $\mathbf{r}$ given in equation (3.6) leads to subchannels in $\mathcal{I}$ that contain no interference, that is, the corresponding rows of $\mathbf{R}$ have only diagonal elements. From equation (3.6) we recall that $r_1 = \lambda_2 = \sqrt{\alpha_2}\sigma_2$; ... ; $r_{K-2} = \lambda_{K-1} = \sqrt{\alpha_{K-1}}\sigma_{K-1}$ so that the corresponding $K-2$ subchannels related to information transfer in (3.8b) and (3.9a) are just permutations of each other. To guarantee equal information rate in both cases, the subchannel associated with r_K must therefore satisfy $\log_2(1+\alpha_1\sigma_1^2) = \log_2(1+r_K^2)$. Substituting r_K given in equation (3.6) on the RHS yields the equality leads to

$$\log_2\left(1+\frac{r_K^2}{\sigma^2}\right) = \log_2\left(1+\frac{\lambda_1^2+\lambda_K^2-\frac{EH}{\eta}}{\sigma^2}\right) \tag{3.16a}$$

$$= \log_2\left(1+\frac{(\beta_1+\alpha_1)\sigma_1^2+p_K\sigma_K^2-(\beta_1\sigma_1^2+p_K\sigma_K^2)}{\sigma^2}\right) \tag{3.16b}$$

$$= \log_2\left(1+\frac{\alpha_1\sigma_1^2}{\sigma^2}\right), \tag{3.16c}$$

where the second equality follows from the fact that $\lambda_1 = \sqrt{\beta_1+\alpha_1}\sigma_1$, $\lambda_K = \sqrt{p_K}\sigma_K$ and $EH/\eta = \beta_1\sigma_1^2 + p_K\sigma_K^2$. Thus, vector $\mathbf{r}$ given in equation (3.6) guarantees that (3.9a)–(3.9b) match (3.8b)–(3.8c) and power allocation (3.13) satisfies the constraints with minimum

total transmit power if (3.8) is feasible.

Finally, if the water filling algorithm allocates power to only the first w strongest subchannels ($w < K-1$) so that $\alpha_{w+1} = \alpha_{w+2} = \cdots = \alpha_{K-1} = 0$, the above development still holds when σ_K is replaced with σ_{w+1} and p_K by p_{w+1} everywhere;thus, the number of the subchannels with nonzero powers $L = w + 1$. For simplicity, Algorithm 1 summarizes the solution to the problem (3.8) for the case $w = K - 1$.

3.3.2 Transmit Power Minimization for SVD Based SWIPT

Recall the SVD based SWIPT scheme discussed in Section 2.4.1 and consider the following optimization problem

$$\underset{\mathbf{P},\mathcal{I},\mathcal{E}}{\text{minimize}} \quad \text{tr}(\mathbf{F}\mathbf{F}^H), \tag{3.17a}$$

$$\text{s.t.} \quad \sum_{i\in\mathcal{I}} \log_2\left(1+\frac{p_i\sigma_i^2}{\sigma^2}\right) \geqslant C, \tag{3.17b}$$

$$\sum_{e\in\mathcal{E}} \eta p_e \sigma_e^2 \geqslant EH, \tag{3.17c}$$

$$\sum_{k\in\mathcal{K}} p_k \leqslant P_t, \tag{3.17d}$$

where $\mathcal{I} \subseteq \mathcal{K}$ and $\mathcal{E} \subseteq \mathcal{K}\setminus\mathcal{I}$ are the sets of subchannels that are assigned for information

Algorithm 2 Solution to the problem (3.17)

1: $[\mathbf{U}, \mathbf{\Sigma}, \mathbf{V}] \leftarrow \text{SVD}(\mathbf{H})$
2: **Initialize** $\mathbf{P}^\star = (P_t/N_t)\cdot\mathbf{I}_{N_t}$, $e^\star = 0$ and $\mathcal{I}^\star = \emptyset$
3: **for** $k = 1$ to K **do**
4: Set $e = k$
5: Set $\mathcal{I} = \{1, 2, \ldots, K\} \setminus \{e\}$
6: Set $p_e = EH/\eta\sigma_e^2$
7: Obtain $\{p_i\}_{i\in\mathcal{I}}$ Using (3.2), (3.3), (3.4) to satisfy (3.17b)
8: **if** $p_e + \sum_{i\in\mathcal{I}} p_i \leqslant \text{tr}(\mathbf{P}^\star)$ **then**
9: Set $\mathbf{P}^\star = \text{diag}(p_1, \ldots, p_{e-1}, p_e, p_{e+1}, \ldots p_K)$, $e^\star = e$ and $\mathcal{I}^\star = \mathcal{I}$
10: **End if**
11: **if** $k = K$, $e^\star = 0$ and $\mathcal{I}^\star = \emptyset$ **then**
12: Problem (3.17) is infeasible for SVD based SWIPT
13: **End for**

exchange and energy transfer, respectively. A similar problem was studied and solved in

[14, 16], but with a maximum power per antenna constraint instead of the total power constraint as in problem (3.17). As in Section 3.2.1, to solve problem (3.17), the index sets for information bearing $\mathcal{I}$ and energy carrying $\mathcal{E}$ subchannels need to be identified. From Appendix A, it is optimal to choose one subchannel for energy harvesting and assign the remaining subchannels information exchange. As previously, expressions (3.2), (3.3) and (3.4) are used to obtain the power allocation to these subchannels to satisfy the rate constraint (3.17b). Since only one subchannel is assigned for energy harvesting, the power required to satisfy the constraint (3.17c) is simply given by $p_e = \frac{EH}{\eta\sigma_e^2}$. Following Section 3.2.1, this means that the optimal power allocation is found by examining all K possible subchannel assignments and choosing the one that leads to minimum transmit power. Algorithm 2 summarizes the proposed solution to problem (3.17).

3.4 Data Rate Maximization With Energy Harvesting and Total Instantaneous Transmit Power Constrains

This section focuses on designing two SS based MIMO SWIPT transceivers that maximize the data rate and achieving a specific amount of energy with a limited total power at the transmitter. We use GTD to design the first transceiver while the second one is build based on SVD.

3.4.1 Data Rate Maximization for GTD based SWIPT

Consider the following optimization problem for the achievable rate maximization:

$$\underset{\mathbf{P},\,\mathbf{r}\preceq\boldsymbol{\lambda},\,\mathcal{I},\,\mathcal{J}}{\text{maximize}} \quad C = \sum_{i\in\mathcal{I}} \log_2\left(1+\frac{R_{ii}^2}{\sigma^2}\right), \tag{3.18a}$$

$$\text{s.t.} \quad \sum_{j\in\mathcal{J}}\sum_{l=j}^{K} \eta R_{jl}^2 \geqslant EH, \tag{3.18b}$$

$$\text{tr}(\mathbf{F}\mathbf{F}^H) \leqslant P_t, \tag{3.18c}$$

Similar to the approach that is used to solve problem (3.8), the solution to problem (3.18) can be done in two steps. The aim in the first step is to obtain the optimal power

allocation $\mathbf{P}^{\star}$ that maximizes the data rate and satisfies the energy harvesting constraint in (3.18b). In the second step we decompose the matrix $\mathbf{\Sigma}(\mathbf{P}^{\star})^{1/2}$ using GTD to construct the precoding and the receiver-side matrices $\mathbf{F}$ and $\mathbf{W}$, respectively.

As discussed in Subsection 3.3.1, the proposed design exploits the key feature of the GTD based SWIPT system, namely, that the transmitter has the ability to allocate the power to the strongest subchannel to jointly send information and energy signals and these transmissions can be separated at the receiver via the linear filtering.

A. Optimal Power Allocation

The power allocation is carried out according to the singular values $\boldsymbol{\sigma}$ of the channel matrix $\mathbf{H}$. As explained in Appendix A, assigning only one subchannel for energy harvesting is optimal. Since the GTD allows the transmitter to any subchannel to carry signals that are used to transfer both information and energy, the transmitter uses the highest gain subchannel for both energy harvesting and information exchange. Thus, the power allocation problem can be written as follows:

$$\underset{\beta_1,\alpha_k}{\text{maximize}} \quad \sum_{k=1}^{K-1} \log_2\left(1+\frac{\alpha_k\sigma_k^2}{\sigma^2}\right), \tag{3.19a}$$

$$\text{s.t.} \quad \eta\beta_1\sigma_1^2 = EH, \tag{3.19b}$$

$$\sum_{k=1}^{K-1} p_k < P_t, \tag{3.19c}$$

$$p_k \geqslant 0, \quad k = \{1,2,\ldots,K-1\} \tag{3.19d}$$

where $p_1 = \beta_1 + \alpha_1, p_2 = \alpha_2, \ldots, p_{K-1} = \alpha_{K-1}$. Note that, the subchannel related to σ_K is not considered in (3.19) and the transmitter applies only small power $p_K > 0$ to it in order to keep the corresponding subchannel active as its presence is necessary for the receiver to be able to perform the signals separation.

Clearly, problem (3.19) is not feasible when there is no power left for the information exchange; *i.e.*, $\alpha_k = 0$ after satisfying the energy constraint EH. In other words, problem (3.19) is feasible if $EH < EH_{\max}$, where $EH_{\max} = \eta(P_t - p_K)\sigma_1^2$.

To obtain $\alpha_k^{\star}$ that are used to maximize the data rate, it is required to find the minimum power $\beta_1^{\star}$ that is required to satisfy EH. $\beta_1^{\star}$ can be computed from (3.19b)

directly as

$$\beta_1^\star = \frac{EH}{\eta\sigma_1^2}. \tag{3.20}$$

The remaining power $P_r = (P_t - \beta_1^\star - p_K)$ is used for information exchange.

The optimal power allocation $\alpha_k^\star$ for information transfer can be obtained via the standard waterfilling algorithm [83] as

$$\alpha_k^\star = \begin{cases} \alpha_w^\star + \sigma^2\left(\frac{1}{\sigma_w^2} - \frac{1}{\sigma_k^2}\right), & k = 1, 2, \ldots, w, \\ 0, & w < k \leqslant K-1, \end{cases} \tag{3.21}$$

where $\alpha_w^\star$ is found as

$$\alpha_w^\star = \frac{1}{w}\left(P_r - \sigma^2 \sum_{k=1}^{w} \frac{1}{\sigma_w^2} - \frac{1}{\sigma_k^2}\right), \tag{3.22}$$

and the water level step is given by

$$w = \max\left\{k \;\middle|\; P_r - \sigma^2 \sum_{i=1}^{k} \frac{1}{\sigma_k^2} - \frac{1}{\sigma_i^2} > 0,\ k = 1, \ldots, K-1\right\}. \tag{3.23}$$

The optimal power allocation matrix is denoted $\mathbf{P}^\star = \text{diag}\left[\beta_1^\star + \alpha_1^\star, \alpha_2^\star, \ldots, \alpha_w^\star, p_K\right]$. Given the optimal power allocation $\mathbf{P}^\star$ is obtained, we need to define the diagonal elements $\mathbf{r}$ of the matrix $\mathbf{R}$ used in the GTD decomposition of $\mathbf{\Sigma}(\mathbf{P}^\star)^{1/2}$.

B. Precoder and Receiver Filter Design via GTD

As discussed in Section 3.2.2, the diagonal elements $\mathbf{r}$ must be multiplicatively majorized by the diagonal elements of $\mathbf{\Sigma}(\mathbf{P}^\star)^{1/2}$, that is, $\mathbf{r} \preceq \boldsymbol{\lambda}$. For notation simplicity, let us assume $w = K-1$; thus, the vector $\mathbf{r}$ that is defined in (3.6) can be used to decompose $\mathbf{\Sigma}(\mathbf{P}^\star)^{1/2}$ to complete the construction of the precoder $\mathbf{F}$ and the linear filter $\mathbf{W}$. Note that using $\mathbf{F}$ and $\mathbf{W}^H$ at the transmitter and the receiver, respectively, results $\mathbf{R}$ which leads to give a total data rate equals to $\left(\sum_{k=1}^{K-1} \log_2\left(1 + \alpha_k^\star \sigma_k^2/\sigma^2\right)\right)$ and satisfies the required energy EH at the receiver. This structure of $\mathbf{R}$ allows the receiver to harvest the energy from the $\mathcal{J} = K-1$ subchannel while the rest of the subchannels; *i.e.*, $\mathcal{I} = \{1, 2, \ldots, K\} \setminus \mathcal{J}$ are used to decode information.

Algorithm 3 Solution to the problem (3.18)

1: $[\mathbf{U}, \mathbf{\Sigma}, \mathbf{V}] \leftarrow \text{SVD}(\mathbf{H})$
2: Set $p_K > 0$
3: Set $EH_{\max} = \eta(P_t - p_K)\sigma_1^2$
4: **if** $EH < EH_{\max}$ **then**
5: Obtain $\beta_1^\star$ from (3.20)
6: Set $P_r = P_t - \beta_1^\star - p_K$
7: Obtain $\left[\alpha_1^\star, \alpha_2^\star, \ldots, \alpha_{K-1}^\star\right]$ (3.21), (3.22) and (3.23) on SNRs $\sigma_1^2, \sigma_2^2 \ldots, \sigma_{K-1}^2$
8: Construct the power allocation matrix $\mathbf{P}^\star = \text{diag}\left[\beta_1^\star + \alpha_1^\star, \alpha_2^\star, \ldots, \alpha_w^\star, p_K\right]$
9: Set vector $\mathbf{r}$ as in (3.6)
10: $[\mathbf{Q}, \mathbf{R}, \mathbf{X}] \leftarrow \text{GTD}(\mathbf{\Sigma}(\mathbf{P}^\star)^{1/2}, \mathbf{r})$
11: Transmit using precoder (2.18) and apply filter (2.20) at the receiver
12: Harvest energy from the subchannel $\mathcal{J}^\star = \{K-1\}$
13: Decode information from the subchannels $\mathcal{I}^\star = \{1, \ldots, K\} \setminus \mathcal{J}^\star$
14: **else**
15: Problem (3.18) is infeasible for GTD based SWIPT
16: **End if**

Finally, to verify that the achievable data rate and the energy harvested at the receiver coincide with the data rate and the energy that are obtained from solving problem (3.19), we follow the discussion presented in Subsection 3.3.1.C. Algorithm 3 summarizes the solution of problem (3.18) for the case $w = K - 1$.

3.4.2 Data Rate Maximization for SVD based SWIPT

Consider the following optimization problem for data rate maximization of the SVD based SWIPT system

$$\underset{\mathbf{P}, \mathcal{I}, \mathcal{E}}{\text{maximize}} \quad C = \sum_{i \in \mathcal{I}} \log_2\left(1 + \frac{p_i \sigma_i^2}{\sigma^2}\right), \tag{3.24a}$$

$$\text{s.t.} \quad \sum_{e \in \mathcal{E}} \eta p_e \sigma_e^2 \geqslant EH, \tag{3.24b}$$

$$\sum_{k \in \mathcal{K}} p_k \leqslant P_t, \tag{3.24c}$$

where $\mathcal{I} \subseteq \mathcal{K}$ and $\mathcal{E} \subseteq \mathcal{K}$ are disjoint sets ; *i.e.*, $\mathcal{I} \bigcap \mathcal{E} = \emptyset$. As discussed in Section 3.3.2, it is optimal to select only one subchannel for energy harvesting and use the remaining subchannel for information exchange. Thus, problem (3.24) feasibility can be examined

by check if the condition $EH < EH_{\max}$ holds, where $EH_{\max} = \eta P_t \sigma_1^2$. Suppose that problem (3.24) is feasible, the optimal solution can be found by examining all K possible subchannel assignments and choose the particular assignment that returns the maximum information rate C. This means that problem (3.24) is solved K times with different fixed sets $\mathcal{I}$ and $\mathcal{E}$ at each time. For fixed sets $\mathcal{I}$ and $\mathcal{E}$, the power is allocated first to satisfy the energy harvesting constraint (3.24b) as follows

$$p_e = \frac{EH}{\eta \sigma_e}, \tag{3.25}$$

then the remaining power $P_r = P_t - p_e$ is used for information exchange. Note that P_r

Algorithm 4 Solution to the problem (3.24)

1: $[\mathbf{U}, \mathbf{\Sigma}, \mathbf{V}] \leftarrow \text{SVD}(\mathbf{H})$
2: Set $EH_{\max} = \eta P_t \sigma_1^2$
3: **if** $EH < EH_{\max}$ **then**
4: **Initialize** $\mathbf{P}^\star = \mathbf{0}_{N_t}$, $e^\star = 0$, $\mathcal{I}^\star = \emptyset$ and $C^\star = 0$
5: **for** $k = 1$ to K **do**
6: Compute p_e from (3.25)
7: Compute $P_r = P_t - p_e$
8: **if** $P_r > 0$ **then**
9: Set $\mathcal{I} = \{1, 2, \ldots, K\} \setminus \{e\}$
10: Obtain $\{p_i\}_{i \in \mathcal{I}}$ that maximizes the information rate C Using (3.26), (3.27) and (3.28)
11: **if** $C > C^\star$ **then**
12: $\mathbf{P}^\star = \text{diag}(p_1, \ldots, p_{e-1}, p_e, p_{e+1}, \ldots p_K)$, $e^\star = e$, $\mathcal{I}^\star = \mathcal{I}$ and $C^\star = C$
13: **End if**
14: **else**
15: Continue
16: **End if**
17: **End for**
18: **End if**

must be always positive; hence, any given assignment that does not satisfy this condition is rejected without any further consideration. In order to maximize the information rate, the standard water filling algorithm [83] is used over the subchannels in the set $\mathcal{I}$ as

follows

$$p_i = \begin{cases} p_w + \sigma^2 \left(\frac{1}{\sigma_w^2} - \frac{1}{\sigma_i^2}\right), & i = 1, 2, \ldots, w \quad \text{and} \quad i \neq e \\ 0, & w < i \leqslant K-1 \quad \text{and} \quad i \neq e \end{cases} \tag{3.26}$$

where p_w is found as

$$p_w = \frac{1}{w}\left(P_r - \sigma^2 \sum_{i=1}^{w} \frac{1}{\sigma_w^2} - \frac{1}{\sigma_i^2}\right), \qquad i \in \mathcal{I}, \tag{3.27}$$

and the water level step is given by

$$w = \max\left\{ i \;\middle|\; P_r - \sigma^2 \sum_{i=1}^{k} \frac{1}{\sigma_k^2} - \frac{1}{\sigma_i^2} > 0, \qquad k = \{1, 2, \ldots K\} \setminus \{e\} \right\}, \tag{3.28}$$

Algorithm 4 summarizes the solution of problem (3.24)

3.5 Energy Harvesting Maximization With Data Rate and Total Instantaneous Transmit Power Constrains

In this section, we present two SS based MIMO SWIPT transceivers. The first one is developed based on GTD while the other one is designed based on SVD. In each transceiver, we concentrate on maximizing the harvested energy and satisfying data rate constraint at the receiver when the transmitter has limited total power.

3.5.1 Energy Harvesting Maximization for GTD Based SWIPT

In this section, the GTD structure is exploited to design a transceiver that maximizes the harvested energy in SS based MIMO SWIPT systems. Consider the following optimization problem for energy harvesting maximization

$$\underset{\mathbf{P}, \mathbf{r} \preceq \boldsymbol{\lambda}, \mathcal{I}, \mathcal{J}}{\text{maximize}} \quad EH = \sum_{j \in \mathcal{J}} \sum_{l=j}^{K} \eta R_{jl}^2, \tag{3.29a}$$

$$\text{s.t.} \qquad \sum_{i \in \mathcal{I}} \log_2\left(1 + \frac{R_{ii}^2}{\sigma^2}\right) \geqslant C, \tag{3.29b}$$

$$\mathrm{tr}(\mathbf{F}\mathbf{F}^H) \leqslant P_t, \tag{3.29c}$$

The solution to problem (3.29) follows the same process that is used to solve problems (3.8) and (3.18) in Subsection 3.3.1 and Subsection 3.4.1, respectively. That is, the power is first allocated according to the singular values $\mathbf{\Sigma}$ of the channel $\mathbf{H}$ then the GTD is used to decompose $\mathbf{\Sigma}\mathbf{P}^{1/2}$ in order to construct the precoder $\mathbf{F}$ and the receiver-side matrix $\mathbf{W}$ that results in a proper $\mathbf{R}$ in which the energy harvesting is maximized and the required data rate is met at the receiver.

A. Optimal Power Allocation

The transmit-side power allocation problem for the proposed transceiver is carried out according to the singular values $\mathbf{\Sigma}$ of the MIMO channel $\mathbf{H}$. Following Appendix A and the fact that the GTD structure allows the transmitter to use a single subchannel to carry both information and energy signals as discussed previously, the power allocation problem can be written as follows:

$$\begin{aligned}
\underset{\beta_1,\,\alpha_k}{\text{maximize}} \quad & \eta\beta_1\sigma_1^2, && \text{(3.30a)}\\
\text{s.t.} \quad & \sum_{k=1}^{K-1} \log_2\left(1+\frac{\alpha_k\sigma_k^2}{\sigma^2}\right) \geqslant C, && \text{(3.30b)}\\
& \sum_{k=1}^{K-1} p_k \leqslant P_t - p_K, && \text{(3.30c)}\\
& p_k \geqslant 0, \quad k=\{1,2,\ldots,K-1\} && \text{(3.30d)}
\end{aligned}$$

where $(p_1 = \beta_1 + \alpha_1, p_2 = \alpha_2, \ldots, p_{K-1} = \alpha_{K-1})$. Like the previous GTD designs, the transmitter applies low power to the weakest subchannel, that is, $p_K > 0$. The presence of the weakest subchannel is important for the signals separation process at the receiver in the GTD systems as discussed earlier in the previous sections.

Clearly, problem (3.30a) is not feasible if $C \geqslant C_{\max}$, where $C_{\max} = \sum_{k=1}^{K-1}\log_2\left(1+\tilde{\alpha_k}\sigma_k^2\right)$ and the powers $\tilde{\alpha}_k$ are obtained using the standard water filling algorithm [83] as explained in equations (3.21), (3.22) and (3.23). Note that P_r in equations (3.22) and (3.23) should be replaced by $(P_t - p_K)$ to comply with the available transmitted power in (3.30).

Algorithm 5 Solution to the problem (3.29)

1: $[\mathbf{U}, \mathbf{\Sigma}, \mathbf{V}] \leftarrow \text{SVD}(\mathbf{H})$
2: Set $p_K > 0$ and $P_r = Pt - p_K$
3: Set $C_{\max} = \sum_{k=1}^{K-1} \log_2\left(1 + \tilde{\alpha_k}\sigma_k^2\right)$, where the powers $\tilde{\alpha_k}$ are obtained from applying (3.21), (3.22) and (3.23) on the subchannels $(\sigma_1, \sigma_2, \ldots, \sigma_{K-1})$
4: **if** $C < C_{\max}$ **then**
5: Obtain $\left[\alpha_1^\star, \alpha_2^\star, \ldots, \alpha_{K-1}^\star\right]$ from (3.10), (3.11) and (3.12)
6: Compute $\beta_1^\star$ from (3.31)
7: Construct the power allocation matrix $\mathbf{P}^\star = \text{diag}\left[\beta_1^\star + \alpha_1^\star, \alpha_2^\star, \ldots, \alpha_w^\star, p_K\right]$
8: Set vector $\mathbf{r}$ as in (3.6)
9: $[\mathbf{Q}, \mathbf{R}, \mathbf{X}] \leftarrow \text{GTD}(\mathbf{\Sigma}(\mathbf{P}^\star)^{1/2}, \mathbf{r})$
10: Transmit using precoder (2.18) and apply filter (2.20) at the receiver
11: Harvest energy from the subchannel $\mathcal{J}^\star = \{K-1\}$
12: Decode information from the subchannels $\mathcal{I}^\star = \{1, \ldots, K\} \setminus \mathcal{J}^\star$
13: **else**
14: Problem (3.30) is infeasible for GTD based SWIPT
15: **End if**

To obtain $\beta_1^\star$ that maximizes EH, we need to find the minimum powers $\alpha_k^\star$ to meet the required rate in constraint (3.30b). Following Theorem 1 in [76], and as explained in Subsection 3.3.1.A, $\alpha_k^\star$ can be computed using equations (3.10), (3.11) and (3.12). Therefore $\beta_1^\star$ can be calculated as follows

$$\beta_1^\star = P_t - \left(p_K + \sum_{k=1}^{w} \alpha_k^\star\right). \tag{3.31}$$

Thus, the optimal power allocation $\mathbf{P}^\star = \text{diag}\left[\beta_1^\star + \alpha_1^\star, \alpha_2^\star, \ldots, \alpha_w^\star, p_K\right]$. Given the optimal power allocation $\mathbf{P}^\star$ is obtained, we need to define the diagonal elements $\mathbf{r}$ of the matrix $\mathbf{R}$ used in the GTD decomposition of $\mathbf{\Sigma}(\mathbf{P}^\star)^{1/2}$.

B. Precoder and Receiver Filter Design via GTD

The precoder $\mathbf{F}$ and the linear filter $\mathbf{W}$ constructions are completed via the GTD decomposition of the diagonal matrix $\mathbf{\Sigma}\mathbf{P}^{1/2}$. GTD is performed on $\mathbf{\Sigma}\mathbf{P}^{1/2}$ when the vector of the diagonal elements $\mathbf{r}$ is chosen properly. However, $\mathbf{r}$ must be multiplicatively majorized by the diagonal elements of $\mathbf{\Sigma}(\mathbf{P}^\star)^{1/2}$, that is, $\mathbf{r} \preceq \boldsymbol{\lambda}$. We note that using $\mathbf{r}$ that is defined in Theorem 3.1 maximizes the objective of problem (3.29) and gives data rate

equivalent to the one in the constraint (3.30b).

Finally, the details introduced in Section Subsection 3.3.1.C can be followed to verify that the amounts of the harvested energy and the information rate at the receiver are identical to the energy and the data rate that attained by solving problem (3.30). Algorithm 5 illustrates the solution of problem (3.29).

3.5.2 Energy Harvesting Maximization for SVD Based SWIPT

The problem of maximizing the harvested energy for the SVD based SWIPT system has been studied in [76]. For the comparison purpose, the work in [76] is revisited here briefly. The problem of energy harvesting maximization is formulated as follows:

$$\underset{\mathbf{P},\mathcal{I},\mathcal{E}}{\text{maximize}} \quad EH = \sum_{e\in\mathcal{E}} \eta p_e \sigma_e^2, \tag{3.32a}$$

$$\text{s.t.} \quad \sum_{i\in\mathcal{I}} \log_2\left(1+\frac{p_i\sigma_i^2}{\sigma^2}\right) \geqslant C, \tag{3.32b}$$

$$\sum_{k\in\mathcal{K}} p_k \leqslant P_t, \tag{3.32c}$$

where $\mathcal{I} \subseteq \mathcal{K}$ and $\mathcal{E} \subseteq \mathcal{K}$ represent the sets of the subchannels that are used for information exchange and for energy harvesting, respectively. Note that $\mathcal{I}$ and $\mathcal{E}$ are disjoint sets.

Obviously, Problem (3.32) is not feasible if $C \geqslant C_{\max}$, where $C_{\max} = \sum_{i=1}^{K-1} \log_2\left(1 + p_i\sigma_i^2/\sigma^2\right)$ and the powers p_i can be obtained by using the standard water filling algorithm [83] as given by equation (3.21), (3.22) and (3.23) and using P_t instead of P_r and replacing α_k with p_i to match the notations in problem (3.32).

Since it is optimal to use only subchannel for the energy harvesting as discussed in Subsection 3.3.2 and Subsection 3.4.2, the optimal solution of problem (3.32) is obtained by examining K subchannels assignments and choose the one that leads to the maximum energy harvesting EH. For each assignment, the transmitter picks up one subchannel wit index e for energy harvesting and allocates powers p_i to the remaining subchannels $\mathcal{I} = \{1,2,\ldots,K\} \setminus \{e\}$ in order to meet the required rate C in (3.32b) and the remaining power is applied on the subchannel e for energy harvesting. The powers p_i that are used for information exchange are calculated based on Theorem 1 in [76] and as explained by

Algorithm 6 Solution to the problem (3.32)

1: $[\mathbf{U}, \mathbf{\Sigma}, \mathbf{V}] \leftarrow \text{SVD}(\mathbf{H})$
2: Obtain $C_{\max} = \sum_{i=1}^{K-1} \log_2\left(1 + p_i \sigma_i^2\right)$ from (3.21), (3.22) and (3.23) and using P_t instead of P_r
3: **if** $C < C_{\max}$ **then**
4: **Initialize** $\mathbf{P}^\star = \mathbf{0}_{N_t}$, $e^\star = 0$, $\mathcal{I}^\star = \emptyset$ and $EH^\star = 0$
5: **for** $e = 1$ to K **do**
6: Set $\mathcal{I} = \{1, 2, \ldots, K\} \setminus \{e\}$
7: Compute p_i from (3.2), (3.3) and (3.4)
8: Compute $p_e = P_t - \sum_{i \in \mathcal{I}} p_i$
9: **if** $p_e > 0$ **then**
10: Obtain EH as in (3.32a).
11: **if** $EH > EH^\star$ **then**
12: $\mathbf{P}^\star = \text{diag}(p_1, \ldots, p_{e-1}, p_e, p_{e+1}, \ldots p_K)$, $e^\star = e$, $\mathcal{I}^\star = \mathcal{I}$ and $EH^\star = EH$
13: **End if**
14: **else**
15: Continue
16: **End if**
17: **End for**
18: **End if**

equations (3.2), (3.3) and (3.4). After obtaining p_i the remaining power p_e that is used for energy harvesting is computed as

$$p_e = P_t - \sum_{i \in \mathcal{I}} p_i. \tag{3.33}$$

Note that p_e must be always positive; therefore, any given assignment that does not meet this condition is not considered as a solution. Algorithm 6 summarizes the solution of problem (3.32)

3.6 Numerical Results

In this section, simulation results are presented to compare the performance of GTD and SVD based precoding methods for SWIPT. A Rayleigh block fading spatially uncorrelated MIMO channel is considered, so that the entries of $\mathbf{H}$ are independent ZMCSCG random variables with variance $\sigma_h^2 = ad^{-\gamma}$ where $a = 0.1$ is the path loss factor, d in meters (m) is the transmitter to receiver distance and $\gamma = 3$ represents the path loss

exponent. A symmetric antenna setup $N_t = N_r = 4$ is assumed in all simulations. The power is measured in watts (W) and the information rate is measured in bits per second per hertz (bps/Hz). The energy conversion efficiency η is set to 0.66. The results are averaged over 10^6 independent channel realizations using Monte Carlo simulations. In all figures, except Figure 3.7, the blue and the red colors refer to the GTD based SWIPT and the SVD based SWIPT curves, respectively.

A. Transmit Power Minimization

The simulation results of the GTD and the SVD based SWIPT designs for transmit power minimization are presented here. The results of both GTD based SWIPT and SVD based SWIPT systems are obtained by solving problems (3.8) and (3.17) using Algorithm 1 and Algorithm 2, respectively. Figure 3.2 shows plots of outage probability versus the instantaneous total transmit power constraint P_t under different data rate C and energy harvesting EH requirements. The outage is defined as an event when one or both of the constraints cannot be satisfied for the given power constraint P_t. Note that identifying which particular constraint fails is not easy especially for the SVD based SWIPT approach since there is no closed-form solution that defines the feasibility of the power allocation problem (3.17) [14, 15]. In addition, the available transmit power in some cases is enough to satisfy only one constraint no matter EH or C. In Figure 3.2a, the outage probability of the GTD based SWIPT decays steeply as a function of the total transmit power. In contrast, the curves representing the SVD based SWIPT decay slowly and exhibit much higher outage probabilities when the required data rate is high. It is also clear that for a constant energy harvesting constraint $EH = 0.3$ mW, increasing the data rate constraint from $C = 6$ bps/Hz to $C = 14$ bps/Hz has significantly less impact on the outage probability of the GTD base system compared to the SVD based one. For example, given energy harvesting constraint $EH = 0.3$ mW and 10% outage probability, increasing the data rate constraint C from 6 to 14 bps/Hz requires the average transmit power to be increased by 0.8 W for the GTD based approach while 3.5 W more power is needed for the SVD based approach. The difference in the performance is explained by the fact that the best eigenchannel in the GTD based precoder can be assigned to carry both information and energy simultaneously, while for the SVD based precoder

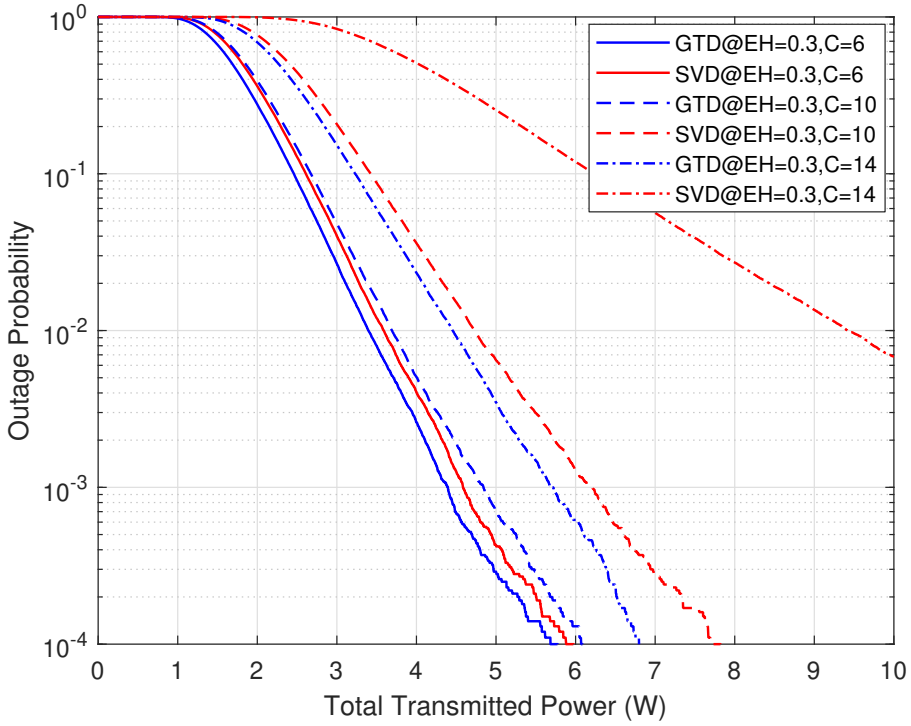

(a) Varying energy harvesting constraint

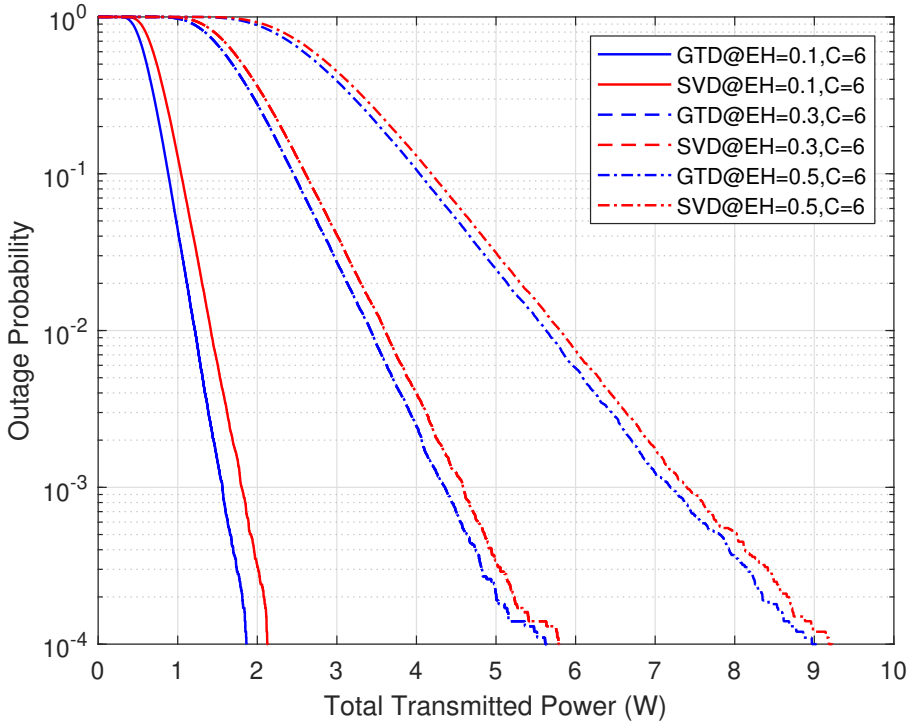

(b) Varying information rate constraint

Figure 3.2: Outage probability vs. total transmit power constraint P_t for different energy harvesting and rate requirements with noise power $\sigma^2 = -60$ dBm and $d = 15$ m (C in bps/Hz, EH in mW).

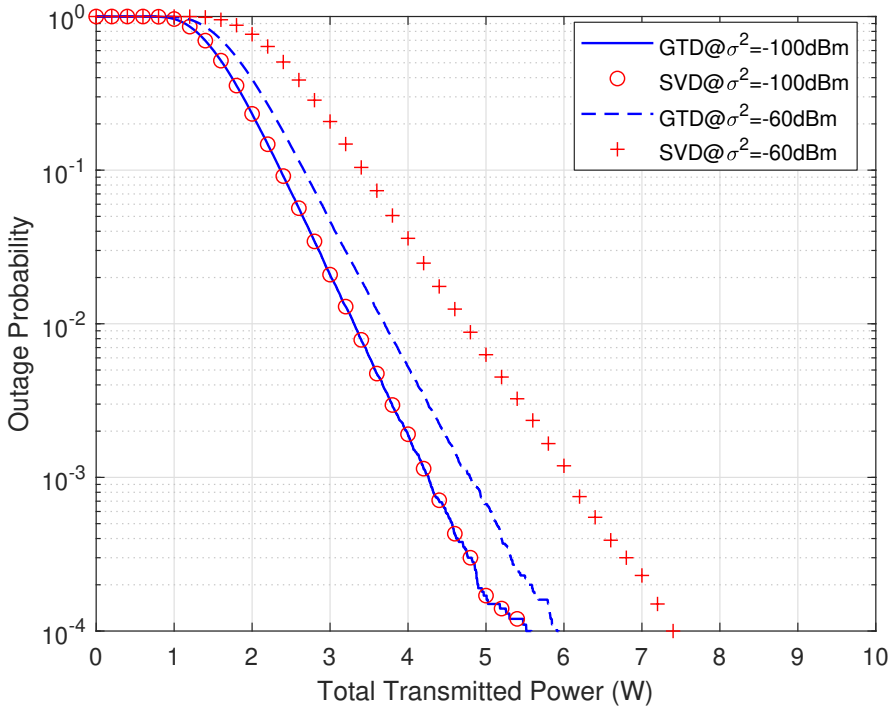

Figure 3.3: Outage probability vs. total transmit power constraint P_t for different σ^2 with $EH = 0.3$ mW, $C = 10$ bps/Hz and $d = 15$ m .

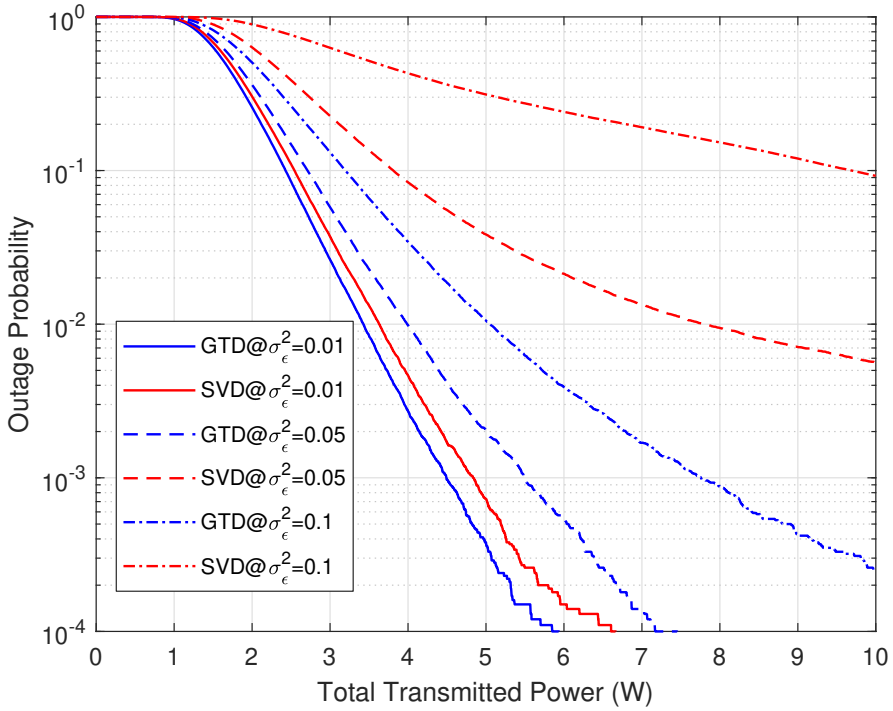

Figure 3.4: Outage probability vs. total transmit power constraint P_t assuming imperfect CSI with noise power $\sigma^2 = -100$ dBm, $EH = 0.3$ mW, $C = 6$ bps/Hz and $d = 15$ m.

each eigenchannel can carry either information or energy, but not both at the same time.

In Figure 3.2b, it can be observed that the GTD system outperforms the SVD system only marginally when the data rate constraint has moderate values such as $C = 6$ bps/Hz. The small gap in the performance between the GTD and the SVD systems is due to the fact that the SVD system always assigns the highest gain subchannel for energy harvesting when the data rate constraint has moderate or low values. In this case, the data rate constraint in the SVD systems is satisfied using the lowest gain subchannels. In the GTD system, the highest gain subchannel is used jointly for data and energy transmission and this explains why the GTD system has better performance its counterpart SVD system.

Figure 3.3 plots the outage probability versus the total transmit power for both GTD and SVD based SWIPT systems under different values of the noise power with $EH = 0.3$ mW and $C = 10$ bps/Hz. It can be noted from Figure 3.3 that both GTD and SVD approaches have equivalent performance when the noise power value is low. This is expected since the data rate constraint is related to the signal-to-noise ratio and low noise powers such as $\sigma^2 = -100$ dBm make the impact of the subchannels gains insignificant toward the satisfaction of the required data rate. On the other hand, the impact of the noise power toward attaining the energy harvesting constraint is negligible in comparison with the impact of the subchannels gains. This leads to the dominance of the energy harvesting constraint over the data rate constraint. Therefore, the transmitter at the SVD approach allocates most of the available transmit power to the highest gain subchannel for energy harvesting while only fractional of the transmit power are applied to the subchannels of the weakest gains for information exchange as the noise power value is low. This type of the subchannel assignment is the reason why both GTD and SVD approaches yield almost equivalent performance knowing that the GTD approach always assign the highest gain subchannel for joint information and energy transmission. The gap in the performance between the GTD and the SVD approaches is evident when the noise power is high. Note that the influence of the subchannels gains toward satisfying the data rate constraint rises as the noise power increases. In fact, the dominance of the energy harvesting becomes less when the required data rate is high and the noise power at high values. In this case, the GTD approach very well outperforms its counterpart the

SVD approach.

Figure 3.4 shows the outage probability versus the total transmit power for the GTD and the SVD approaches considering that the channel matrix is subject to a channel estimation error and therefore the channel is imperfectly known at both the transmitter and the receiver. The energy harvesting and the data rate constraints are assumed to be 0.3 mW and 10 bps/Hz, respectively. The noise power is set to -100 dBm and the distance between the transmitter and the receiver is assumed to be 15 m. The case of imperfect CSI knowledge follows [84] ; *i.e.*, the channel is imperfectly known at both the transmitter and the receiver with a parameter σ_ϵ^2 that is used to capture the quality of the channel estimation. According to [84], the parameter σ_ϵ^2 can take any value from 0 to 0.1. Note that the channel is perfectly estimated when $\sigma_\epsilon^2 = 0$, more details can be found in [84] about σ_ϵ^2 for different channel estimation schemes. In general, the imperfect channel estimation leads to inter-stream interference. The presence of the interference is beneficial for energy harvesting but detrimental for the achievable rate. In this case, the noise power is negligible in comparison with the power due to the interference and hence the achievable rate is determined based on the value of the signal-to-interference ratio. This fact is illustrated in the plots of Figure 3.4. It can be observed from Figure 3.4 that both GTD and SVD approaches have a comparable performance when the estimated channel is close to the actual one. However, the GTD approach significantly shows better performance that the SVD approach for the case of poor channel estimation. The dramatic difference between the two techniques can be highlighted by considering a case of poor channel estimation ; *i.e.*, $\sigma_\epsilon^2 = 0.1$ and moderate power, rate and energy harvesting constraints, namely, $P_t = 3.5$ W, $C = 6$ bps/Hz, and $EH = 0.3$ mW. Under these conditions, the GTD based system shows 7% outage probability, while the SVD based system has 52% outage probability, making the system unusable. The reason behind this difference in the performance is because the GTD experiences less interference than the SVD approach due to the fact that the highest gain eigenchannel at the GTD approach is used jointly for information and energy transmission.

Having demonstrated that for given instantaneous transmit power constraint P_t, the probability that a GTD based system fails to meet the energy harvesting and information

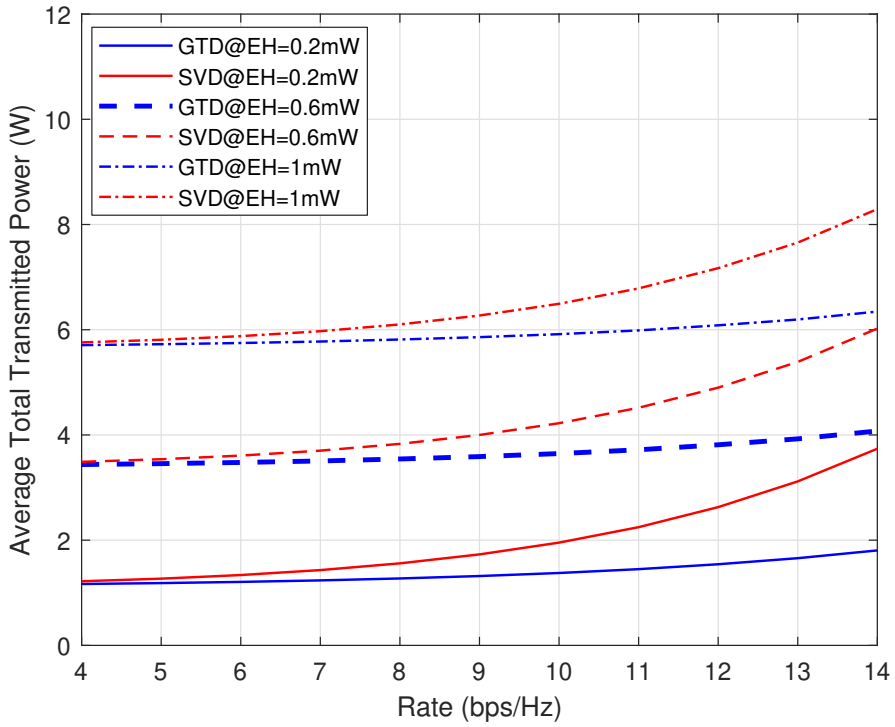

(a) Varying energy harvesting constraint

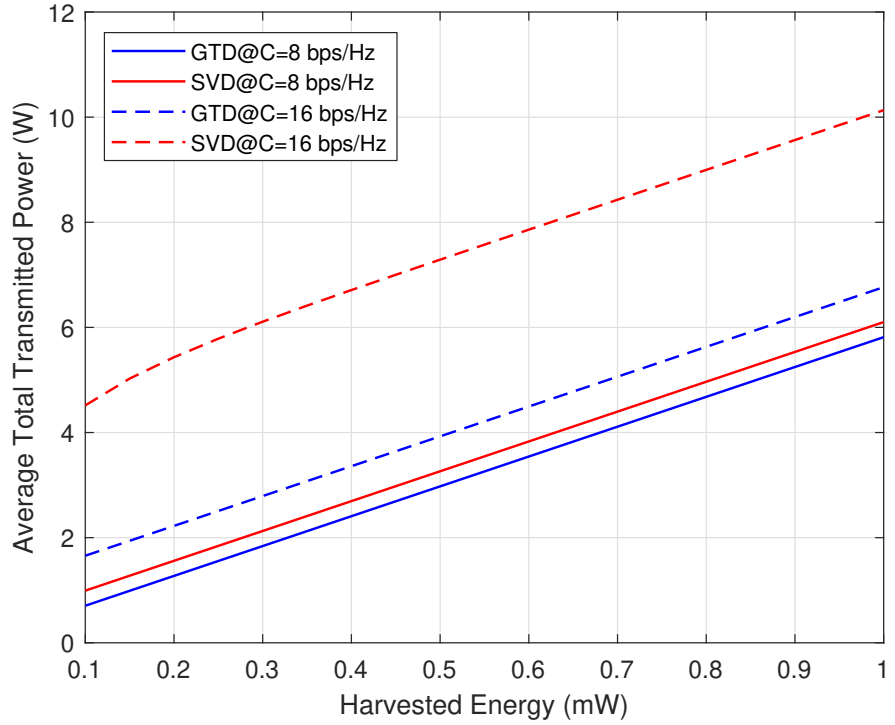

(b) Varying information rate constraint

Figure 3.5: Average total transmitted power with optimum power allocation and no instantaneous power constraint, $P_t = +\infty$.$d = 15$ m.

rate targets is orders of magnitude lower than with SVD based system, in Figure 3.5 we examine the average transmitted powers of both systems when the instantaneous power constraint is relaxed as $P_t = +\infty$. Note that the SVD based SWIPT in this case becomes similar to those investigated in [16] and [14]. The considered setup guarantees that both SWIPT strategies always succeed in meeting the constraints, while minimizing the total transmit power.

Figure 3.5a plots the average total transmit power versus rate constraint for both precoding schemes. For a given value of EH, increasing the rate requirement for the GTD based system shows only mild increase in the average transmit power. In contrast, the curves representing the SVD based system rise sharply for the higher values of the rate constraint. For example, increasing the rate constraint C from 9 to 13 bps/Hz while holding EH fixed at 0.6 mW requires increasing the average total transmitted power by 0.3 W and 1.4 W for the GTD and SVD based approaches, respectively. The average total transmit power as a function of energy harvesting constraint is examined in Figure 3.5b. The results clearly show that using GTD based SWIPT leads to significant saving of transmitted power in comparison with the SVD based SWIPT, especially for higher rate constraints. For example, EH = 0.4 mW, C = 16 bps/Hz can be achieved using average power of 3.6 W with GTD, while approximately 7 W are required with SVD.

Figure 3.6 shows the affect of the distance between the transmitter and the receiver on the average total transmitted power under different values of energy harvesting EH and rate C constraints. In Figure 3.6a, It can be observed that for moderate rate C and any value of EH increasing the distance requires approximately equal increment in Pt at both the GTD and the SVD approaches. In contrast, Figure 3.6b shows that, when the rate C is high and EH is fixed, the GTD based SWIPT in comparison with the SVD based SWIPT requires significantly low increment in P_t when the distance is increased.

To investigate the relative performance of the two SWIPT schemes in more detail, Figure 3.7 plots the ratio between the average total transmit power for the GTD and SVD based systems versus the rate and energy harvesting constraints. As in Figures 3.5 and 3.6, the scenario of no instantaneous power constraint ($P_t = +\infty$) is considered. The results clearly show that a significant saving in the transmitted power can be achieved

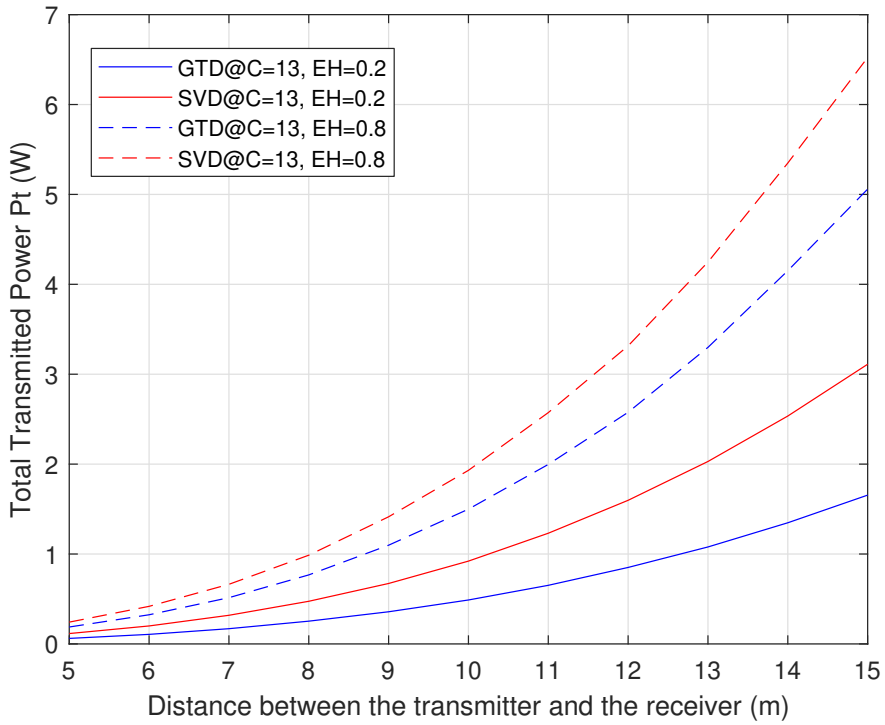

(a) Varying energy harvesting constraint with fixed information rate constraint

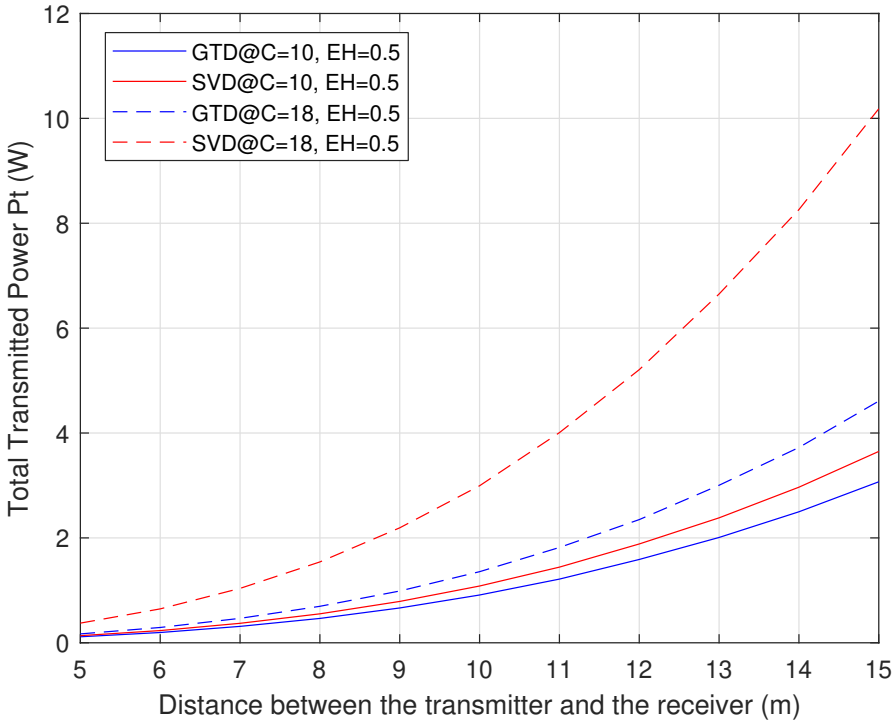

(b) Varying information rate constraint with fixed energy harvesting constraint

Figure 3.6: Average total transmitted power with optimum power allocation and no instantaneous power constraint, $P_t = +\infty$ vs. distance (C in bps/Hz and EH in mW).

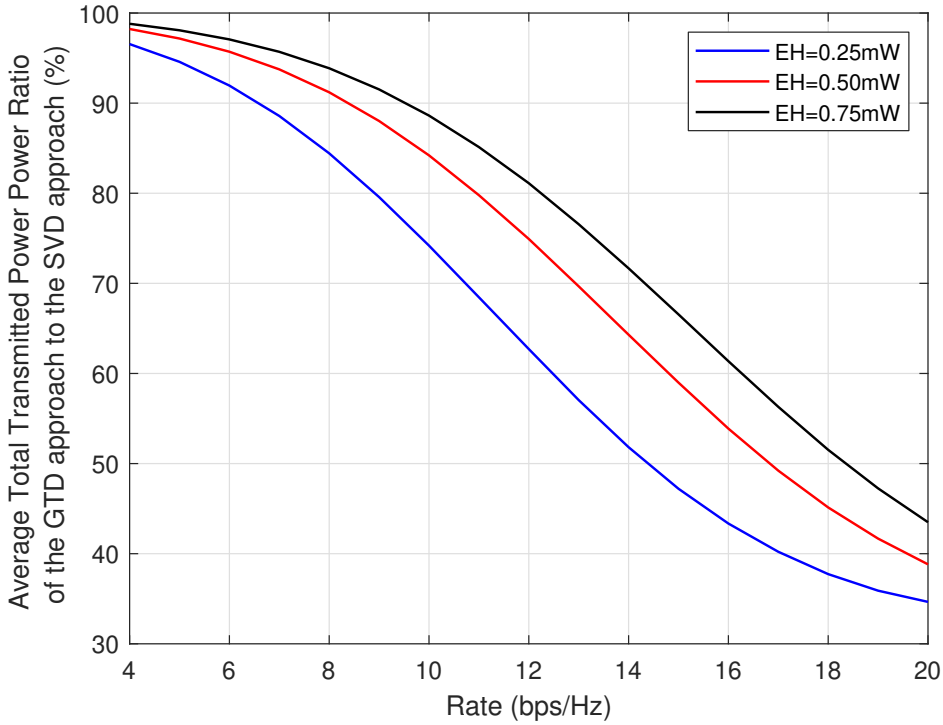

(a) Varying energy harvesting constraint

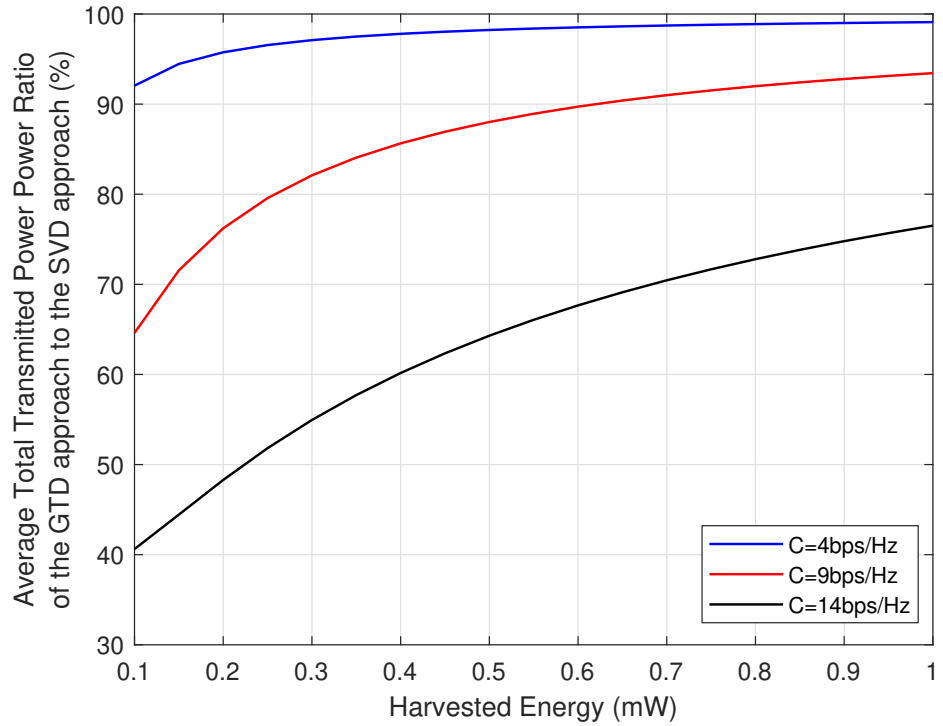

(b) Varying information rate constraint

Figure 3.7: Average total transmitted power with optimum power allocation and no instantaneous power constraint, $P_t = +\infty$ with $d = 15$ m.

for a wide range of system parameter values by using the proposed GTD based approach instead of the conventional SVD based approach specially when the data rate constraint is large and the noise power is high $\sigma^2 = -60$ dBm. It is also noticeable that both the SVD and GTD based approaches have an equivalent performance when the noise power is low; *i.e.*, $\sigma^2 = -100$ dBm regardless the amount of data rate and energy harvesting constraint. However, both approaches yield a comparable performance when data rate constraint has moderate or low values and the noise power is high.

B. Data Rate Maximization

In the following, the simulation results are introduced to evaluate the GTD and the SVD approaches for data rate maximization. The results of the GTD approach are obtained by solving problem (3.18) using Algorithm 3 while the results of the SVD approach are obtained by solving (3.24) using Algorithm 4.

Figure 3.8 shows the maximum achievable rate under different values of the total transmit power P_t under different energy harvesting requirements. It is observed that the GTD based SWIPT always achieves higher data rate than its counterpart SVD based SWIPT. For example, when $Pt = 5$ and the energy harvesting constraint $EH = 0.1$mW, the GTD approach attains approximately $C = 22$ bps/Hz while the SVD approach achieves data rate 17 bps/Hz. This is because the GTD based SWIPT has the ability to use the highest gain subchannel jointly for data and energy transmission which is not possible in the SVD based SWIPT.

The plots in Figure 3.9 shows the maximum achievable rate versus the energy harvesting constraint EH for multiple values of total transmit power P_t. The curves of both systems degrade rapidly as the values of EH increases when P_t is low. However, when Pt is high both systems improve and the loss in the achievable rate is relatively low as the EH value increases.

C. Energy Harvesting Maximization

The simulation results are presented in this section to evaluate the performance of the proposed transceiver designs for energy harvesting maximization. The results of the GTD based SWIPT are obtained from solving problem (3.29) optimally using Algorithm 5 while the SVD based SWIPT results are obtained by solving problem (3.32) using Algorithm 6.

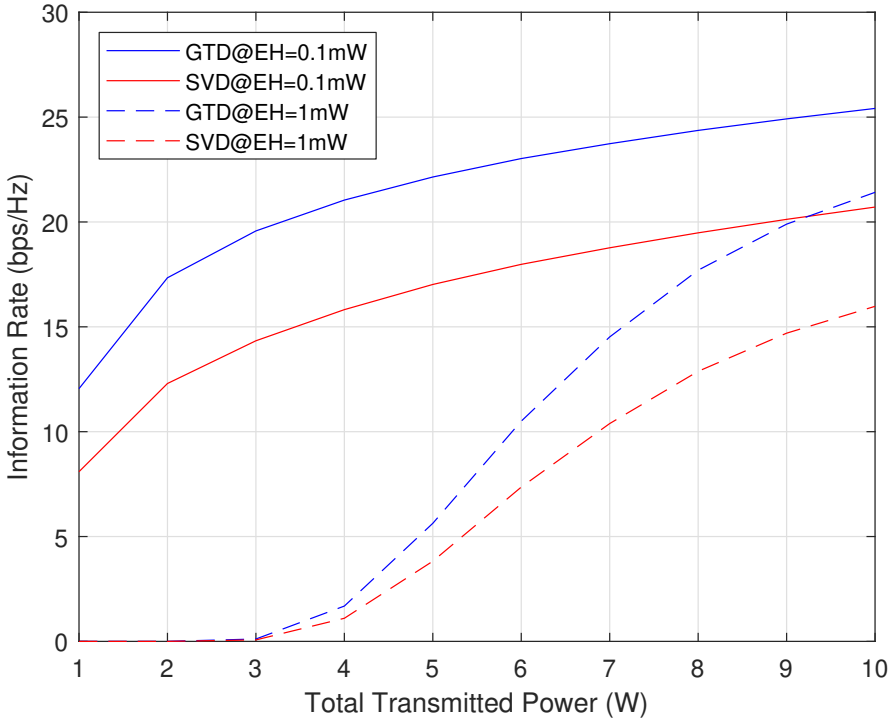

Figure 3.8: Maximum achievable rate vs. total transmitted power Pt for different energy harvesting requirements with d=15 m.

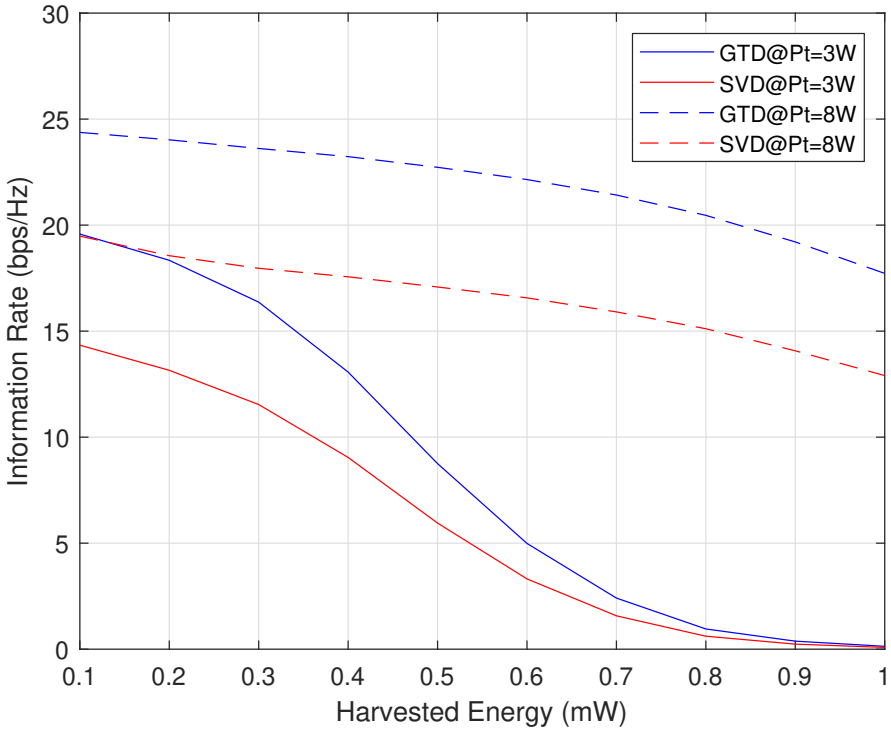

Figure 3.9: Maximum achievable rate vs. harvested energy EH for different available total transmit power with d = 15 m.

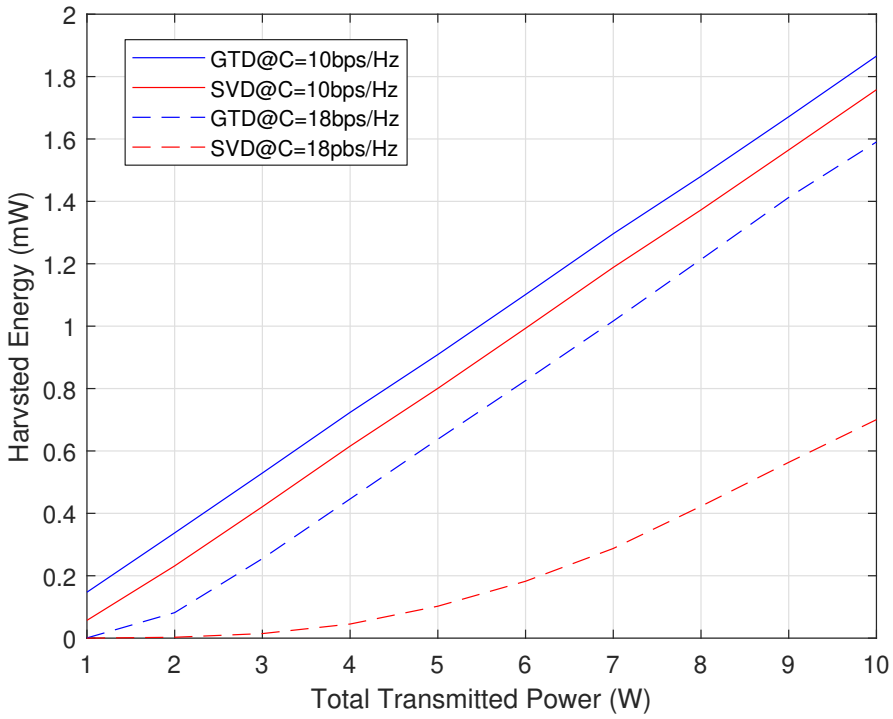

Figure 3.10: Maximum harvested energy vs. total transmitted power P_t for different energy harvesting requirements with d=15 m.

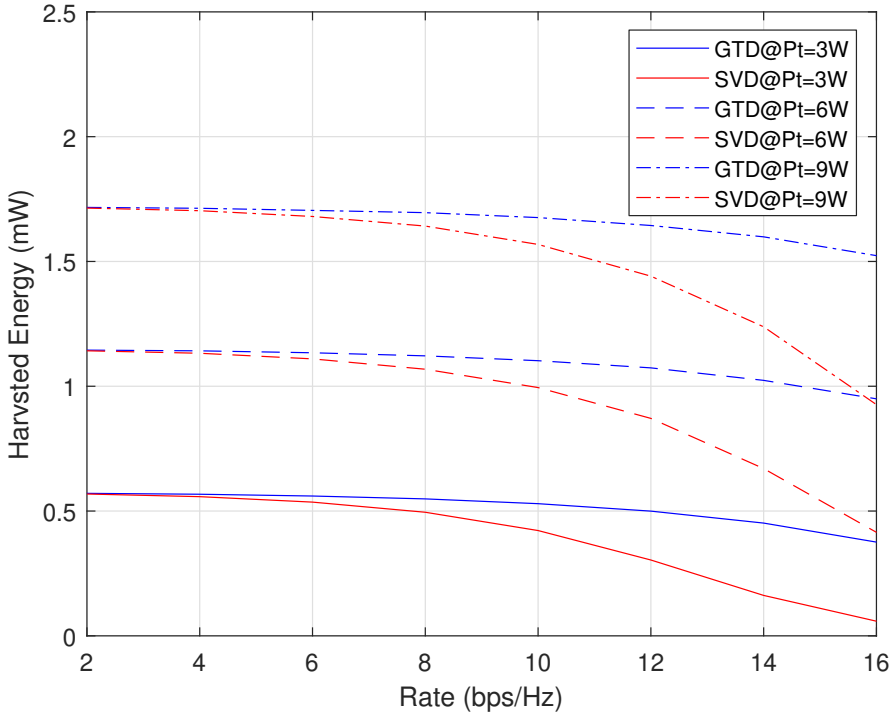

Figure 3.11: Maximum harvested energy vs. data rate C for different available total transmit power with d = 15 m.

Figure 3.10 shows the maximum harvested energy EH versus the total transmitted power P_t under different data rate C constraints. It can be noted from Figure 3.10 that the maximum harvested energy is significantly reduced when the rate constraint C is largely increased . In contrast, the GTD based SWIPT shows a relatively low reduction in the harvested energy if the rate constraint C is increases. For example, at $P_t = 6$ W, the energy harvested by the SVD approach is reduced by approximately 0.81 mW when C increases from 10 bps/Hz to 18 bps/Hz while the GTD losses only 0.27 mW under the same conditions.

In Figure 3.11, it can be observed that the GTD approach and the SVD approach have equivalent performance when the rate requirement is low. When the rate requirement increases, the SVD based SWIPT curves starts to diminish rapidly in comparison with the GTD based SWIPT.

3.7 Summary

In this chapter, a new SWIPT approach, based on the GTD, in a point-to-point MIMO communication system was proposed. The optimal structure of the GTD that attains the optimal performance in GTD based SWIPT was derived and introduced in Theorem 3.1. The GTD structure is exploited to create an interfering subchannel to satisfy the energy harvesting requirement while maintaining the best subchannels for information exchange. Based on the developments in Theorem 3.1, three transceiver designs for transmit power minimization, data rate maximization and energy harvesting maximization were introduced. For each design, an optimal solution that obtains jointly the power allocation and the subchannel assignment was developed. The proposed GTD designs were compared against the state-of-art SVD designs. Both theoretical and numerical results showed that GTD based SWIPT well outperforms the SVD based SWIPT. Although extra process are required in designing the precoder and the receive-side matrix in the proposed GTD approaches, the power allocation in all of these approaches is obtained by examining only one fixed subchannel assignment at the transmitter. This is in contrast to the state-of-the art SVD approaches which require to examine all the possible subchannel assignments.

Chapter 4

Transceiver Design for SS Based MIMO SWIPT With per Subchannel Transmit Power Constraint

4.1 Introduction

This chapter studies SS based MIMO SWIPT transceiver systems where the transmitter is constrained by limited transmit power per subchannel. This limited power constraint leads to a complex SVD based transceiver designs whereby the optimal power allocation and subchannel assignment require solution to a mixed-integer optimization problem [14, 16]. This complexity is also evident in GTD based SWIPT transceiver designs. In GTD based SWIPT, further complexity is introduced due to signal separation process at the receive side requiring optimal design for precoder $\mathbf{F}$ and receiver side matrix $\mathbf{W}$. However, the GTD structure allows the highest gain subchannels to be used for joint information and energy transmission, which result in better performance than conventional SVD designs. Such flexibility is not possible in SVD based SWIPT transceiver designs since each subchannel should carry one type of signals either energy or information signals [14–16, 76].

This chapter presents three transceiver designs for each GTD and SVD based SWIPT. The first design that focuses on minimizing the total transmit power while meeting specific

energy harvesting and information rate is presented in Section 4.2. In this section, both optimal and suboptimal GTD based SWIPT designs are developed. For comparison purpose, the SVD based SWIPT design that introduced [14, 16] is briefly introduced in this section. The second design is presented in Section 4.3 and studies the case of maximizing the energy harvesting while satisfying a particular data rate constraint at the receiver. In this section, a suboptimal design is developed for the GTD transceiver while an optimal design is considered for the SVD transceiver. The last design that considers the case of maximizing the total throughput of the MIMO link with energy harvesting constraint is developed in Section 4.4. Both suboptimal GTD and optimal SVD approaches were proposed in this section. Simulation results are introduced in the Section 4.5 to evaluate the performance of the developed designs. Finally, Section 4.6 summarizes Chapter 4.

4.2 Transmit Power Minimization With Energy Harvesting and Data Rate Constraints

This section presents two SS based SWIPT transceivers. The first transceiver is developed based on GTD while the second transceiver uses the SVD as introduced in [14, 16]. Both transceivers are designed to minimize the total transmitted power and achieve data rate and energy harvesting constraints assuming limited transmit power per each subchannel. For the GTD based SWIPT transceiver, optimal and suboptimal solutions are developed. The optimal solution is presented in Subsection 4.2.1 where the power allocation and the transmit-side subchannel assignment are obtained via solving mixed-integer second order cone problem (MISCOP). Additionally, Theorem 4.1 is proposed in Subsection 4.2.1 to find the receive-side subchannel assignment. In Subsection 4.2.2, the suboptimal solution is presented where the power allocation is obtained by examining a few number of subchannel assignments at the transmitter while the receive-side subchannel assignment is identified from Theorem 4.1. Subsection 4.2.3 introduces the SVD based SWIPT transceiver that developed in [14, 16].

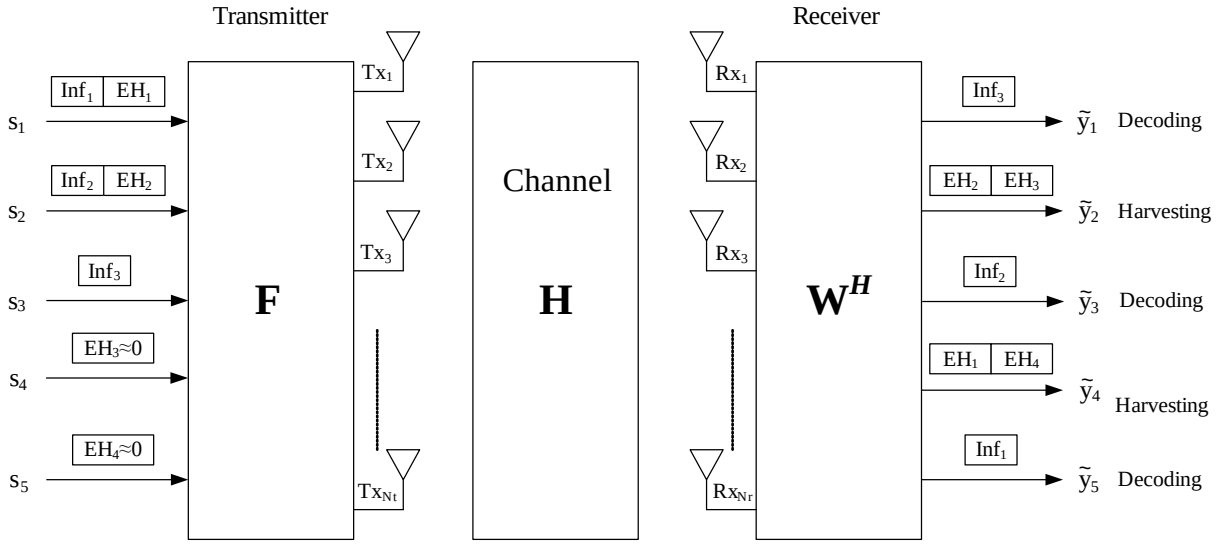

Figure 4.1: GTD based SWIPT with $P_{\max}$ per subchannel Constraint.

4.2.1 Transmit Power Minimization for GTD Based SWIPT (Optimal Design)

We focus in this section on minimizing the total transmitted power at the transmitter while guaranteeing that the receiver gets specific amounts of data rate and energy. The following optimization problem describes the objective of the system design:

$$\underset{\mathbf{P},\, \mathbf{r}\preceq\boldsymbol{\lambda},\, \mathcal{I}_{\mathrm{RX}},\, \mathcal{J}_{\mathrm{RX}}}{\text{minimize}} \quad \mathrm{tr}(\mathbf{F}\mathbf{F}^{H}), \tag{4.1a}$$

$$\text{s.t.} \quad \sum_{i\in\mathcal{I}_{\mathrm{RX}}} \log_2\left(1+\frac{R_{ii}^2}{\sigma^2}\right) \geqslant C, \tag{4.1b}$$

$$\sum_{j\in\mathcal{J}_{\mathrm{RX}}} \sum_{l=j}^{K} \eta R_{jl}^2 \geqslant EH, \tag{4.1c}$$

$$0 \leqslant p_k \leqslant P_{\max}, \tag{4.1d}$$

where $\mathcal{I}_{\mathrm{RX}} \subset \mathcal{K}$ and $\mathcal{J}_{\mathrm{RX}} \subset \mathcal{K}$ are disjoint sets represent the subchannels from which the information is decoded and the energy is harvested at the receiver, respectively. The set $\mathcal{K}$ denotes to the total number of subchannels. The precoder matrix $\mathbf{F}$ is defined in equation (2.18), λ represents the positive diagonal elements of $\mathbf{\Sigma}\mathbf{P}^{1/2}$ and σ denote to the noise power while $P_{\max}$ is the maximum transmit power per subchannel at the transmitter.

As discussed in Chapter 3, problem (4.1) cannot be solved directly since the power

allocation $\mathbf{P}$ is embedded in the matrix $\mathbf{R}$. Furthermore, the optimal power allocation $\mathbf{P}^\star$ and the subchannel assignment $\mathcal{I}_{\mathrm{RX}}^\star$ and $\mathcal{J}_{\mathrm{Rx}}^\star$ should be obtained jointly in order to construct the precoder $\mathbf{F}$ and the receive-side filter $\mathbf{W}$.

To solve (4.1), a similar solution that proposed for GTD based SWIPT designs in the previous chapter is used here. This solution consists of two steps as discussed earlier. The first step is to find the optimal power allocation $\mathbf{P}^\star$. In the second step we apply GTD on $\mathbf{\Sigma}(\mathbf{P}^\star)^{1/2}$ to construct the precoding and the receiver-side matrices $\mathbf{F}$ and $\mathbf{W}$, respectively. The proposed approach takes advantage of the key feature of the GTD based system, namely, that the transmitter can allocate power both to any subchannel for joint information and energy transmissions while these transmissions can be separated at the receiver via linear filtering as illustrated in Figure 4.1.

A. Optimal Power Allocation

Similar to GTD based designs developed in the previous chapter, the power allocation is carried out according to the positive singular values $\boldsymbol{\sigma}$ of the channel matrix $\mathbf{H}$. Taking into account that the GTD structure allows the transmitter to use any single subchannel to carry both information and energy as discussed previously, the problem of transmit-side power allocation can be written as follows:

$$\underset{\alpha_i,\,\beta_j,\,a_i,\,b_j}{\text{minimize}} \quad \sum_{i\in\mathcal{K}}\alpha_i + \sum_{j\in\mathcal{K}}\beta_j, \tag{4.2a}$$

$$\text{s.t.} \quad \prod_{i\in\mathcal{K}}\left(1+\frac{a_i\alpha_i\sigma_i^2}{\sigma^2}\right) \geqslant 2^C, \tag{4.2b}$$

$$\sum_{j\in\mathcal{K}}\eta b_j\beta_j\sigma_j^2 \geqslant EH,, \tag{4.2c}$$

$$0 \leqslant \alpha_i + \beta_j \leqslant P_{\max},\ \forall\ i=j,\ i\in\mathcal{K},\ j\in\mathcal{K}, \tag{4.2d}$$

$$\sum_{i\in\mathcal{K}}a_i + \sum_{j\in\mathcal{K}}b_j \leqslant K,\ i\in\mathcal{K},\ j\in\mathcal{K}, \tag{4.2e}$$

$$0 \leqslant \alpha_i \leqslant P_{\max},\ 0 \leqslant \beta_j \leqslant P_{\max}, \forall\ i\neq j,\ i\in\mathcal{K},\ j\in\mathcal{K} \tag{4.2f}$$

$$a_i\in\{0,1\},\ b_j\in\{0,1\}, \tag{4.2g}$$

where α_i and β_j are the powers allocated by the transmitter to information and energy transfer on the i-th and j-th stream, respectively. Note that the diagonal entries of $\mathbf{P}$ are

given as $p_k = \alpha_k + \beta_k, k \in \mathcal{K}$. The variables a_i and b_j are binary and denote the usage of each subchannel at the transmitter as illustrated in the Table 4.1. In fact, a_i and b_j are used to define the subchannel assignment at the transmitter as will be explained later in next subsection. Constraint (4.2b) represents the required data rate and it is transformed into the product form instead of the sum-log form to facilitate the solution as discussed below.

Problem (4.2) is nonlinear because of the presence of product form of the data rate constraint in (4.2b) and has a combinatorial nature due to the use of binary variables in constraints (4.2b) and (4.2c). In fact, the power minimization problem of the SVD based SWIPT that is studied in [14, 16] has similar formulation to problem (4.2). Hence, a similar technique that is used to solve the power allocation problem of the SVD based SWIPT can be applied to solve problem (4.2). This technique transforms the power allocation problem of the SVD based SWIPT into mixed-integer second order optimization problem (MISCOP) by following two steps. In the first step, the product between the binary and the continuous variables are linearized. In the second step, the product form in the data rate constraint is transformed into multiple-layers of second-order-rotated-conic (SORC) constraints.

To follow up the technique mentioned above, propositions 1 and 2 in [14] are revisited. The first proposition is used to linearize the products of the variables $a_i\alpha_i$ and $b_j\beta_j$ whereas the second proposition transforms the constraint (4.2b) into $m+1$ layers of SORC constraints.

Table 4.1: Binary variables cases

Binary variables		Index status	Subchannel use
a_i	b_j		
1	1	$i = j$	Information exchange and energy transfer
1	0	$i = j$ or $i \neq j$	Information exchange only
0	1	$i = j$ or $i \neq j$	Energy transfer only
0	0	$i = j$	The subchannel is not used

Proposition 4.1 ([14]). *Consider a binary variable $\omega \in \{0,1\}$ and a continuous variable $x \in [x_{\min}, x_{\max}]$. Constraint $y = \omega x$ can be linearized as follows*

$$\omega x_{\min} \leqslant y \leqslant x - (1-\omega)x_{\min}, \tag{4.3}$$

$$x - (1-\omega)x_{\max} \leqslant y \leqslant \omega x_{\max}. \tag{4.4}$$

To linearize the products of the variables $a_i\alpha_i$ that are appeared in (4.2b), Proposition 4.1 is used as explained below. Let us define $\tilde{\alpha}_i = a_i\alpha_i,\ i \in \mathcal{K}$. According to Proposition 4.1, the equality $\tilde{\alpha}_i,\ i \in \mathcal{K}$ can be represented by the linear constraints (4.3) and (4.4) by setting $y \equiv \tilde{\alpha}_i$, $\omega \equiv a_i$ and $x \equiv \alpha_i \in [0, P_{\max}]$. Likewise, the products of the variables $b_j\beta_j$ in constraint (4.2c) can be represented by the linear constraints (4.3) and (4.4). Therefore, problem (4.2) can be written as

$$\underset{\alpha_i,\, \tilde{\alpha}_i,\, \beta_j,\, \tilde{\beta}_j,\, a_i,\, b_j}{\text{minimize}} \quad \sum_{i\in\mathcal{K}} \alpha_i + \sum_{j\in\mathcal{K}} \beta_j, \tag{4.5a}$$

$$\text{s.t.} \quad \prod_{i\in\mathcal{K}} \left(1 + \frac{\tilde{\alpha}_i \sigma_i^2}{\sigma^2}\right) \geqslant 2^C, \tag{4.5b}$$

$$\sum_{j\in\mathcal{K}} \eta\tilde{\beta}_j\sigma_j^2 = EH, \tag{4.5c}$$

$$\tilde{\alpha}_i \leqslant a_i P_{\max},\ \tilde{\alpha}_i \leqslant \alpha_i, \tag{4.5d}$$

$$\tilde{\alpha}_i \geqslant \alpha_i - (1-a_i)P_{\max},\ \tilde{\alpha}_i \geqslant 0, \tag{4.5e}$$

$$\tilde{\beta}_j \leqslant b_j P_{\max},\ \tilde{\beta}_j \leqslant \beta_j, \tag{4.5f}$$

$$\tilde{\beta}_j \geqslant \beta_j - (1-b_j)P_{\max},\ \tilde{\beta}_j \geqslant 0, \tag{4.5g}$$

$$\text{Constraints (4.2d), (4.2e), (4.2f) and (4.2g).} \tag{4.5h}$$

Note that constraints (4.5d)-(4.5g) are presented due to the use of Proposition 4.1. Next, Proposition 4.2 is introduced to transform the product form of the data rate constraint into multiple-layers SORC constraints.

Proposition 4.2 ([85], *p.105*, [14],[16]). *The geometric mean constraint (GMC) $x_1 \ldots x_{2^m} \geqslant t^{2^m},\ x_q \geqslant 0,\ q = 1,\ldots,2^m$ is convex and can be represented by (m+1)-layers of SORC constraints. These layers of the SORC constraints are constructed by defining the 2^m original*

x-variables to be the variables of level 0 ; i.e., $x_q \equiv x_{0,q}$. *For each two variables of level 0 a new variable of level 1 is added; thus, the number of the new level 1 variables* $x_{1,q}$ *is* 2^{m-1}. *Similarly, a new variable of level 2 is added for each two variables of level 1; hence, adding* 2^{m-2} *variables of level 2. This process of adding a new level of variables continues until level m becomes with a single variable* $x_{m,1}$. *Therefore the (m+1) layers of the SORC constraints can be written as:*

$$\begin{aligned}
&\text{layer } 1: && x_{0,2q-1}x_{0,2q} \geqslant x_{1,q}^2,\\
&\text{layer } 2: && x_{1,2q-1}x_{1,2q} \geqslant x_{2,q}^2,\ x_{2,q},\ x_{1,2q-1},\\
& && \vdots\\
&\text{layer } m: && x_{m-1,1}x_{m-1,2} \geqslant x_{m,1}^2,\ x_{m,1},\ x_{m-1,1},\\
&\text{layer } m+1: && x_{m,1} \geqslant t,
\end{aligned} \tag{4.6}$$

where x_{mi} *and* t *are real and positive numbers.*

To explain Proposition 4.2, let us assume the following geometric mean constraint $x_1x_2x_3x_4x_5x_6x_7x_8 \geqslant t^8$. This constraint can be represented by 4 layers of SORC constraints as follows:

$$\begin{aligned}
&\text{layer } 1: && x_{0,1}x_{0,2} \geqslant x_{1,1}^2,\ x_{0,3}x_{0,4} \geqslant x_{1,2}^2,\ x_{0,5}x_{0,6} \geqslant x_{1,3}^2,\ x_{0,7}x_{0,8} \geqslant x_{1,4}^2,\\
&\text{layer } 2: && x_{1,1}x_{1,2} \geqslant x_{2,1}^2,\ x_{1,3}x_{1,4} \geqslant x_{2,2}^2,\\
&\text{layer } 3: && x_{2,1}x_{2,2}^2 \geqslant x_{3,1}^2,\\
&\text{layer } 4: && x_{3,1}^2 \geqslant t.
\end{aligned} \tag{4.7}$$

To transform (4.2b) to GMC form, a similar method that is used in [14, 16] is followed here. This method starts by defining $m = \lceil \log_2 K \rceil$, $\mu = 2^m$ and setting $x_{0,q} = \log_2(1 + \tilde{\alpha}_i\sigma_i^2/\sigma^2) \geqslant 0$, $q \in \mathcal{K}$, $x_{0,i} = 1$, $q = K+1, \ldots, \mu$ and $t = 2^{C/\mu}$. This method brings (4.2b) into GMC, and hence, Proposition 4.2 is used to construct the SORC layers as given in (4.6). To clarify this process, suppose that $K = 6$. In this case $m = 3$ and $\mu = 8$; therefore, $q = \{1, 2, \ldots, 8\}$. The SORC layers can be written as in (4.7) where

$x_{0,q} = \log_2(1 + \tilde{\alpha}_i\sigma_i^2/\sigma^2),\ i \in \mathcal{K},$ and $q \in \{1,2,\ldots,6\}$ while $x_{0,q} = 1,\ q \in \{7,8\}$.

After applying Proposition 4.2 to transform constraint (4.5b) into multiple SORC constraints as illustrated above, problem (4.5) can be rewritten as:

$$\underset{\alpha_i,\,\tilde{\alpha}_i,\,\beta_j,\,\tilde{\beta}_j,\,a_i,\,b_j}{\text{minimize}} \quad \sum_{i\in\mathcal{K}}\alpha_i + \sum_{j\in\mathcal{K}}\beta_j, \tag{4.8a}$$

$$\text{s.t.} \quad x_{n-1,2q-1}x_{n-1,2q} \geqslant x_{n,q}^2,\ n = 1,\ldots,m,\ q = 1,\ldots,2^{m-n}, \tag{4.8b}$$

$$x_{m,1} \geqslant t,\ t = 2^{C/\mu}, \tag{4.8c}$$

$$x_{0,q} = 1 + \frac{\tilde{\alpha}_i\sigma_i^2}{\sigma^2},\ i \in \mathcal{K},\ q \in \mathcal{K}, \tag{4.8d}$$

$$x_{0,q} = 1,\ q = K+1,\ldots,\mu, \tag{4.8e}$$

$$x_{n,q} \geqslant 0,\ n = 0,\ldots,m, q = 1,\ldots,2^{m-n}, \tag{4.8f}$$

$$\sum_{j\in\mathcal{K}}\eta\tilde{\beta}_j\sigma_j^2 \geqslant EH, \tag{4.8g}$$

$$\tilde{\alpha}_i \leqslant a_iP_{\max},\ \tilde{\alpha}_i \leqslant \alpha_i, \tag{4.8h}$$

$$\tilde{\alpha}_i \geqslant \alpha_i - (1-a_i)P_{\max},\ \tilde{\alpha}_i \geqslant 0, \tag{4.8i}$$

$$\tilde{\beta}_j \leqslant b_jP_{\max},\ \tilde{\beta}_j \leqslant \beta_j, \tag{4.8j}$$

$$\tilde{\beta}_j \geqslant \beta_j - (1-b_j)P_{\max}, \quad \tilde{\beta}_j \geqslant 0, \tag{4.8k}$$

$$0 \leqslant \alpha_i + \beta_j \leqslant P_{\max},\ \forall\ i = j,\ i \in \mathcal{K},\ j \in \mathcal{K}, \tag{4.8l}$$

$$0 \leqslant \alpha_i \leqslant P_{\max},\ 0 \leqslant \beta_j \leqslant P_{\max}, \forall\ i \neq j,\ i \in \mathcal{K},\ j \in \mathcal{K}, \tag{4.8m}$$

$$\sum_{i\in\mathcal{K}}a_i + \sum_{j\in\mathcal{K}}b_j \leqslant K,\ i \in \mathcal{K},\ j \in \mathcal{K}, \tag{4.8n}$$

$$a_i \in \{0,1\},\ b_j \in \{0,1\}. \tag{4.8o}$$

According to [14, 16] the formulation of (4.8) is MISOCP and can be solved via CVX package [86]. Unlike the SVD based SWIPT power allocation problem which has been introduced in [14, 16], problem (4.8) contains two binary variables to allow the transmitter to send information and energy signals jointly using any single subchannel. Another major difference between problem (4.8) and the SVD based SWIPT power allocation probelm is the presence of constraint (4.8l). This is imposed to prevent the transmitter from applying more power than $P_{\max}$ to any particular subchannel used for joint transmission. Constraint (4.8l) is not existed in the power allocation problem of SVD based SWIPT

since the SVD structure prevents the use of the joint transmissions.

B. Transmit-Side Optimal Subchannel Assignment

After obtaining the optimal power allocation, the subchannel assignment at the transmitter should be identified. This can be done by examining the binary variables a_i and b_j that are obtained in the optimal solution of problem (4.8). Towards this direction, let us defined the set of the subchannels assigned for information exchange as $\mathcal{I}_{\mathrm{TX}}$ and let $\mathcal{J}_{\mathrm{TX}}$ denote to the set of the subchannels assigned for energy harvesting. The sets $\mathcal{I}_{\mathrm{TX}}$ and $\mathcal{J}_{\mathrm{TX}}$ are found as

$$\mathcal{I}_{\mathrm{TX}}^{\star} := \big\{i : i \in K \wedge a_i = 1\big\}, \tag{4.9a}$$

$$\mathcal{J}_{\mathrm{TX}}^{\star} := \big\{j : j \in \mathcal{K} \wedge b_j = 1\big\}. \tag{4.9b}$$

Therefore, the set $\mathcal{U} = \mathcal{I}_{\mathrm{TX}}^{\star} \bigcup \mathcal{J}_{\mathrm{TX}}^{\star}$ contains all the subchannels that are used in the optimal solution of problem (4.8), where $\mathcal{U} \subseteq \mathcal{K}$. In addition to allocating power to transmit one type of signals either information or energy, the presence of constraint (4.8l) in problem (4.8) allows the transmitter of allocating power to any subchannel for joint information and energy transmission. For future convenience, we refer to the subchannels that are used to carry information and energy signals jointly as the "joint subchannels" while the subchannels that are used to carry one type of signals as the "clear subchannels". Let $\mathcal{Z}$ and $\mathcal{N}$ denote to the sets of the joint subchannels and the clear subchannel, respectively. Thus, $\mathcal{Z}$ can be easily identified as $\mathcal{Z} = \mathcal{I}_{\mathrm{TX}}^{\star} \bigcap \mathcal{J}_{\mathrm{TX}}^{\star}$ while $\mathcal{N} = \mathcal{U} \setminus \mathcal{Z}$.

While in the SVD based SWIPT the condition $\mathcal{Z} = \emptyset$ is mandatory[14, 16], it does not need to hold in the GTD based SWIPT. A necessary condition for all SS based SWIPT schemes is, however, that each single stream at the receive-side carries only one type of signal, either information to be decoded or energy to be harvested [14, 16]. Therefore, the transmitted signals carried by each joint subchannel in the set $\mathcal{Z}$ is separated at the receiver into two parts using the linear filter $\mathbf{W}$. Note that the constraint (4.8n) is imposed to force the transmitter to comply with the SS based SWIPT requirement as explained in the following remarks.

Remark 4.1. When the optimal solution of problem (4.8) returns a set of joint subchannels $\mathcal{Z} \neq \emptyset$, the constraint (4.8n) implies that a set of different subchannels $\hat{\mathcal{Z}}$ is left out of the optimization problem (4.8) and are not part of power allocation. The set $\hat{\mathcal{Z}}$ can be defined as $\hat{\mathcal{Z}} = \{|\mathcal{U}| + 1, \ldots, |\mathcal{U}| + |\mathcal{Z}|\}$ where $\left|\hat{\mathcal{Z}}\right| = |\mathcal{Z}|$. The subchannels in $\hat{\mathcal{Z}}$ are corresponded to the lowest gain subchannels and the transmitter applies only low power $p_{\hat{z}} > 0$ to them in order to keep these streams active since their presence is important for the receiver to be able to perform the signal separation.

Remark 4.2. When the optimal solution returns a set of joint subchannels $\mathcal{Z} = \emptyset$, the constraint (4.8n) implies that all the K available subchannels are part of the power allocation (4.8) and the GTD based SWIPT is reduced to the SVD based SWIPT. Note that in this case $\hat{\mathcal{Z}} = \emptyset$ and $\mathcal{U} = \mathcal{K}$.

C. Precoder and Filter Design via GTD

The design process consists of two distinct cases when: 1) $\mathcal{Z} \neq \emptyset$ 2) $\mathcal{Z} = \emptyset$. We concentrate here in the first case since it is when GTD and SVD based systems are different, while the second case corresponds to a scenario where both methods are the same, as discussed in Remark 4.2. Thus, we consider only the first case here, and return to the second case at the end.

The signals that are carried in the joint subchannels should be separated at the receiver to comply with the SS schemes requirements as discussed previously. However, the separation process requires both the transmitter and the receiver to use a properly designed precoder $\mathbf{F}$ and filter $\mathbf{W}$, respectively. The precoder and the filter design can be accomplished via the GTD decomposition of the diagonal matrix $\mathbf{\Sigma}(\mathbf{P}^{\star})^{1/2}$ where $\mathbf{P}^{\star}$ is the optimal power allocation matrix that is obtained from solving problem (4.8) and also contains the low powers $p_{\hat{z}}$ on its diagonal as discussed in Remark 4.1. The GTD decomposition of $\mathbf{\Sigma}(\mathbf{P}^{\star})^{1/2}$ requires to define the vector $\mathbf{r}$ properly in order to design the precoder and the filter suitably. Note that the vector $\mathbf{r}$ should be multiplicatively majorized by the vector $\boldsymbol{\lambda}$, where $\boldsymbol{\lambda}$ represents the diagonal elements of the matrix $\mathbf{\Sigma}(\mathbf{P}^{\star})^{1/2}$.

The vector $\boldsymbol{\lambda}$ can be written based on the sets $\mathcal{U}$ and $\hat{\mathcal{Z}}$ as follows

$$\boldsymbol{\lambda} = \begin{bmatrix} \lambda_1 \\ \lambda_2 \\ \vdots \\ \lambda_{|\mathcal{U}|} \\ \lambda_{|\mathcal{U}|+1} \\ \vdots \\ \lambda_{|\mathcal{U}|+|\mathcal{Z}|} \end{bmatrix}. \tag{4.10}$$

The first elements of $\boldsymbol{\lambda}$, starting from the first element and up to the $|\mathcal{U}|$-th element, can be expressed according to the usage of each subchannel as

$$\lambda_u = \begin{cases} \lambda_z, & z \in \mathcal{Z} \text{ and } \mathcal{Z} \subseteq \mathcal{U}, \\ \lambda_n, & n \in \mathcal{N} \text{ and } \mathcal{N} \subset \mathcal{U}, \end{cases} \tag{4.11}$$

where $u = 1, \ldots, |\mathcal{U}|$. Note that λ_z represents the joint subchannels and can be written as

$$\lambda_z = \sqrt{\alpha_z^\star + \beta_z^\star}\sigma_z, \quad z \in \mathcal{Z}, \tag{4.12}$$

while λ_n represents the clear subchannels and can be expressed as

$$\lambda_n = \begin{cases} \sqrt{\alpha_n^\star}\sigma_n, & \forall n \in \mathcal{I}_{\text{TX}}, \\ \sqrt{\beta_n^\star}\sigma_n, & \forall n \in \mathcal{J}_{\text{TX}}. \end{cases} \tag{4.13}$$

The last elements of $\boldsymbol{\lambda}$, starting from the element $|\mathcal{U}| + 1$, and up to the $|\mathcal{U}| + |\mathcal{Z}|$-th element, can be written as

$$\lambda_{\hat{z}} = \sqrt{p_{\hat{z}}}\sigma_{\hat{z}}, \quad \hat{z} \in \hat{\mathcal{Z}},\ \hat{\mathcal{Z}} = \left\{ |\mathcal{U}| + 1, \ldots, |\mathcal{U}| + |\mathcal{Z}| \right\}. \tag{4.14}$$

The form of $\mathbf{r}$ that is used to perform the GTD decomposition of $\boldsymbol{\Sigma}(\mathbf{P}^\star)^{1/2}$ to design the precoder and the filter that lead to the desired signals separation at the receiver is

defined as

$$r_d = \lambda_n, \tag{4.15a}$$

$$r_e = \frac{\lambda_{\check{z}}\lambda_{\hat{z}}}{\sqrt{\lambda_{\check{z}}^2 + \lambda_{\hat{z}}^2 - \frac{EH_{\check{z}}}{\eta}}}, \tag{4.15b}$$

$$r_w = \sqrt{\lambda_{\check{z}}^2 + \lambda_{\hat{z}}^2 - \frac{EH_{\check{z}}}{\eta}}, \tag{4.15c}$$

where $EH_{\check{z}} = \eta\left(\beta_{\check{z}}^{\star}\sigma_{\check{z}}^2 + p_{\hat{z}}\sigma_{\hat{z}}^2\right)$ and the following indexing[1] is defined: $d = 1,\ldots,|\mathcal{N}|$, $e = |\mathcal{N}|+1, |\mathcal{N}|+3,\ldots,L-1$, $w = |\mathcal{N}|+2, |\mathcal{N}|+4,\ldots,L$, $L = |\mathcal{U}|+\left|\hat{\mathcal{Z}}\right|$ and $\check{z} = z_{\max},\ldots,z_{min}$. Note that $L \leqslant K$ and represents the number of all the subchannels that have non-zero powers while $z_{\max}$ and z_{min} denote to the maximum and minimum elements in the set $\mathcal{Z}$. To complete the GTD decomposition of the matrix $\mathbf{\Sigma}(\mathbf{P}^{\star})^{1/2}$, the following proposition and corollary are presented.

Proposition 4.3. *The vector* $\mathbf{r}$ *defined in* (4.15) *is multiplicatively majorized by the vector* $\boldsymbol{\lambda}$ *that is given in* (4.10).

Proof: See Appendix C. ■

Corollary 4.1. *Using the vector* $\mathbf{r}$ *that is defined in* (4.15) *yields a GTD decomposition*

[1]The indexing in (4.15) should be interpreted as a sequence of tuples in the order given above. For example, in (4.15b) we have $\left((e,\check{z},\hat{z})\right) = \left((|\mathcal{N}|+1, z_{\max}, |\mathcal{U}|+1),\ldots,(L-1, z_{min}, L)\right)$

of the matrix $\mathbf{\Sigma}(\mathbf{P}^{\star})^{1/2}$ *with the following* $\mathbf{R}$

$$\mathbf{R} = \begin{pmatrix} R_{1,1} & 0 & \cdots & \cdots & \cdots & \cdots & \cdots & \cdots & \cdots & 0_{1,L} \\ & \ddots & \cdots & \cdots & \cdots & \cdots & \cdots & \cdots & \cdots & \vdots \\ & & \ddots & \cdots & \cdots & \cdots & \cdots & \cdots & \cdots & \vdots \\ & & & R_{|\mathcal{N}|,|\mathcal{N}|} & 0 & \cdots & \cdots & \cdots & \cdots & 0 \\ & & & & R_{|\mathcal{N}|+1,|\mathcal{N}|+1} & R_{|\mathcal{N}|+1,|\mathcal{N}|+2} & \cdots & \cdots & \cdots & R_{|\mathcal{N}|+1,L} \\ & & & & & R_{|\mathcal{N}|+2,|\mathcal{N}|+2} & 0 & \cdots & \cdots & 0 \\ & & & \mathit{0} & & & \ddots & \cdots & \cdots & \vdots \\ & & & & & & & \ddots & \cdots & \vdots \\ & & & & & & & & R_{L-1,L-1} & R_{L-1,L} \\ & & & & & & & & & R_{L,L} \end{pmatrix}, \tag{4.16}$$

where the diagonal elements of $\mathbf{R}$ *coincides with elements of the vector* $\mathbf{r}$ *that is given in* (4.15).

Proof: Corollary 4.1 is a result of Theorem 2.1 and can be proved by following the GTD algorithm introduced in Section 2.3.2. ■

The form of $\mathbf{R}$ in (4.16) guarantees that the energy streams at rows $e \in \mathcal{E}$ have non-zero off-diagonal elements (inter-stream interference) while the ones dedicated to information transfer at rows $w \in \mathcal{W}$ have only diagonal entries (no inter-stream interference). The "flexible" subchannels corresponding to rows $d \in \mathcal{D}$ are always interference free at the receiver regardless of the type of signal they carry.

D. Harvested Energy and Achievable Rate

After decomposing the matrix $\mathbf{\Sigma}(\mathbf{P}^{\star})^{1/2}$ using GTD, the transmitter uses the precoder $\mathbf{F} = \mathbf{V}(\mathbf{P}^{\star})^{1/2}\mathbf{X}$ as in (2.18) while the receiver applies the filter $\mathbf{W} = \mathbf{Q}^{T}\mathbf{U}^{H}$. This leads to the end-to-end signal model as in (2.20) with the matrix $\mathbf{R}$ as described in (4.16).

The following theorem is presented to identify the optimal subchannel assignment at the receiver and to compute the energy harvested and the achievable rate of the proposed design.

Theorem 4.1. *Consider the end-to-end signal of the GTD based SWIPT stated in* (2.20). *Given the matrix* $\mathbf{R}$ *as described in* (4.16), *the rate of data decoded from the set* $\mathcal{I}_{\mathrm{RX}}^{\star} = \mathcal{W} \bigcup \bar{\mathcal{D}}$ *satisfies the data rate constraint* (4.1b) *while the energy harvested from the subchannels in the set* $\mathcal{J}_{\mathrm{RX}}^{\star} = \mathcal{E} \bigcup \tilde{\mathcal{D}}$ *satisfies the energy harvesting constraint* (4.1c). *The achievable rate is obtained from the subchannels in the set* $\mathcal{I}_{\mathrm{RX}}^{\star}$ *is calculated as follows*

$$C_{\mathrm{RX}} = \sum_{w \in \mathcal{W}} C_w + \sum_{\bar{d} \in \bar{\mathcal{D}}} C_{\bar{d}},\ \bar{\mathcal{D}} \subseteq \mathcal{D}, \tag{4.17}$$

where

$$C_w = \log_2 \left(1 + \frac{r_w^2}{\sigma^2}\right),\ w \in \mathcal{W}, \tag{4.18}$$

and

$$C_{\bar{d}} = \log_2 \left(1 + \frac{r_{\bar{d}}^2}{\sigma^2}\right),\ \bar{d} \in \bar{\mathcal{D}}. \tag{4.19}$$

The amount of the harvested energy from the subchannels in the set $\mathcal{J}_{\mathrm{RX}}^{\star}$ *is written as*

$$EH_{\mathrm{RX}} = \sum_{e \in \mathcal{E}} EH_e + \sum_{\tilde{d} \in \tilde{\mathcal{D}}} EH_{\tilde{d}},\ \tilde{\mathcal{D}} \subseteq \mathcal{D}, \tag{4.20}$$

where

$$EH_e = \eta \left(r_e^2 + \frac{1}{r_e^2}\left(\lambda_{\tilde{z}}^2 - r_e^2\right)\left(r_e^2 - \lambda_{\tilde{z}}^2\right)\right),\ e \in \mathcal{E}, \tag{4.21}$$

and

$$EH_{\tilde{d}} = r_{\tilde{d}}^2,\ \tilde{d} \in \tilde{\mathcal{D}}. \tag{4.22}$$

Proof: See Appendix D ■

The achievable rate of the data that is decoded from the subchannels in set $\mathcal{W}$ matches the rate of the data that is transmitted by the subchannels in the set $\mathcal{Z}$. Also, the energy harvested from the subchannels in the set $\mathcal{E}$ is equivalent to the energy that is transferred by the subchannels in the set $\mathcal{Z}$. Note that the subchannels in the set $\mathcal{Z}$ are used by the transmitter for joint data and energy transmissions.

Additionally, the rate of the data decoded or the energy harvested at the receiver from the subchannels in the set $\mathcal{D}$ are identical to the data rate or the energy amount that are transferred by the subchannels in the set $\mathcal{N}$. The sets $\bar{\mathcal{D}}$ and $\tilde{\mathcal{D}}$ are disjoint

; *i.e.*, $\bar{\mathcal{D}} \bigcap \tilde{\mathcal{D}} = \emptyset$ whereas $\bar{\mathcal{D}} \bigcup \tilde{\mathcal{D}} = \mathcal{D}$. To explain how to define the elements of $\bar{\mathcal{D}}$ and $\tilde{\mathcal{D}}$, the following four cases are presented. Moreover, these cases also express the relation between the optimal subchannel assignment at the transmitter $\mathcal{I}_{\text{Tx}}^{\star}$ and $\mathcal{J}_{\text{Tx}}^{\star}$ and the optimal subchannel assignment at the receiver $\mathcal{I}_{\text{Rx}}^{\star}$ and $\mathcal{J}_{\text{Rx}}^{\star}$. Note that $\mathcal{I}_{\text{Tx}}^{\star}$ and $\mathcal{J}_{\text{Tx}}^{\star}$ are obtained from solving problem (4.8) while $\mathcal{I}_{\text{Rx}}^{\star}$ and $\mathcal{J}_{\text{Rx}}^{\star}$ are defined according to Theorem 4.1.

- Case 1: The achievable rate obtained by decoding the information from the subchannels in $\mathcal{W}$ and the energy harvested from the subchannels $\mathcal{E}$ do not satisfy the data rate and the energy harvesting constraints (4.1b) and (4.1c), respectively, if $\mathcal{I}_{\text{TX}}^{\star} \neq \mathcal{J}_{\text{TX}}^{\star} \neq \mathcal{Z}$, $\left|\mathcal{I}_{\text{Tx}}^{\star}\right| > |\mathcal{Z}|$ and $\left|\mathcal{J}_{\text{Tx}}^{\star}\right| > |\mathcal{Z}|$. This means subset of the subchannels $\bar{\mathcal{D}} \subset \mathcal{D}$ are used for information decoding and the other subset of the subchannels in $\tilde{\mathcal{D}} \subset \mathcal{D}$ are used for energy harvesting to satisfy the constraints (4.1b) and (4.1c) as illustrated in equations (4.17) and (4.20). This implies that $\mathcal{I}_{\text{Rx}}^{\star} = \mathcal{W} \bigcup \bar{\mathcal{D}}$ and $\mathcal{J}_{\text{Tx}}^{\star} = \mathcal{E} \bigcup \tilde{\mathcal{D}}$, where $\bar{\mathcal{D}} \bigcup \tilde{\mathcal{D}} = \mathcal{D}$. Note that the set $\mathcal{D}$ is equivalent to the set $\mathcal{N}$ as defined in (4.15a).

  To clarify this case, we introduce the following illustrative example. Suppose that the total number of the available subchannels $K = 6$. Consider the optimal solution of problem (4.8) returned the following binary variables vectors $\mathbf{a} = [1,1,1,0,0,0]$ and $\mathbf{b} = [1,1,0,1,0,0]$. Based on equation (4.9), the optimal subchannel assignment at the transmitter is defined as $\mathcal{I}_{\text{Tx}}^{\star} = \{1,2,3\}$ and $\mathcal{J}_{\text{Tx}}^{\star} = \{1,2,4\}$. Note that the elements of sets $\mathcal{I}_{\text{Tx}}^{\star}$ and $\mathcal{J}_{\text{Tx}}^{\star}$ represents the indices of the subchannels. Thus, the set of the subchannels that is used in the power allocation of problem (4.1) is defined as $\mathcal{U} = \mathcal{I}_{\text{Tx}}^{\star} \bigcup \mathcal{J}_{\text{Tx}}^{\star} = \{1,2,3,4\}$. The set of the joint subchannel $\mathcal{Z} = \mathcal{I}_{\text{Tx}}^{\star} \bigcap \mathcal{J}_{\text{Tx}}^{\star} = \{1,2\}$ and the set of the clear subchannel $\mathcal{N} = \mathcal{U} \setminus \mathcal{Z} = \{3,4\}$ while the set $\hat{\mathcal{Z}} = \left\{|\mathcal{U}|+1,\ldots,|\mathcal{U}|+|\mathcal{Z}|\right\} = \{5,6\}$. According to equation (4.15) and Theorem 4.1, the receiver has three types of sets. The first set of the flexible subchannels $\mathcal{D} = \{1,2\}$, the information subchannels set $\mathcal{W} = \{4,6\}$ and the energy subchannels set $\mathcal{E} = \{3,5\}$. Since $\left|\mathcal{I}_{\text{Tx}}^{\star}\right| > |\mathcal{Z}|$ and $\left|\mathcal{I}_{\text{Tx}}^{\star}\right| > |\mathcal{Z}|$, the information decoded from the subchannels in $\mathcal{W}$ does not satisfy the data rate constraint while the energy harvested form the subchannels in $\mathcal{E}$ does not meet the energy requirements at the

receiver. Hence, the subchannels in the set $\mathcal{D}$ are used to fulfill the data rate and the energy harvesting requirements at the receiver as follows. The set $\mathcal{D}$ is divided into two sets $\bar{\mathcal{D}} = \{3\}$ and $\tilde{\mathcal{D}} = \{4\}$. The subchannel in the set $\bar{\mathcal{D}}$ is used for information decoding while the subchannel in the set $\tilde{\mathcal{D}}$ is used for energy harvesting in order to complete the data rate and the energy harvesting requirements at the receiver as illustrated in (4.17) and (4.20).

- Case 2: The energy harvested from the subchannels in $\mathcal{E}$ satisfies the energy harvesting constraint (4.1c) if $\mathcal{J}_{\text{Tx}}^{\star} = \mathcal{Z}$, and hence, the subchannels in $\mathcal{D}$ (equivalent to the set $\mathcal{N}$) are used for information decoding in addition to those subchannels in $\mathcal{W}$. This means $\mathcal{I}_{\text{Rx}}^{\star} = \mathcal{W} \bigcup \bar{\mathcal{D}}$ and $\mathcal{J}_{\text{Tx}}^{\star} = \mathcal{E}$, where $\bar{\mathcal{D}} = \mathcal{D}$ and $\tilde{\mathcal{D}} = \emptyset$.

- Case 3: The achievable rate obtained by decoding the information form the subchannels in $\mathcal{W}$ satisfies the data rate constraint (4.1b) if $\mathcal{I}_{\text{TX}}^{\star} = \mathcal{Z}$, and hence, the subchannels in $\mathcal{D}$ (equivalent to the set $\mathcal{N}$) are used for energy harvesting in addition to those subchannels in $\mathcal{E}$. In this case $\mathcal{I}_{\text{Rx}}^{\star} = \mathcal{W}$ and $\mathcal{J}_{\text{Tx}}^{\star} = \mathcal{E} \bigcup \tilde{\mathcal{D}}$, where $\tilde{\mathcal{D}} = \mathcal{D}$ and $\bar{\mathcal{D}} = \emptyset$.

- Case 4: The energy harvested from the subchannels in $\mathcal{E}$ and the data rate obtained by decoding the information from the subchannels in $\mathcal{W}$ satisfy the energy harvesting and the data rate constraints (4.1c) and (4.1b), respectively, if $\mathcal{I}_{\text{TX}}^{\star} = \mathcal{J}_{\text{TX}}^{\star} = \mathcal{Z}$, and hence, $\mathcal{D} = \emptyset$ (implied that $\mathcal{N} = \emptyset$). In this case $\mathcal{I}_{\text{Rx}}^{\star} = \mathcal{W}$ and $\mathcal{J}_{\text{Tx}}^{\star} = \mathcal{E}$.

E. Special Case

This section studies the case when the optimal solution of problem (4.8) returns no joint subchannels ; *i.e.*, $\mathcal{Z}^{\star} = \emptyset$. This means the GTD based SWIPT is reduced to the SVD based SWIPT since there is no subchannel carrying more than one type of signals.

This special case is remarked when all the available powers per each subchannels are required at the strongest or the weakest subchannels to satisfy the energy harvesting constraint (4.1c) or the date rate constraint (4.1b). For example, if the energy harvesting

constraint and the data rate constraint has the following amounts:

$$EH = \sum_{j=1}^{J} \eta P_{\max} \sigma_j^2, \tag{4.23a}$$

$$C = \sum_{i=J+1}^{K} \log_2 \left(1 + \frac{P_{\max} \sigma_i^2}{\sigma^2}\right), \tag{4.23b}$$

the optimal solution of problem (4.8) returns $\mathcal{Z}^\star = \emptyset$. However, this case occurs rarely and is not observed in the numerical simulations.

In general, the optimal GTD design has an exponential complexity due to the combinatorial nature of the power allocation problem (4.8) [14, 16]. Furthermore, the required signals separation at the receiver leads to more complicated and non systematic design due to the presence of the sets $\mathcal{N}$ and $\mathcal{D}$ at the transmitter and the receiver, respectively, as explained in the above cases. Therefore, the proposed approach is used for benchmarks only.

4.2.2 Transmit Power Minimization for GTD Based SWIPT (Sub-optimal Design)

In this section, a suboptimal approach is proposed for the GTD based SWIPT to tackle the high complexity of the optimal approach that is developed in Section 4.2.1. The high complexity of the optimal approach is arose from the combinatorial nature of the power allocation problem (4.8) which grows exponentially with the number of the subchannels K.

The proposed solution in this section exploits the fact that the strongest subchannels are preferred to satisfy both data rate and energy harvesting constraints. Combining this fact with the concept that the GTD allows the transmitter to use any subchannel jointly for information and energy transmission, the strongest subchannels are used jointly to carry information and energy signals. Hence, the power allocation is carried out over a limited number of subchannel assignments that always guarantees joint transmissions. Therefore, no binary variables are required here since the power allocation is obtained over fixed subchannel assignments.

A. Optimal Power Allocation for Fixed Transmit-Side Subchannel Assignment

Consider the following power allocation problem with fixed subchannel assignment

$$\underset{\alpha_i,\beta_j}{\text{minimize}} \quad \sum_{i\in\mathcal{I}_{\text{TX}}} \alpha_i + \sum_{j\in\mathcal{J}_{\text{TX}}} \beta_j, \tag{4.24a}$$

$$\text{s.t.} \quad \sum_{i\in\mathcal{I}_{\text{Tx}}} \log_2\left(1+\frac{\alpha_i\sigma_i^2}{\sigma^2}\right) \geqslant C, \tag{4.24b}$$

$$\sum_{j\in\mathcal{J}_{\text{Tx}}} \eta\beta_j\sigma_j^2 = EH, \tag{4.24c}$$

$$0 \leqslant \alpha_i \leqslant P_{\max},\ 0 \leqslant \beta_j \leqslant P_{\max}, \tag{4.24d}$$

$$\mathcal{U} = \mathcal{I}_{\text{TX}} \cup \mathcal{J}_{\text{TX}},\ |\mathcal{U}| < K, \tag{4.24e}$$

$$0 \leqslant \alpha_u + \beta_u \leqslant P_{\max},\ u \in \mathcal{U}, \tag{4.24f}$$

where $\mathcal{I}_{\text{TX}}$ and $\mathcal{J}_{\text{TX}}$ are fixed sets. Unlike problem (4.8) that is introduced to obtain the optimal power allocation and the subchannel assignment in the previous section, the formulation of problem (4.24) has no binary variables. Therefore, the subchannel assignment in problem (4.24) ; *i.e.*, the sets $\mathcal{I}_{\text{Tx}}$ and $\mathcal{J}_{\text{Tx}}$ should be defined in advance. In fact, a provisional number of subchannel assignments should be examined and choose the one that provides the least total transmit power. A systematic procedure for finding the provisional subchannel assignments that lead to desired power allocation is given in Algorithm 7. The obtained power allocation matrix $\mathbf{P}$ is a diagonal matrix whose diagonal entries given as $p_u = \alpha_u + \beta_u, u = 1,\ldots,|\mathcal{U}|$.

In Algorithm 7, steps 2 and 3 specify the minimum numbers of the highest gains subchannels $J_{\min}$ and $I_{\min}$ that are required to satisfy the energy harvesting EH and the data rate C constraints, respectively, when the maximum transmit power per subchannel $P_{\max}$ is applied. In step 4, problem (4.24) feasibility is presented. Because $J_{\min}$ and $I_{\min}$ are computed by applying $P_{\max}$ to the highest gains subchannels, problem (4.24) feasibility is not limited only to the condition given in step 4. In fact, any of the examined subchannel assignments that are defined in steps 7-15 could provide no solution. In general, the total number of the provisional subchannel assignments that are examined to obtain the desire

Algorithm 7 Solution to problem (4.24)

1: Initialize $P^{(0)} = \infty$, $\mathbf{P} = \mathbf{0}_K$.
2: Set $J_{\min}$ so the following condition is satisfied $\sum_{j=1}^{J_{\min}-1} \eta P_{\max} \sigma_j^2 < EH \leqslant \sum_{j=1}^{J_{\min}} \eta P_{\max} \sigma_j^2$
3: Set $I_{\min}$ so the following condition is satisfied $\sum_{i=1}^{I_{\min}+1} \log_2\left(1 + P_{\max}\sigma_i^2/\sigma^2\right) > C \geqslant \sum_{i=1}^{I_{\min}} \log_2\left(1 + P_{\max}\sigma_i^2/\sigma^2\right)$
4: **if** $J_{\min} + I_{\min} > K$ **then**
5: Problem (4.24) is infeasible and stop.
6: **else**
7: **for** $k = 1 : K - I_{\min} - 1$ **do**
8: $\mathcal{J}_{\text{Tx}}^{(k)} = \{1, 2, \ldots, J_{\min}\}$
9: $\mathcal{I}_{\text{Tx}}^{(k)} = \{1, 2, \ldots, K - J_{\min}\}$
10: Use CVX to solve (3.5) and obtain $P^{(k)} = \sum_{i \in \mathcal{I}_{\text{Tx}}} \alpha_i + \sum_{j \in \mathcal{J}_{\text{Tx}}} \beta_j$
11: **if** $P^{(k)} < P^{(0)}$ **then**
12: $\mathcal{I}_{\text{Tx}} = \mathcal{I}_{\text{Tx}}^{(k)}$, $\mathcal{J}_{\text{Tx}} = \mathcal{J}_{\text{Tx}}^{(k)}$, $P^{(0)} = P^{(k)}$ and $\mathbf{P} = \mathbf{P}^{(k)}$
13: **end if**
14: $J_{\min} = J_{\min} + 1$
15: **end for**
16: **end if**
17: **if** steps 7-15 returns no solution **then**
18: Problem (4.24) is infeasible.
19: **end if**

power allocation $\mathbf{P}$ is $K - I_{\min} - 1$.

The sets of the joint subchannels $\mathcal{Z}$ and the clear subchannels $\mathcal{N}$ are specified after finding the power allocation $\mathbf{P}$. Due to steps 8 and 9 in Algorithm 7, all the subchannel assignments that are examined in problem (4.24) guarantee the presence of the joint subchannels ; *i.e.*, $\mathcal{Z} \neq \emptyset$ where $\mathcal{Z} = \mathcal{I}_{\text{TX}} \bigcap \mathcal{J}_{\text{TX}}$. Furthermore, all the clear subchannels in the set $\mathcal{N}$, whenever existed, are used either for information exchange or energy harvesting where $\mathcal{N} = \mathcal{U} \setminus \mathcal{Z}$. It is worth noting that constraint (4.24e) leave a set of weakest subchannels $\hat{\mathcal{Z}}$ out of the problem (4.24). This is inline with Remark 4.1 that is discussed in Subsection 4.2.1 as those weakest subchannels are important for the system to separate the signals carried by the joint subchannels at the receiver. The set of those weakest subchannels $\hat{\mathcal{Z}}$ is defined as $\hat{\mathcal{Z}} = \left\{ |\mathcal{U}|+1, \ldots, |\mathcal{U}|+|\mathcal{Z}| \right\}$ and the transmitter applies only low power $p_{\hat{z}} > 0$ to them in order to keep the streams active as discussed in Remark 4.1.

B. Precoder and Filter Design via GTD

Similar to the approach that is proposed Subsection 4.2.1, the precoder $\mathbf{F}$ and the filter $\mathbf{W}$ are designed via the GTD decomposition of the diagonal matrix $\mathbf{\Sigma}(\mathbf{P})^{1/2}$. Including the low powers $p_{\hat{z}}$ in the matrix $\mathbf{P}$ gives the first and last batch of elements in $\boldsymbol{\lambda}$ of the diagonal matrix $\mathbf{\Sigma}(\mathbf{P})^{1/2}$ as

$$\lambda_z = \sqrt{\alpha_z + \beta_z}\sigma_z, \qquad z \in \mathcal{Z}, \tag{4.25a}$$

$$\lambda_{\hat{z}} = \sqrt{p_{\hat{z}}}\sigma_{\hat{z}}, \qquad \hat{z} \in \hat{\mathcal{Z}}. \tag{4.25b}$$

The remaining subchannels that are corresponded to the clear subchannels ; *i.e.*, the subchannels in the set $\mathcal{N}$ can be written as

$$\lambda_n = \begin{cases} \sqrt{\alpha_n^{\star}}\sigma_n, & \text{if } |\mathcal{I}_{\mathrm{Tx}}| > |\mathcal{Z}|, \\ \sqrt{\beta_n^{\star}}\sigma_n, & \text{if } |\mathcal{J}_{\mathrm{Tx}}| > |\mathcal{Z}|, \end{cases} \tag{4.26}$$

where $n \in \mathcal{N}$. Equation (4.26) implied that the subchannels in the set $\mathcal{N}$ carry one type of signals ; *i.e.*, either information or energy signals. The use of the subchannels in the set $\mathcal{N}$ is because the way of the provisional subchannel assignments are defined in the steps 8 and 9 of Algorithm 7.

The form of $\mathbf{r}$ that leads to the desired signals separation at the receiver for this approach is similar to the form of $\mathbf{r}$ that is given in equation (4.15). Thus, the structure of $\mathbf{R}$ at the receiver is similar to that one given by equation (4.16). Therefore, Theorem 4.1 can also be used to define the subchannel assignment at the receiver. In contrast to the optimal approach, the subchannel assignment at the receiver in this approach has more systematic order as will be explained in the next subsection.

C. Energy Harvested and Achievable Rate

According to Theorem 4.1, the receiver decodes the data from the set $\mathcal{I}_{\mathrm{Rx}} = \mathcal{W} \bigcup \bar{\mathcal{D}}$ and harvests energy from the subchannels $\mathcal{J}_{\mathrm{Tx}} = \mathcal{E} \bigcup \tilde{\mathcal{D}}$ where $\bar{\mathcal{D}} \bigcup \tilde{\mathcal{D}} = \mathcal{D}$. As stated in equation (4.15a), the streams that are transmitted by the subchannels in the set $\mathcal{N}$ are equivalent to the streams that are received by the subchannels in the set $\mathcal{D}$. Based on equation (4.26), the subchannels in the set $\mathcal{N}$ are used to transmit only type of signals,

and hence by equation (4.15a), the subchannels in the set $\mathcal{D}$ are used at the receiver either for information decoding ; *i.e.*, $\tilde{\mathcal{D}} = \emptyset$ or energy harvesting ; *i.e.*, $\bar{\mathcal{D}} = \emptyset$. In the following, we explain at which cases $\bar{\mathcal{D}} = \emptyset$ or $\tilde{\mathcal{D}} = \emptyset$.

Based on Theorem 4.1, the energy harvested from $e \in \mathcal{E}$ is

$$EH_e = \eta \left(r_e^2 + \frac{1}{r_e^2} \left(\lambda_{\check{z}}^2 - r_e^2 \right) \left(r_e^2 - \lambda_{\hat{z}}^2 \right) \right). \tag{4.27}$$

Substituting the corresponding $\lambda's$ and $r's$ as given in (4.25a) and (4.15) to (4.27) yields

$$EH_e = \eta \left(\beta_{\check{z}} \sigma_{\check{z}}^2 + p_{\hat{z}} \sigma_{\hat{z}}^2 \right) \approx \eta \beta_{\check{z}} \sigma_{\check{z}}^2, \tag{4.28}$$

since $p_{\hat{z}} \sigma_{\hat{z}}^2 \approx 0$. Note that $\check{z} = z_{\max}, \ldots, z_{\min}$, where $z_{\max}$ and $z_{\max}$ are maximum and the minimum elements in the set $\mathcal{Z}$. Now, if $|\mathcal{J}_{\mathrm{Tx}}| = |\mathcal{Z}|$ (that imply also $|\mathcal{J}_{\mathrm{Tx}}| < |\mathcal{I}_{\mathrm{Tx}}|$), the energy harvested from the streams $\mathcal{E}$ satisfies the constraint (4.1c) with equality;hence, $\mathcal{J}_{\mathrm{Tx}} = \mathcal{E}$ and $\tilde{\mathcal{D}} = \emptyset$. On the other hand, if $|\mathcal{J}_{\mathrm{Tx}}| > |\mathcal{Z}|$ (that imply also $|\mathcal{J}_{\mathrm{Tx}}| > |\mathcal{I}_{\mathrm{Tx}}|$), by (4.26) and (4.15a) the all receive-side streams by the subchannels in $\mathcal{D}$ are also used for energy harvesting in addition to those in $\mathcal{E}$; *i.e.*, $\mathcal{J}_{\mathrm{Tx}} = \mathcal{E} \bigcup \mathcal{D}$ and $\tilde{\mathcal{D}} = \mathcal{D}$. Constraint (4.1c) is then satisfied from the energy harvested from the subchannels in $\mathcal{J}_{\mathrm{RX}}$.

Since the information bearing subchannels are interference-free by construction, the achievable rate can be obtained from (2.21a). As with energy harvesting, there are two cases that arise from (4.26), that is: 1) $|\mathcal{I}_{\mathrm{Tx}}| = |\mathcal{Z}|$ (that imply also $|\mathcal{I}_{\mathrm{Tx}}| < |\mathcal{J}_{\mathrm{Tx}}|$), and 2) $|\mathcal{I}_{\mathrm{Tx}}| > |\mathcal{Z}|$ (that imply also $|\mathcal{I}_{\mathrm{Tx}}| > |\mathcal{J}_{\mathrm{Tx}}|$). Concentrating on the former, recalling that $r_k = R_{kk}$, and using (4.25a) and (4.15c) in (2.21a) yields the rate of stream $w \in \mathcal{W}$ as

$$C_w = \log_2 \left(1 + \frac{\alpha_{\check{z}} \sigma_{\check{z}}^2}{\sigma} \right). \tag{4.29}$$

In this case, the total rate $\sum_{w \in \mathcal{W}} C_w = C$ so that the constraint (4.1b) is satisfied and $\mathcal{I}_{\mathrm{RX}} = \mathcal{W}$ while $\bar{\mathcal{D}} = \emptyset$. In the case of $|\mathcal{I}_{\mathrm{TX}}| > |\mathcal{Z}|$, by (4.26) and (4.15a) the $|\mathcal{N}|$ receive-side streams in $\mathcal{D}$ are also used for information transfer so that the total rate of streams $\mathcal{I}_{\mathrm{Rx}} = \mathcal{W} \cup \mathcal{D}$ satisfies the constraint (4.1b) and $\bar{\mathcal{D}} = \mathcal{D}$.

Although the proposed approach in this section yields suboptimal power allocation,

there are two main advantages in this approach over the optimal approach that is proposed in Subsection 4.2.1. The first advantage is that the power allocation can be obtained in polynomial time complexity since the power allocation process is carried over a limited number of the subchannel assignments (less than K). This is in contrast with the optimal approach which has high complexity that increases exponentially with K [14, 16]. The second advantage is that the suboptimal approach has more systematic design than the optimal approach since the clear subchannels in the suboptimal design are only assigned either for information exchange or energy transfer.

4.2.3 Transmit Power Minimization for the SVD Based SWIPT

In this section, the SVD based SWIPT system that is presented [14, 16] is revisited with brief details. The focus will be on the optimal design in order to compare with proposed GTD solutions that are developed in Subsection 4.2.1 and Subsection 4.2.2.

The problem of the power minimization of the SVD based SWIPT is formulated as follows [14, 16]

$$\begin{aligned}
\underset{\mathbf{P},a_i}{\text{minimize}} \quad & \text{tr}(\mathbf{F}\mathbf{F}^H), && \text{(4.30a)}\\
\text{s.t.} \quad & \prod_{i\in\mathcal{K}}\left(1+\frac{a_i p_i \sigma_i^2}{\sigma^2}\right) \geqslant 2^C, && \text{(4.30b)}\\
& \sum_{i\in\mathcal{K}}(1-a_i)\eta p_i \sigma_i^2 \geqslant EH, && \text{(4.30c)}\\
& 0 \leqslant p_i \leqslant P_{\max},\ a_i \in \{0,1\},\ i \in \mathcal{K}. && \text{(4.30d)}
\end{aligned}$$

Unlike the GTD based SWIPT system, the power allocation problem of the SVD based SWIPT system has only single binary variable vector. This is due to the structure of the SVD since any subchannel should be used either for information exchange ; *i.e.*, $a_i = 1$ or energy transfer ; *i.e.*, $a_i = 0$.

According to [14, 16], problem (4.30) can be transformed into MISOCP by following Proposition 4.1 and Proposition 4.2 as written below

$$\begin{aligned}
\underset{p_i,\,\tilde{p}_i,\,a_i}{\text{minimize}} \quad & \sum_{i\in\mathcal{K}} p_i, && \text{(4.31a)}\\
\text{s.t.} \quad & x_{n-1,2q-1}x_{n-1,2q} \geqslant x_{n,q}^2,\ n = 1,\ldots,m,\ q = 1,\ldots,2^{m-n}, && \text{(4.31b)}
\end{aligned}$$

$$x_{m,1} \geqslant t,\ t = 2^{C/\mu}, \tag{4.31c}$$

$$x_{0,q} = 1 + \frac{\tilde{p}_i \sigma_i^2}{\sigma^2},\ i \in \mathcal{K},\ q \in \mathcal{K}, \tag{4.31d}$$

$$x_{0,q} = 1,\ i = K+1, \ldots, \mu, \tag{4.31e}$$

$$x_{n,q} \geqslant 0,\ n = 0, \ldots, m,\ q = 1, \ldots, 2^{m-n}, \tag{4.31f}$$

$$\sum_{i \in \mathcal{K}} \eta (p_i - \tilde{p}_i) \sigma_i^2 \geqslant EH, \tag{4.31g}$$

$$\tilde{p}_i \leqslant a_i P_{\max},\ \tilde{p}_i \leqslant p_i,\ i \in \mathcal{K}, \tag{4.31h}$$

$$\tilde{p}_i \geqslant p_i - (1 - a_i) P_{\max}, \tilde{p}_i \geqslant 0,\ i \in \mathcal{K}, \tag{4.31i}$$

$$0 \leqslant p_i \leqslant P_{\max},\ a_i \in \{0,1\},\ i \in \mathcal{K}. \tag{4.31j}$$

Similar to problem (4.8), problem (4.31) can be solved via standard optimization packages such as CVX [86].

4.2.4 RF Powers at the Transmit Antenna

This chapter studies GTD and SVD based SWIPT approaches under the assumption of maximum transmit power per each subchannel. In general and from the practical implementation perspective, transmitters in MIMO wireless communication systems deal with the RF transmit power at the antenna instead of the subchannel. In this subsection, the case of the actual RF power that is used at each of the transmit antennas is briefly studied. In following, an illustrative example is presented To highlight the difference between the concepts of per subchannel/antenna maximum transmit power.

Suppose that the objective of the GTD and the SVD based SWIPT approaches is to minimize the total transmit power that satisfy energy harvesting and data rate constraints that are equal to 0.75 mW and 10 bps/Hz, respectively. The transmitter and the receiver in both approaches are equipped with equal number of antenna that is $N_t = N_r = 6$. The maximum transmit power per each subchannel is set to 0.5 W. A Rayleigh fading channel spatially uncorrelated is assumed in this example. The channel entries are i.i.d ZMCSCG variables with variance $\sigma_h^2 = ad^{-\gamma}$ where $a = 0.1$ is the path loss factor, $d = 12$ m is the distance between the transmitter and the receiver and $\gamma = 3$ denotes the path loss exponent. The noise variance σ^2 is set to -50 dBm and the energy conversion efficiency η is set to 0.66.

Table 4.2: Transmit powers per subchannel and per antenna for GTD and SVD based SWIPT systems.

No.	Subchannel gain (σ_i)	GTD based SWIPT			SVD based SWIPT		
		$P_{sub.}$ (W)	$P_{Ant.}$ (W)	Subchannel use	$P_{sub.}$ (W)	$P_{Ant.}$ (W)	Subchannel use
1	0.0369	0.5	0.2349	EH+Inf	0.5	0.4893	EH
2	0.0251	0.5	0.2951	EH+Inf	0.5	0.0096	EH
3	0.0203	0.3466	0.0340	EH+Inf	0.3460	0.5431	EH
4	0.0120	10^{-6}	0.1653	Separation	0.0031	0.0296	Inf
5	0.0067	10^{-6}	0.0896	Separation	0.0029	0.1161	Inf
6	0.0023	10^{-6}	0.5277	Separation	0.0012	0.1654	Inf

Table 4.2 shows the transmit power that is used at each subchannel and antenna in both GTD and SVD based SWIPT systems. The gains of the subchannels σ_i are obtained by taking SVD of the channel matrix. The transmit powers per subchannel $\boldsymbol{P_{sub}}$ for the GTD and the SVD approaches are calculated by following the solutions developed in Subsection 4.2.1 and Subsection 4.2.3, respectively. On the other hand, the transmit powers per antennas $\boldsymbol{P_{Ant}}$ for both GTD and SVD approaches are computed by following equations (2.18) and (2.16) that are presented in Section 2.4.

It should be noted that the total amount of the transmit power that is used at the subchannels is equivalent to the total amount to the transmit that is used at the antennas in each of the GTD and the SVD approaches. This is because of the orthogonality of the precoders that are used at the transmitters in each approach, as illustrated in equations (2.18) and (2.16). We can observe that the transmit powers are sorted in more balanced manner at the antennas in comparison to the transmit powers per subchannels especially in the GTD approach. This means that using power amplifiers that support relatively higher power than the value of the maximum power per subchannel would be a reasonable choice. Note that the GTD is only studied theoretically in this work and hence the practical implementation aspects that are related to the realization of GTD and SVD approaches, such as the use of power amplifiers and precoder designs, are left for future works.

4.3 Energy Harvesting Maximization With Data Rate and per Subchannel Transmit Power Constrains

In this section, two SS based SWIPT transceivers are developed to maximize the energy harvested and meet the required data rate at the receiver where the transmitter is characterized by limited transmit power per each subchannel. The first transceiver is designed using GTD and presented in Subsection 4.3.1. The second transceiver is developed based on SVD and introduced in Subsection 4.3.2.

4.3.1 Energy Harvesting Maximization for GTD Based SWIPT

The focus in this section is on designing a GTD based SWIPT transceiver to maximize the energy harvesting. The proposed design relies on the structure of the GTD which allows any of the available subchannels to carry more than one type of signals. In this design, per subchannel power constraint is assumed at the transmitter. Note that the proposed approach in this section is different from the one in Subsection 3.5.1 since the latter uses instantaneous total power constraint at the transmitter. However, the difference in the power constraint between both approaches results in different solutions for each one.

The following optimization problem describes the design objective of the GTD transceiver:

$$\underset{\mathbf{P},\,\mathbf{r}\preceq\boldsymbol{\lambda},\,\mathcal{J}_{\mathrm{Tx}},\,\mathcal{I}_{\mathrm{Rx}}}{\text{maximize}} \quad EH = \sum_{j\in\mathcal{J}_{\mathrm{RX}}}\sum_{l=j}^{K}\eta R_{jl}^{2}, \tag{4.32a}$$

$$\text{s.t.} \quad \sum_{i\in\mathcal{I}_{\mathrm{RX}}}\log_2\left(1+\frac{R_{ii}^{2}}{\sigma^{2}}\right)\geqslant C, \tag{4.32b}$$

$$0\leqslant p_k\leqslant P_{\max},\ k\in\mathcal{K}, \tag{4.32c}$$

where $\mathcal{K}$ denotes the set of all the available subchannels while $\mathcal{J}_{\mathrm{Tx}}\subset\mathcal{K}$ and $\mathcal{I}_{\mathrm{Rx}}\subset\mathcal{K}$ represent the sets of the subchannels that are assigned for energy harvesting and information decoding at the receiver, respectively. $P_{\max}$ is the maximum available power per subchannel at the transmitter and $\mathbf{P}$ denote to the power allocation matrix while $\boldsymbol{\lambda}$ represents the positive diagonal elements of the matrix $\boldsymbol{\Sigma}\mathbf{P}^{1/2}$.

Similar to the solutions that already developed for all the previous GTD designs, the

solution of problem (4.32) can be obtained in two steps. The first step is to obtain the power allocation $\mathbf{P}$ where the same method that is used to find the power allocation $\mathbf{P}$ in suboptimal GTD design is followed in this section. The second step involves applying the GTD on $\mathbf{\Sigma}(\mathbf{P})^{1/2}$ to design the precoder $\mathbf{F}$ at the transmitter and the linear filter $\mathbf{W}$ at the receiver.

A. Power Allocation and Transmit-Side Subchannel Assignment

The transmitter allocates the power according to the positive singular values $\boldsymbol{\sigma}$ of the channel matrix $\mathbf{H}$. Considering the fact that the GTD gives the transmitter the flexibility to use any subchannel to carry both information and energy signals, the power allocation problem at the transmitter for a fixed subchannel assignment can be written as follows:

$$\underset{\beta_j,\alpha_i}{\text{maximize}} \quad EH = \sum_{j\in\mathcal{J}_{\text{TX}}} \eta\beta_j\sigma_j^2, \tag{4.33a}$$

$$\text{s.t.} \quad \sum_{i\in\mathcal{I}_{\text{TX}}} \log_2\left(1+\frac{\alpha_i\sigma_i^2}{\sigma^2}\right) \geqslant C, \tag{4.33b}$$

$$\mathcal{U} = \mathcal{I}_{\text{Tx}} \cup \mathcal{J}_{\text{Tx}},\ |\mathcal{U}| < K, \tag{4.33c}$$

$$0 \leqslant \alpha_u + \beta_u \leqslant P_{\max},\ \alpha_u \geqslant 0,\ \beta_u \geqslant 0,\ u \in \mathcal{U}, \tag{4.33d}$$

where the β_j and α_i denote to th power allocated the transmitter for energy and information transfer on the j-th and i-th streams. The sets $\mathcal{I}_{\text{Tx}}$ and $\mathcal{J}_{\text{Tx}}$ represent the subchannels assigned at the transmitter for information exchange and energy transfer, respectively while K denote to the total numbers of the available subchannels. Like the suboptimal GTD approach that is introduced in Section 4.2.2, the power allocation in problem (4.33) is obtained by examined a few number of predefined subchannel assignments and select the one that returns the highest amount of energy as illustrated in Algorithm 8.

The first step in Algorithm 8 specifies the minimum number of the subchannels $I_{\min}$ that is required to obtain the least amount of the rate that is higher than required rate C in constraint (4.33b). The process of specifying $I_{\min}$ ensures that the highest gain subchannels can be used for joint information and energy transmissions. Clearly, problem (4.33) is not feasible if the required $I_{\min}$ to satisfy the data rate constraint C is equal or greater than the total number of available subchannels K as mentioned in the second step

of Algorithm 8. According to step 6 in Algorithm 8, the total number of the examined subchannel assignments does not exceed $K - I_{\min}$. Each subchannel assignment is defined in an iterative manner based on steps 7 and 8. It is obvious from steps 7 and 8 that in each iteration, the number of the subchannels assigned for information increases while the number of the energy subchannels decreases. The reason for this process is to allow more transmit power to be used for energy harvesting at the highest gain subchannels since the moderate and the low gains subchannels could be used to satisfy part of the data rate constraint. This process continues as long as the energy obtained increases at each iteration and stops when the amount of energy obtained starts to diminish as depicted in the conditions provided by steps 10 and 13. The conditions in steps 10 and 13 can be interpreted as follows. The process of updating the subchannel assignment stops when the amount of the energy that is obtained by the newly updated subchannel assignment is less than the amount of the energy obtained from the old subchannel assignment.

The subchannel assignment that returns the highest harvested energy consists of the sets $\mathcal{J}_{\text{Tx}}$ and $\mathcal{I}_{\text{Tx}}$. The set $\mathcal{U} = \mathcal{I}_{\text{Tx}} \bigcup \mathcal{J}_{\text{Tx}}$ contains all the subchannels that are used in the power allocation problem (4.33), where $\mathcal{U} \subset \mathcal{K}$. Steps 7 and 8 in Algorithm 8 ensures the presence of the joint subchannels set $\mathcal{Z}$. Note that the joint subchannels set refers to the subchannels that are used by the transmitter to transfer information and energy jointly and can be found as $\mathcal{Z} = \mathcal{I}_{\text{Tx}} \bigcap \mathcal{J}_{\text{Tx}}$. Also, depending on the data rate constraint (4.33b), the selected subchannel assignment may return a set of clear subchannels. The set of clear subchannels $\mathcal{N}$ contains the subchannels that are used by the transmitter to send either information or energy signals and can be specified as $\mathcal{N} = \mathcal{U} \setminus \mathcal{Z}$.

According to Remark 4.1, the presence of the set $\mathcal{Z}$ leads to $\hat{\mathcal{Z}} \neq \emptyset$, where $\hat{\mathcal{Z}} = \mathcal{K} \setminus \mathcal{U}$. The set $\hat{\mathcal{Z}}$ consists all the weakest subchannels that are not used in problem (4.33) where $\left|\hat{\mathcal{Z}}\right| = |\mathcal{Z}|$. As discussed in Remark 4.1, the subchannels in the set $\hat{\mathcal{Z}}$ are important for the GTD based SWIPT systems to perform the signal separation at the receiver. Moreover, these subchannels can also contribute to increase the energy harvesting amount; therefore, the transmitter applies the maximum power to each subchannel in the set $\hat{\mathcal{Z}}$; *i.e.*, $p_{\hat{z}} = P_{\max}$.

Finally, the obtained power allocation $\mathbf{P}$ is diagonal matrix whose its first $|\mathcal{U}|$-th

Algorithm 8 Solution to problem (4.33)

Find $I_{\min}$ that satisfies the following condition: $\sum_{i=1}^{I_{\min}-1} \log_2\left(1 + P_{\max}\sigma_i^2/\sigma^2\right) \leqslant C < \sum_{i=1}^{I_{\min}} \log_2\left(1 + P_{\max}\sigma_i^2/\sigma^2\right)$.
if $I_{\min} \geqslant K$ **then**
    Problem (4.33) is infeasible
else
    Set $I = I_{\min}$, $EH^{(0)} = 0$, and $\mathbf{P} = \mathbf{0}_K$.
    for $k = 1 : K - I_{\min}$ **do**
        Set $\mathcal{I}_{\text{Tx}}^{(k)} = \{1, 2, \ldots, I\}$
        Set $\mathcal{J}_{\text{Tx}}^{(k)} = \{1, 2, \ldots, K - I\}$
        Use CVX to obtain α_i and β_j and compute $EH^{(k)} = \sum_{i \in \mathcal{J}_{\text{Tx}}^{(k)}} \eta\beta_j\sigma_j^2$
        if $EH^{(k)} > EH^{(0)}$ **then**
            Set $\mathcal{I}_{\text{Tx}} = \mathcal{I}_{\text{Tx}}^{(k)}$, $\mathcal{J}_{\text{Tx}} = \mathcal{J}_{\text{Tx}}^{(k)}$, $EH^{(0)} = EH^{(k)}$ and $\mathbf{P} = \mathbf{P}^{(k)}$.
            $I = I + 1$.
        else
            Stop this algorithm and returns $\mathcal{I}_{\text{Tx}} = \mathcal{I}_{\text{Tx}}^{(k-1)}$, $\mathcal{J}_{\text{Tx}} = \mathcal{J}_{\text{Tx}}^{(k-1)}$, and $\mathbf{P} = \mathbf{P}^{(k-1)}$.
        End if
    End for
End if

diagonal entries are $p_u = \alpha_u + \beta_u$ while the last $\left|\hat{\mathcal{Z}}\right|$ entries $p_{\hat{z}}$ are set to $P_{\max}$ as discussed above. Note that, all K available subchannels are used in this design since the objective is to achieve a maximum amount of energy harvesting.

B. Precoder and Filter Design via GTD

The precoder and the filter design process is carried out by applying the GTD on the diagonal matrix $\mathbf{\Sigma P}^{1/2}$. To apply the GTD, the elements of $\mathbf{r}$ are required to be defined properly such that the resulted $\mathbf{R}$ at the receiver leads to satisfy the rate constraint (4.32b) and also leads to energy harvesting amount equivalent to the sum of the energy that is transferred by the subchannels in the sets $\mathcal{J}_{\text{Tx}}$ and $\hat{\mathcal{Z}}$. Note that $\mathbf{r}$ must be multiplicatively majorized by the diagonal elements of $\mathbf{\Sigma P}^{1/2}$; *i.e.*, $\mathbf{r} \preceq \boldsymbol{\lambda}$. The elements of $\boldsymbol{\lambda}$ in this design have a similar form to those defined in equations (4.25a), (4.25b), and (4.26) that are introduced Subsection 4.2.2.

The element of $\mathbf{r}$ that gives the required streams separation at the receiver can be defined as in (4.15). Following Proposition 4.3 and Corollary 4.1, the end-to-end signal

at the receiver described by (2.20) has matrix $\mathbf{R}$ equivalent to the one defined in equation (4.16). It is worth noting that the index L should be replaced by K in equations (4.15) and (4.16) since all the available subchannels in the system are utilized to maximize the harvested energy.

C. Harvested Energy and Achievable Rate

Since the matrix $\mathbf{R}$ at the receive-side has a similar form to that one in equation (4.16), Theorem 4.1 can be used to verify the energy harvested and the achievable rate in this GTD design. It is worth noting that Theorem 4.1 considers the energy harvesting as a constraint, however, the main point in Theorem 4.1 was to show that the amounts of the energy harvested and the rate of the data decoded at the receiver side coincides with amounts of the energy and the data rate that are obtained by the power allocation at the transmitter side. Furthermore, Theorem 4.1 has defined the optimal subchannel assignment at the receiver. Therefore, Theorem 4.1 is also applicable in this design to define the subchannel assignment at the receiver ; *i.e.*, $\mathcal{I}_{\mathrm{Rx}}$ and $\mathcal{J}_{\mathrm{Tx}}$. In addition to that, equation (4.17) in Theorem 4.1 can be used to show that the data rate achieved at the receiver is equal to the data rate in constraint (4.33b) while equation (4.20) can be applied to verify that the amount of the harvested energy is equal to total amount of the energy transferred by transmitter.

According to Theorem 4.1, the receiver uses subchannels in the set $\mathcal{I}_{\mathrm{Rx}} = \mathcal{W} \bigcup \bar{\mathcal{D}}$ to decode the data while the subchannels in set $\mathcal{J}_{\mathrm{Tx}} = \mathcal{E} \bigcup \tilde{\mathcal{D}}$ are used for energy harvesting, where $\bar{\mathcal{D}} \bigcup \tilde{\mathcal{D}} = \mathcal{D}$. Note that the elements of the sets $\mathcal{D}$, $\mathcal{E}$ and $\mathcal{W}$ are defined in Subsection 4.2.1.C. Based on equation (4.15), the streams that are transmitted by the subchannels in the set $\mathcal{N}$ are equivalent to the streams that are received by the subchannels in the set $\mathcal{D}$. Hence, the receiver uses the subchannels in the set $\mathcal{D}$ for information decoding when $|\mathcal{I}_{\mathrm{Tx}}| > |\mathcal{Z}|$ and this implies that $\mathcal{I}_{\mathrm{Rx}} = \mathcal{W} \bigcup \mathcal{D}$ and $\mathcal{J}_{\mathrm{Tx}} = \mathcal{E}$, where $\bar{\mathcal{D}} = \mathcal{D}$ and $\tilde{\mathcal{D}} = \emptyset$. On the other hand, the receiver uses the subchannels in the set $\mathcal{D}$ for energy harvesting when $|\mathcal{J}_{\mathrm{Tx}}| > |\mathcal{Z}|$ and this implies that $\mathcal{I}_{\mathrm{Rx}} = \mathcal{W}$ and $\mathcal{J}_{\mathrm{Tx}} = \mathcal{E} \bigcup \mathcal{D}$ where $\bar{\mathcal{D}} = \emptyset$ and $\tilde{\mathcal{D}} = \mathcal{D}$. However, the cases that are regarding the use of the set $\mathcal{D}$ in this design are analogous to those that are presented in Subsection 4.2.2.C where more

details can be found there.

4.3.2 Energy Harvesting Maximization for the SVD based SWIPT System

In this section, SVD is used to design a transceiver that maximizes the energy harvesting for the SS based MIMO SWIPT systems. Although the work in [76] studied the energy harvesting maximization of the SVD based SWIPT system as discussed in Section 3.5.2, the study in this section has different aspects regarding the power allocation and subchannel assignment. The authors in [76] have shown that assigning one subchannel at the transmitter to transfer energy is optimal in order to maximize the harvested energy at the receiver. However, this is valid when the transmitter has the instantaneous total transmit power constraint. In this section, the transmitter is constrained by a limited transmit power per subchannel and such constraint forces the transmitter to use more than one subchannel in order to maximize the harvested energy.

The following optimization problem describes the design objective of this section

$$\underset{p_i,a_i}{\text{maximize}} \quad EH = \sum_{i\in\mathcal{K}}(1-a_i)\eta p_i\sigma_i^2, \tag{4.34a}$$

$$\text{s.t.} \quad \prod_{i\in\mathcal{K}}\left(1+\frac{a_i p_i\sigma_i^2}{\sigma^2}\right) \geqslant 2^C, \tag{4.34b}$$

$$0 \leqslant p_i \leqslant P_{\max},\ a_i \in \{0,1\},\ i \in \mathcal{K}. \tag{4.34c}$$

Problem (4.34) is similar in structure to problem (4.30) in Subsection 4.2.3. Therefore, Proposition 4.1 and Proposition 4.2 can be used in problem (4.34) to linearize the products of the variables $a_i p_i$ and to transform constraint (4.34b) into multiple SORC constraints. After applying Proposition 4.1 and Proposition 4.2, probelm (4.34) can be written as follows

$$\underset{p_i,\,\tilde{p}_i,\,a_i}{\text{maximize}} \quad EH = \sum_{i\in\mathcal{K}}\eta(p_i-\tilde{p}_i)\sigma_i^2, \tag{4.35a}$$

$$\text{s.t.} \quad x_{n-1,2q-1}x_{n-1,2q} \geqslant x_{n,q}^2,\ n=1,\ldots,m,\ q=1,\ldots,2^{m-n}, \tag{4.35b}$$

$$x_{m,1} \geqslant t,\ t = 2^{C/\mu}, \tag{4.35c}$$

$$x_{0,q} = 1 + \frac{\tilde{p}_i \sigma_i^2}{\sigma^2},\ i \in \mathcal{K},\ q \in \mathcal{K}, \tag{4.35d}$$

$$x_{0,q} = 1,\ i = K+1, \ldots, \mu, \tag{4.35e}$$

$$x_{n,q} \geqslant 0,\ n = 0, \ldots, m,\ q = 1, \ldots, 2^{m-n}, \tag{4.35f}$$

$$\tilde{p}_i \leqslant a_i P_{\max},\ \tilde{p}_i \leqslant p_i,\ i \in \mathcal{K}, \tag{4.35g}$$

$$\tilde{p}_i \geqslant p_i - (1 - a_i) P_{\max}, \tilde{p}_i \geqslant 0,\ i \in \mathcal{K}, \tag{4.35h}$$

$$0 \leqslant p_i \leqslant P_{\max},\ a_i \in \{0, 1\},\ i \in \mathcal{K}. \tag{4.35i}$$

Constraints (4.35b)-(4.35f) are imposed using Proposition 4.2 where $m = \lceil \log_2 K \rceil$ and $\mu = 2^m$. Constraints (4.35g) and (4.35h) are due to the use of Proposition 4.1. The formulation of (4.35) is MISOCP and can be solved numerically by using CVX [86].

4.4 Data Rate Maximization With Energy Harvesting and per Subchannel Transmit Power Constrains

In this section, two different transceivers are proposed to maximize the data rate in SS based SWIPT systems. The first transceiver is presented in Subsection 4.4.1 and developed based on the GTD. The second transceiver is introduced in Subsection 4.4.2 and designed using SVD.

4.4.1 Data Rate Maximization for GTD Based SWIPT System

In the following, we use GTD to design a point-to-point MIMO SWIPT transceiver for data rate maximization. The transceiver design objective can be formulated in the following optimization problem

$$\underset{\mathbf{P},\, \mathbf{r} \preceq \boldsymbol{\lambda},\, \mathcal{I}_{\mathrm{Rx}},\, \mathcal{J}_{\mathrm{Tx}}}{\text{maximize}} \quad C = \sum_{i \in \mathcal{I}_{\mathrm{Rx}}} \log_2 \left(1 + \frac{R_{ii}^2}{\sigma^2}\right), \tag{4.36a}$$

$$\text{s.t.} \quad \sum_{j \in \mathcal{J}_{\mathrm{RX}}} \sum_{l=j}^{K} \eta R_{jl}^2 \geqslant EH, \tag{4.36b}$$

$$0 \leqslant p_k \leqslant P_{\max},\ k \in \mathcal{K}. \tag{4.36c}$$

The design problem in (4.36) can be solved by following the same methods that are used for designing the power minimization and energy maximization transceivers in Subsection 4.2.2 and Subsection 4.3.1. The design process is implemented in two steps. In first step, the power allocation $\mathbf{P}$ is found by following a similar process that is used in Subsection 4.2.2. The second step targets the precoder and the linear filter designs.

A. Power Allocation and Transmit-Side Subchannel Assignment

The first step of the transceiver design begins with power allocation at the transmitter. The power is allocated in the transmitter based on the singular values $\boldsymbol{\sigma}$ of the channel matrix $\mathbf{H}$. The power allocation problem at the transmitter is formulated as

$$\underset{\alpha_i,\beta_j}{\text{maximize}} \quad C = \sum_{i\in\mathcal{I}_{\text{TX}}} \log_2\left(1+\frac{\alpha_i\sigma_i^2}{\sigma^2}\right), \tag{4.37a}$$

$$\text{s.t.} \quad \sum_{j\in\mathcal{J}_{\text{TX}}} \eta\beta_j\sigma_j^2 \geqslant \bar{EH}, \tag{4.37b}$$

$$\mathcal{U} = \mathcal{I}_{\text{Tx}} \cup \mathcal{J}_{\text{Tx}},\ |\mathcal{U}| < K, \tag{4.37c}$$

$$0 \leqslant \alpha_u + \beta_u \leqslant P_{\max},\ \alpha_u \geqslant 0,\ \beta_u \geqslant 0,\ u \in \mathcal{U}, \tag{4.37d}$$

where α_i and β_j are the powers allocated by the transmitter for information exchange and energy transfer, respectively, while $\mathcal{I}_{\text{TX}}$ and $\mathcal{J}_{\text{TX}}$ represent the sets of the subchannels assigned at the transmitter for information exchange and energy transfer, respectively. Note that $\bar{EH} \leqslant EH$ and the reason for this treatment to the energy harvesting constraint (4.37b) will be explained later.

Similar to the power allocation that is obtained for the designs in Subsection 4.2.2 and Subsection 4.3.1, the power allocation in this design is found by examining a limited number of subchannel assignments as show in Algorithm 9.

The solution developed in Algorithm 9 starts with defining the minimum number of the subchannels $J_{\min}$ that returns the least amount of energy that is higher than the required EH in constraint (4.36b). It is obvious that if $J_{\min}$ is equal or greater than the total number of the available subchannels K, problem (4.36) is infeasible as illustrated in the condition at the second step of Algorithm 9. Assuming problem (4.36) is feasible, the total number of the subchannels assignments that are examined in this solution are

Algorithm 9 Solution to problem (4.37)

1: Find $J_{\min}$ that satisfies the following condition: $\sum_{i=1}^{J_{\min}-1} \eta P_{\max} \sigma_j^2 \leqslant EH < \sum_{i=1}^{J_{\min}} \eta P_{\max} \sigma_j^2$.
2: **if** $J_{\min} \geqslant K$ **then**
3: Problem (4.37) is infeasible.
4: **else**
5: Initialize $J = J_{\min}$, $C^{(0)} = 0$, $\mathcal{I}_{\text{Tx}} = \emptyset$, $\mathcal{J}_{\text{Tx}} = \emptyset$ and $\mathbf{P} = \mathbf{0}_K$.
6: **for** $k = 1 : K - J_{\min}$ **do**
7: Set $\mathcal{J}_{\text{Tx}}^{(k)} = \{1, 2, \ldots, J\}$
8: Set $\mathcal{I}_{\text{Tx}}^{(k)} = \{1, 2, \ldots, K - J\}$
9: Set $\mathcal{U}^{(k)} = \mathcal{I}_{\text{Tx}}^{(k)} \bigcup \mathcal{J}_{\text{Tx}}^{(k)}$
10: Set $\hat{\mathcal{Z}}^{(k)} = \mathcal{K} \setminus \mathcal{U}^{(k)}$
11: Compute $\hat{EH} = \sum_{\hat{z} \in \hat{\mathcal{Z}}} \eta P_{\max} \sigma_{\hat{z}}^2$.
12: **if** $\hat{EH} < EH$ **then**
13: Compute $\bar{EH} = EH - \hat{EH}$
14: Use CVX to solve problem (4.37) and obtain α_i and β_j and compute $C^{(k)} = \sum_{i \in \mathcal{I}_{\text{Tx}}^{(k)}} \log_2 \left(1 + \alpha_i \sigma_i^2 / \sigma^2\right)$.
15: **if** $C^{(k)} > C^{(0)}$ **then**
16: $\mathcal{I}_{\text{Tx}} = \mathcal{I}_{\text{Tx}}^{(k)}$, $\mathcal{J}_{\text{Tx}} = \mathcal{J}_{\text{Tx}}^{(k)}$, $C^{(0)} = C^{(k)}$ and $\mathbf{P} = \mathbf{P}^{(k)}$.
17: $J = J + 1$
18: **else**
19: Stop this algorithm and returns $\mathcal{I}_{\text{Tx}} = \mathcal{I}_{\text{Tx}}^{(k-1)}$, $\mathcal{J}_{\text{Tx}} = \mathcal{J}_{\text{Tx}}^{(k-1)}$, and $\mathbf{P} = \mathbf{P}^{(k-1)}$.
20: End if
21: End If
22: **if** $\hat{EH} \geqslant EH$ **then**
23: Set $\mathcal{J}_{\text{Tx}} = \hat{\mathcal{Z}}$, $\mathcal{I}_{\text{Tx}} = \mathcal{K} \setminus \mathcal{J}_{\text{Tx}}$
24: Return $p_k = P_{\max}$, $\mathbf{P} = \text{diag}[p_1, \ldots, p_K]$ and stop this algorithm.
25: End if
26: End for
27: End if

in general $K - J_{\min}$. Steps 7 and 8 define the provisional subchannel assignments that are used to obtain the required power allocation matrix. It is worth noting that steps 7 and 8 in Algorithm 9 guarantee the presence of the joint subchannels ; *i.e.*, $\mathcal{Z} \neq \emptyset$. This also implies that $\hat{\mathcal{Z}} \neq \emptyset$ where $\hat{\mathcal{Z}}$ represent the set of the weakest subchannels that are left out of problem (4.37). The existence of $\hat{\mathcal{Z}}$ is also consistence with Remark 4.1 that is introduced in Subsection 4.2.1.B. The set $\hat{\mathcal{Z}}$ can be found as $\hat{\mathcal{Z}} = \mathcal{K} \setminus \mathcal{U}$ as illustrated in step 10, where $\mathcal{K}$ denotes to the set of the total available subchannels while $\mathcal{U} = \mathcal{I}_{\text{Tx}} \bigcup \mathcal{J}_{\text{Tx}}$ represents the set of the all subchannels that are used to solve in problem (4.37). In general, the presence of the subchannels in the set $\hat{\mathcal{Z}}$ is necessary for the received streams separation process as discussed in Remark 4.1. Furthermore, the

subchannels in $\hat{\mathcal{Z}}$ can also be used in this design to contribute towards the satisfaction of the the energy harvesting constraint (4.36b). Therefore, the transmitter applies maximum transmit power $P_{\max}$ to these subchannels as illustrated in step 11 of Algorithm 9.

Depending on the energy harvesting constraint (4.36b), the energy $\hat{EH}$ that is computed in step 11 could either satisfy a part or all the required EH in (4.36b). The cases that are related to the amount of $\hat{EH}$ are introduced in Algorithm 9 by steps 12 and 22. In case of $\hat{EH} < EH$, the transmitter uses the subchannels that are defined in steps 7 and 8 to solve problem (4.37) where $\bar{EH}$ is found as described in step 13. The subchannel assignment are update iteratively until the assignment that return the highest achievable rate is found. Note that in this case the selected subchannel assignment guarantees the presence of the joint subchannels set $\mathcal{Z} = \mathcal{I}_{\text{Tx}} \bigcap \mathcal{J}_{\text{Tx}}$ while there is a possibility that the clear subchannels set $\mathcal{N} = \mathcal{U} \setminus \mathcal{Z}$ is existed. The obtained power allocation in this case is a diagonal matrix $\mathbf{P}$ and its first$|\mathcal{U}|$ elements are equal to $p_u = \alpha_u + \beta_u$ while the last $\left|\hat{\mathcal{Z}}\right|$ elements are set to $p_{\hat{z}}$ where $p_{\hat{z}} = P_{\max}$.

On the other hand, if $\hat{EH} \geqslant EH$, the subchannel assignment follows step 23 in Algorithm 9 while the power allocation matrix is set as in step 24. Note that in this case there is no joint subchannel set, ; *i.e.*, $\mathcal{Z} = \emptyset$ since the information subchannels set $\mathcal{I}_{\text{Tx}}$ and the energy harvesting subchannels set $\mathcal{J}_{\text{Tx}}$ are disjoint ; *i.e.*, $\mathcal{I}_{\text{Tx}} \bigcap \mathcal{J}_{\text{Tx}} = \emptyset$.

B. Precoder and Filter Design

In this step, the construction of the precoder $\mathbf{F}$ and the receiver-side matrix $\mathbf{W}$ are accomplished by applying GTD on the matrix $\mathbf{\Sigma P}^{1/2}$. However, applying GTD requires defining the elements of the vector $\mathbf{r}$ suitably to ensure that the resulted matrix $\mathbf{R}$ at the end-to-end received signal gives the same achievable rate and energy harvesting that are obtained by solving (4.37). Note that $\mathbf{r}$ must be multiplicatively majorized by the diagonal elements of $\mathbf{\Sigma P}^{1/2}$; *i.e.*, $\mathbf{r} \preceq \boldsymbol{\lambda}$. Considering the case when the subchannel assignment at the transmitter returns $\mathcal{Z} \neq \emptyset$, the elements of $\boldsymbol{\lambda}$ coincides with those given in equations (4.25a), (4.25b) and equation (4.26). We note that defining the element of $\mathbf{r}$ as in equation (4.15) results in matrix $\mathbf{R}$ that achieves equivalent data rate to the one obtained by solving problem (4.36) and satisfies the required EH in constraint (4.36b). The resulted $\mathbf{R}$ at the receiver coincides with the one that is given in equation (4.16).

Note that the index L should be replaced by K in equations (4.15) and (4.16) since all the available subchannels in the system are used in solving problem (4.37).

C. Energy Harvested and Achievable Rate

This section completes the design process by defining the receiver side subchannel assignment. Since matrix $\mathbf{R}$ given in equation (4.16) is resulted at receiver, Theorem 4.1 can be applied to define the subchannel assignment at the receiver ; *i.e.*, $\mathcal{I}_{\mathrm{Rx}}$ and $\mathcal{J}_{\mathrm{Tx}}$. Also, Theorem 4.1 is applicable to verify that the achievable rate and the energy harvested at the receiver coincide with the data rate and energy harvesting obtained by solving (4.37).

Based on Theorem 4.1, the subchannels in the set $\mathcal{I}_{\mathrm{Rx}} = \mathcal{W} \bigcup \bar{\mathcal{D}}$ are used at the receiver for information decoding while the subchannels in the set $\mathcal{J}_{\mathrm{Tx}} = \mathcal{E} \bigcup \tilde{\mathcal{D}}$ are employed for energy harvesting at the receiver where $\bar{\mathcal{D}} \bigcup \tilde{\mathcal{D}} = \mathcal{D}$. The streams that are received by the subchannels in sets $\bar{\mathcal{D}}$ and $\tilde{\mathcal{D}}$ are identical to the stream that are transmitted by the subchannels in the set $\mathcal{N}$ as given by equation (4.15). According to the solution provided by Algorithm 9, all the subchannels in the set $\mathcal{N}$ should convoy either information or energy signals. Therefore, all the subchannels in the set $\mathcal{D}$ used for information decoding at the receiver when $|\mathcal{I}_{\mathrm{Tx}}| > |\mathcal{Z}|$. This implies that $\mathcal{I}_{\mathrm{Rx}} = \mathcal{W} \bigcup \mathcal{D}$ and $\mathcal{J}_{\mathrm{Tx}} = \mathcal{E}$ where $\bar{\mathcal{D}} = \mathcal{D}$ while $\tilde{\mathcal{D}} = \emptyset$. Contrarily, all the subchannels in the set $\mathcal{D}$ are used for energy harvesting when $|\mathcal{J}_{\mathrm{Tx}}| > |\mathcal{Z}|$. This indicates that $\mathcal{I}_{\mathrm{Rx}} = \mathcal{W}$ and $\mathcal{J}_{\mathrm{Tx}} = \mathcal{E} \bigcup \mathcal{D}$ where $\tilde{\mathcal{D}} = \mathcal{D}$ while $\bar{\mathcal{D}} = \emptyset$.

Finally, we remark that equation (4.20) introduced in Theorem 4.1 can be applied to verify the energy that is transferred by the transmitter using the subchannels in the sets $\mathcal{J}_{\mathrm{Tx}}$ and $\hat{\mathcal{Z}}$ matches the energy harvested at the receiver from the streams in the set $\mathcal{J}_{\mathrm{Tx}}$. Meanwhile, equation (4.17) given in Theorem 4.1 can be used to show that the rate of the information exchanged by the transmitter using the subchannels in the set $\mathcal{I}_{\mathrm{Tx}}$ equals to the rate of the information that is decoded at the receiver from the streams in the set $\mathcal{I}_{\mathrm{Rx}}$.

D. Special Case

This part focuses on special case that leads to have $\mathcal{Z} = \emptyset$. This case occurs when $\hat{EH} \geqslant EH$ as illustrated in step 22 in Algorithm 9. In this case, the transmitter assigns

the weakest subchannels for energy transfer ; *i.e.*, $\mathcal{J}_{\text{Tx}} = \hat{\mathcal{Z}}$ while the strongest subchannel are used for information exchange that is $\mathcal{I}_{\text{Tx}} = \mathcal{K} \setminus \mathcal{J}_{\text{Tx}}$. Therefore, the joint subchannels are not existed at the transmitter and the subchannel assignment at receiver is identical to the subchannel assignment at transmitter ; *i.e.*, $\mathcal{I}_{\text{Rx}} = \mathcal{I}_{\text{Tx}}$ and $\mathcal{J}_{\text{Tx}} = \mathcal{J}_{\text{Tx}}$. The GTD design in this case is reduced to the SVD design.

4.4.2 Data Rate Maximization for the SVD Based SWIPT System

The aim in this section is to design a point-to-point SVD based MIMO SWIPT transceiver for maximizing the data rate. The following optimization problem is introduced for the proposed design

$$\underset{p_i, a_i}{\text{maximize}} \quad C = \sum_{i \in \mathcal{K}} \log_2 \left(1 + \frac{a_i p_i \sigma_i^2}{\sigma^2}\right), \tag{4.38a}$$

$$\text{s.t.} \quad \sum_{i \in \mathcal{K}} (1 - a_i) \eta p_i \sigma_i^2 \geqslant EH, \tag{4.38b}$$

$$0 \leqslant p_i \leqslant P_{\max},\ a_i \in \{0,1\},\ i \in \mathcal{K}. \tag{4.38c}$$

The problem above can be simplified by linearizing product term $a_i p_i$ in (4.38a) and (4.38b) using Proposition 4.1. Therefore, problem (4.38) can be reformulated as follows:

$$\underset{p_i, \tilde{p}_i, a_i}{\text{maximize}} \quad C = \sum_{i \in \mathcal{K}} \log_2 \left(1 + \frac{\tilde{p}_i \sigma_i^2}{\sigma^2}\right), \tag{4.39a}$$

$$\text{s.t.} \quad \sum_{i \in \mathcal{K}} \eta (p_i - \tilde{p}_i) \sigma_i^2 \geqslant EH, \tag{4.39b}$$

$$\tilde{p}_i \leqslant a_i P_{\max},\ \tilde{p}_i \leqslant p_i,\ i \in \mathcal{K}, \tag{4.39c}$$

$$\tilde{p}_i \geqslant p_i - (1 - a_i) P_{\max}, \tilde{p}_i \geqslant 0,\ i \in \mathcal{K}, \tag{4.39d}$$

$$0 \leqslant p_i \leqslant P_{\max},\ a_i \in \{0,1\},\ i \in \mathcal{K}, \tag{4.39e}$$

where (4.39c) and (4.39d) constraints are used to linearize the product term $a_i p_i$. Problem (4.39) can be solved numerically using CVX package.

4.5 Numerical Results

In this section, simulation results are presented to compare the performance of GTD and SVD based precoding methods for SWIPT. A Rayleigh block fading spatially uncorrelated MIMO channel $\mathbf{H}$ with symmetric antenna setup $N_t = N_r = 6$ is assumed in all simulations. The elements of $\mathbf{H}$ are independent ZMCSCG variables with variance $\sigma_h^2 = ad^{-\gamma}$ where $a = 0.1$ is the path loss factor, $d = 12$ m is the distance between the transmitter and the receiver and $\gamma = 3$ represents the path loss exponent. The noise power σ^2 is set to -50 dBm and the energy conversion efficiency η is set to 0.66. The power is measured in watts (W) and the information rate is measured in bits per channel use (bps/Hz). In all the simulations, the results are averaged over 10000 independent channel realizations using Monte Carlo simulations. In all figures, the blue color refers to GTD based SWIPT plots while the red color refers to the SVD based SWIPT plots.

A. Transmit Power Minimization

This section presents numerical results to evaluate the GTD and the SVD based SWIPT transceiver designs for power minimization. In Figure 4.2, the plots with lines refer to the optimal the GTD and the SVD optimal solution designs that are developed in Subsection 4.2.1 and Subsection 4.2.3, respectively, while the plots with makers denote the suboptimal GTD design that is presented in Subsection 4.2.2. Figure 4.2 shows the outage probability of the GTD and the SVD designs for different data rate C and energy harvesting EH requirements. In Figure 4.2a, the GTD designs have remarkably less outage probability than the SVD design. For example, at maximum transmit power per subchannel $P_{\max} = 1$ W, both optimal and suboptimal GTD designs shows outage probability roughly equal to 3% while the optimal SVD design shows outage probability up to 30% when $C = 15$ bps/Hz and $EH = 0.6$ mW. In Figure 4.2b, when EH is fixed, it can be observed that the large increase in the data rate requirement leads to a significant rise in $P_{\max}$ at the SVD design in comparison with GTD designs. For example, increasing C from 10 bps/Hz to 18 bps/Hz while maintaining outage probability up to 10% and $EH = 0.35$ mW, forces the SVD design to increase $P_{\max}$ approximately by 0.7 W. On the other hand, the GTD designs need to rise $P_{\max}$ by only 0.35 W to maintain the same

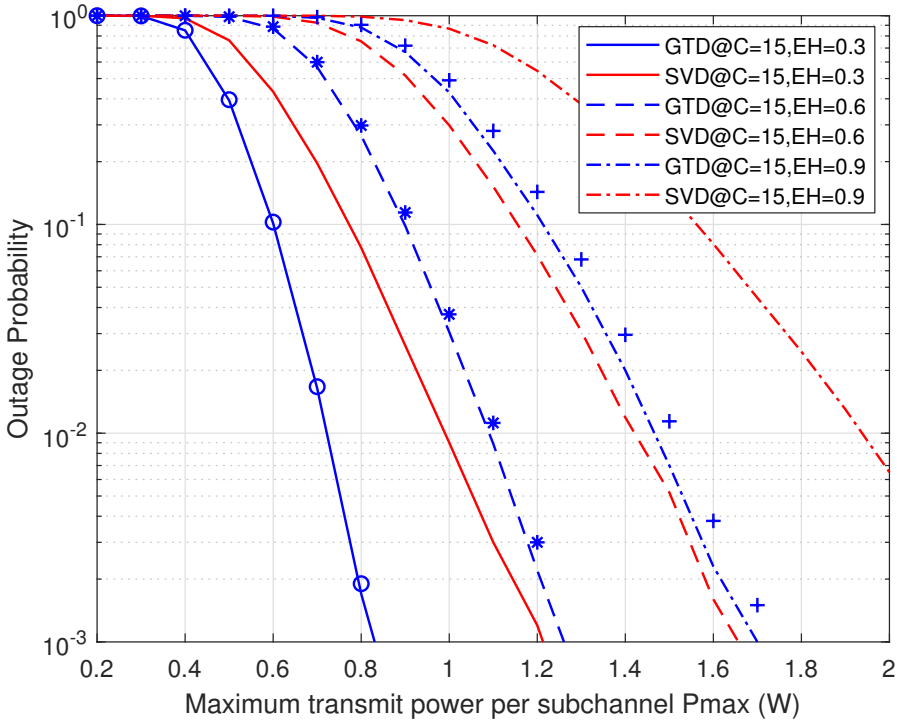

(a) Varying energy harvesting constraint

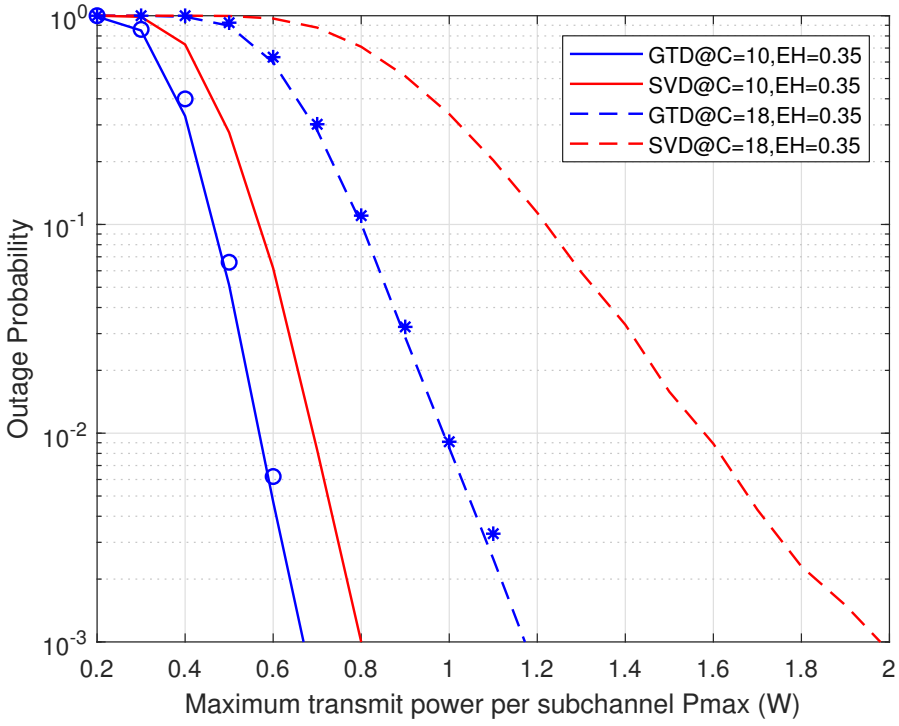

(b) Varying information rate constraint

Figure 4.2: Outage probability vs. maximum transmit power per subchannel $P_{\max}$ for different energy harvesting and rate requirements (C in bps/Hz, EH in mW).

conditions above.

The improvement in the performance of the GTD designs over its counterpart the SVD design is due to the fact that the highest gain subchannels can be used jointly for information and energy transfer which is not allowed in the SVD design. Also, it can be noted that the optimal and the suboptimal GTD designs both yield a comparable performance. This is because the two designs assign the highest gain subchannels for joint information and energy transmissions. However, there is a minor loss in the performance of the suboptimal GTD design in comparison to the optimal GTD design and this is expected since the power allocation is carried out over limited number of the subchannel assignments in the suboptimal design.

B. Energy Harvesting Maximization

In this section, the results of the GTD and the SVD energy harvesting maximization transceiver designs are introduced. The results of the optimal GTD approach are obtained by following similar approach to that is introduced in Subsection 4.2.1 while the results of the suboptimal GTD approach are obtained according to the development that is presented in Subsection 4.3.1. The results of the SVD approach are obtained based on the setup that is developed in Subsection 4.3.2.

Figure 4.3 plots the harvested energy EH versus the maximum transmit power per subchannel $P_{\max}$ considering different values of data rate requirements C. In Figure 4.3, the energy harvested in the GTD based SWIPT approach increases steeply with the rise of $P_{\max}$. In contrast, the plots representing the SVD based SWIPT approach show relatively low increase in the harvested energy as $P_{\max}$ increases. For example, the energy harvested by the GTD approach increases by 1 mW each time $P_{\max}$ has 0.5 W rise when C = 8 bps/Hz while the SVD approach gains approximately 0.6 mW. Furthermore, the GTD approach maintains more harvested energy than the SVD approach and at the same time attains higher data rate when $P_{\max}$ is fixed. This can be shown when $P_{\max}$ is set to 0.8 W, the GTD approach maintains 0.28 mW more energy and 4 bps/Hz higher data rate than the SVD approach.

Figure 4.4 shows the harvested energy against the data rate constraint for different $P_{\max}$. It is very clear that the GTD approach shows significantly high harvested energy

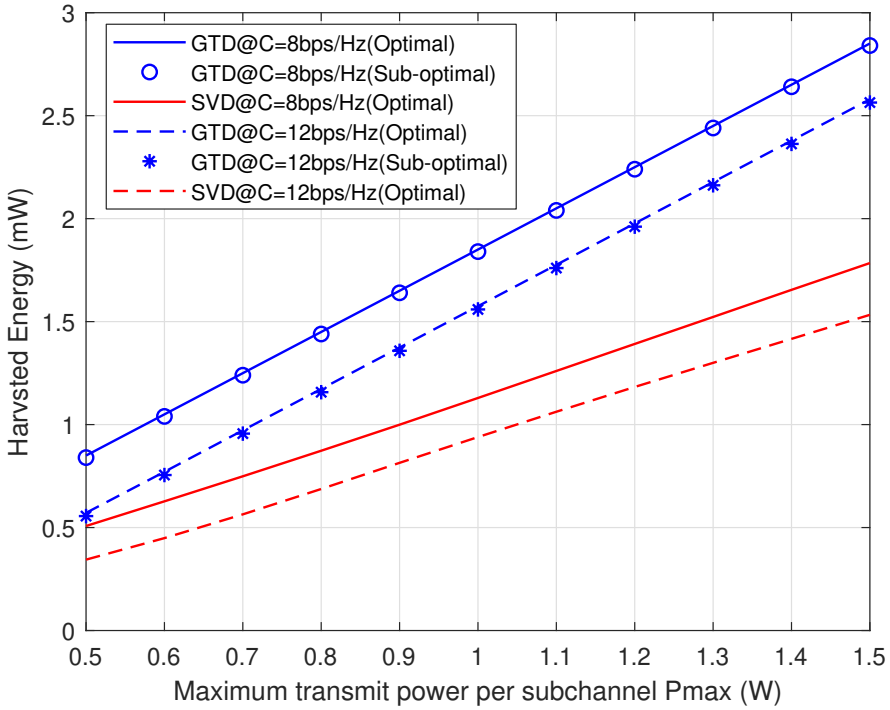

Figure 4.3: Harvested energy vs. maximum transmit power per subchannel $P_{\max}$ for different data rate requirements C.

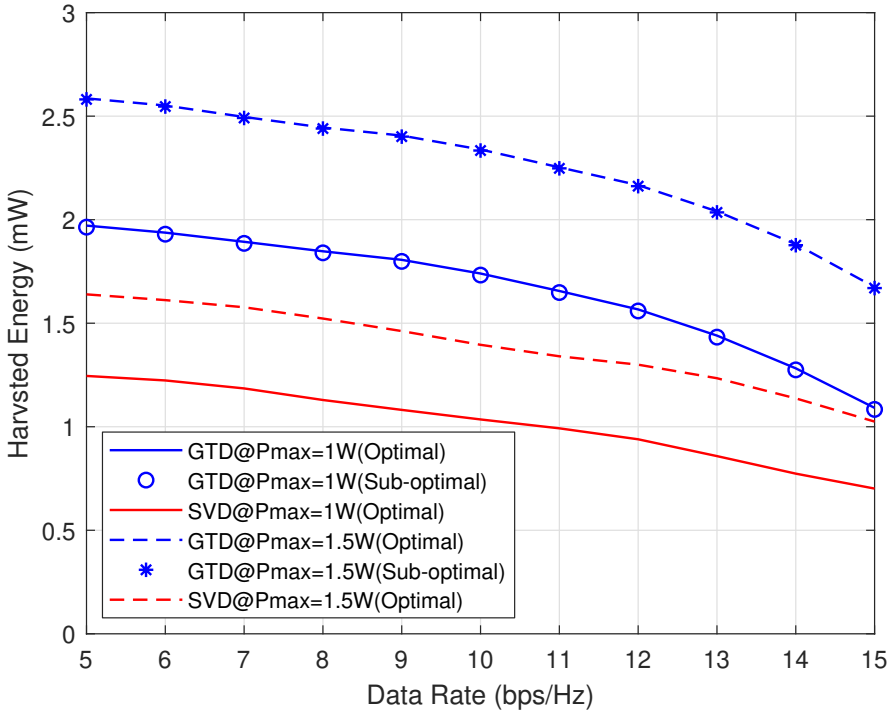

Figure 4.4: Harvested energy vs. data rate C for different values of $P_{\max}$.

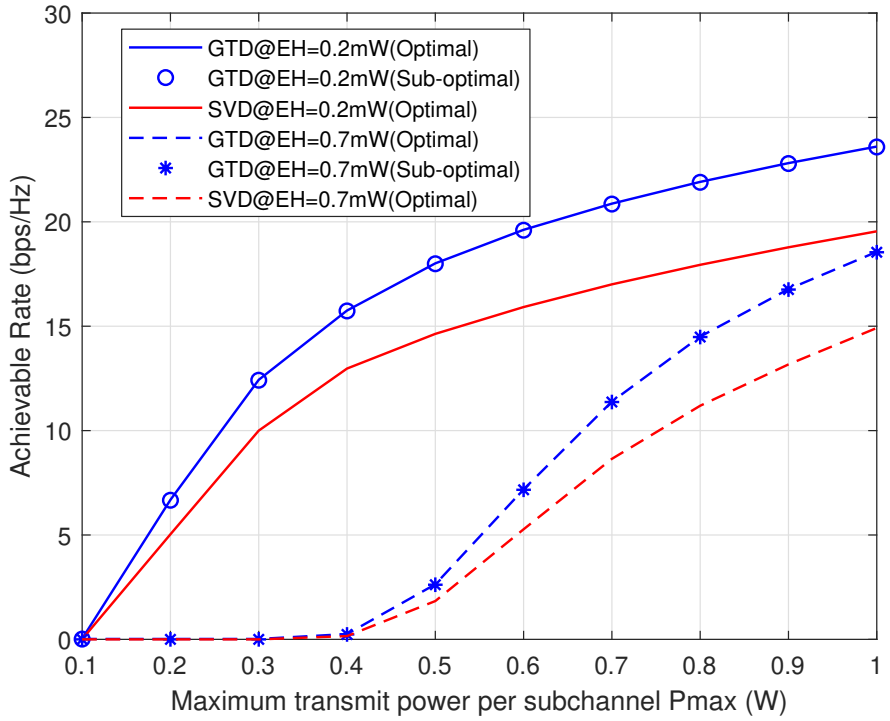

Figure 4.5: Achievable rate vs. maximum transmit power per subchannel $P_{\max}$ for different energy harvesting requirements EH.

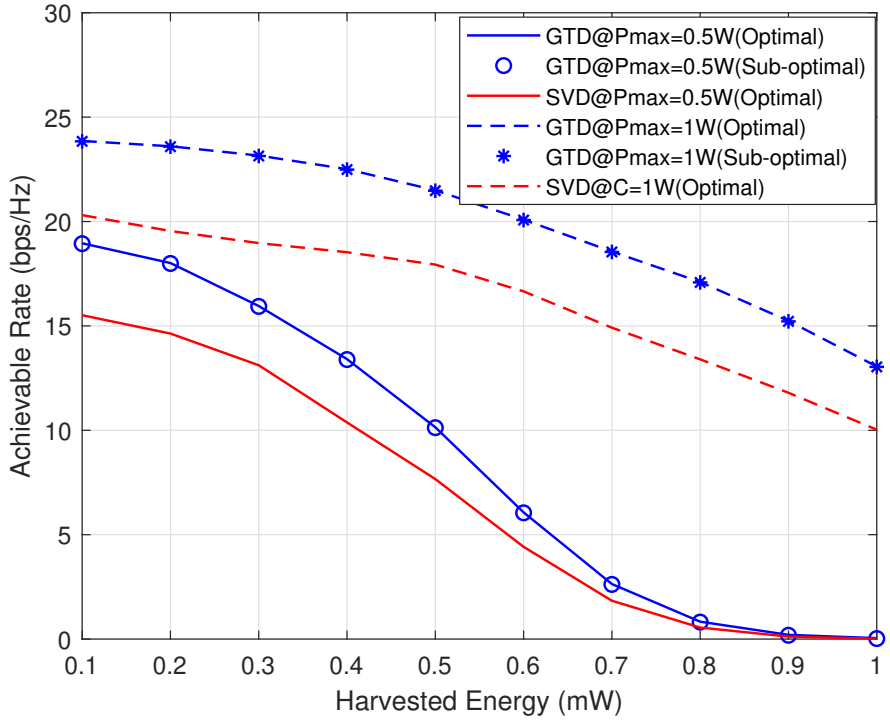

Figure 4.6: Achievable rate vs. energy harvesting constraint EH for different $P_{\max}$.

in comparison to SVD approach for any value of C and $P_{\max}$. For example, when C is fixed to 10 bps/Hz and $P_{\max}$ is set to 1.5 W, the GTD approach can scavenge 40% more energy than the SVD approach.

The superior performance that is introduced by the GTD approach is because the highest gain subchannel at the transmitter are always preserved for energy and information transfer. Unlike the GTD approach, any subchannel in the SVD approach is used either for information exchange or energy transfer.

It can be observed from the plots in Figure 4.3 and Figure 4.4 that both the optimal and the suboptimal GTD designs have equivalent performance. This is expected since both solutions use the subchannels of the highest gains for joint information and energy jointly.

B. Data Rate Maximization

This section introduces simulation results to evaluate the GTD and SVD based SWIPT designs for data rate maximization. The results of the optimal are obtained by following the MISCOP solution that is developed in Subsection 4.2.1 and the results of the of the suboptimal GTD are obtained based on the developments in Subsection 4.4.1. The results of the SVD design are plotted based on the solution in Subsection 4.4.2.

In Figure 4.5, the achievable rate C of the GTD and the SVD designs are plotted versus the maximum transmit power per subchannel $P_{\max}$ under different energy harvesting EH constraints. It can be observed that when $P_{\max}$ is sufficient to satisfy EH constraint the GTD design achieves higher rate than the SVD design. Consider for example $P_{\max}$ = 0.6 W and EH = 0.2 mW, the achievable rate when using GTD design is approximately 19.5 bps/Hz while the SVD design achieves 14.5 bps/Hz. Also, it can be noted from Figure 4.5 that the achievable rate in the GTD design improves significantly with the rise of $P_{\max}$ in comparison with SVD design. It is worth noting that both designs have zero data rate when $P_{\max}$ is relatively low. This is expected since the both approaches have equivalent feasibility and the EH constraints are not satisfied when $P_{\max}$ is low.

Figure 4.6 plots the achievable rate of the GTD and the SVD design versus the EH for different $P_{\max}$ constraints. Similar to Figure 4.5, the curves in Figure 4.6 illustrate that the GTD design achieves better performance than the SVD design. The difference

in the performance between the two design is due to the flexible use of the subchannels in the GTD design where the information and energy signals can be transmitted jointly using any subchannel. Note that such flexibility does not exist in the SVD design.

Similar to energy harvesting maximization case, the results of the optimal and suboptimal GTD approaches show equivalent performance as the highest gains subchannels are used jointly for data and energy transfer.

4.6 Summary

In this chapter, the GTD and the SVD based SWIPT systems were restudied by considering maximum transmit power per subchannel constraint instead of the instantaneous total power constraint that is used in the previous chapter. Unlike the developments proposed in the previous chapter, the deigns in this chapter require to develop new power allocation and subchannel assignment in order to comply with the limitations that are imposed by the new transmit power constraint. In all the GTD based SWIPT transceiver designs, the GTD structure was exploited to allow the transmitter to convoy information and energy signals jointly using the highest gain subchannels.

The first design developed in this chapter was the GTD based SWIPT transmit power minimization transceiver. Although the examined optimization problem of this particular design is combinatorial and nonlinear, MISCOP formulation was proposed to obtain jointly the optimal power allocation and subchannel assignment at the transmitter. The form of $\mathbf{r}$ that is used to decompose $\mathbf{\Sigma}(\mathbf{P}^{\star})^{1/2}$ in order to design precoder $\mathbf{F}$ and the receive-side matrix $\mathbf{W}$ introduced in this chapter. To complete the transceiver design, Theorem 4.1 proposed to define the optimal subchannel assignment at the receiver. However, the optimal solution has in general exponential complexity due to the MISCOP formulation of the joint power allocation and subchannel assignment problem. Hence, a suboptimal solution that obtains near-optimal power allocation by examining only a limited number of subchannel assignments developed in this chapter. The suboptimal solution is used in the next sections to design GTD transceivers for energy harvesting maximization and data rate maximization.

For comparison purpose, SVD based SWIPT transceivers for transmit power minimization, energy harvesting maximization and data rate maximization were also presented in

this chapter. Note that SVD design for transmit power minimization was introduced in [14, 16] whereas the SVD designs for energy harvesting maximization and data rate maximization were developed in this chapter. In all the SVD designs, the optimal power allocation and subchannel assignment were obtained jointly by adopting the MISCOP formulation that is developed in [14, 16].

The numerical results showed that GTD based designs significantly outperform the state-of-the-art SVD designs. The outstanding improvements that introduced in the GTD designs arose from the fact that the highest gain subchannels are used jointly to transfer information and energy signals.

Chapter 5

SS Based MIMO SWIPT Systems with Non-linear Energy Harvesting Model

5.1 Introduction

Energy harvesting (EH) circuit; *i.e.*, the rectifier plays an important role in SWIPT. The rectifier is used to convert the harvested RF signals to a DC voltage. The rectifier in its simplest form consists of a diode, low-pass filter and load as shown in Figure 5.1 [87]. Note that real-world applications may use more complicated rectifiers that involve various elements such as Schottky diodes and also designed based on different topologies such as single and multiple diodes [88].

The early studies of SWIPT, including the references mentioned in Section 2.2, have assumed that the conversion efficiency of the rectifier is constant and the input/output relation at the rectifier is always linear. Measurements and circuit simulations of rectifier implementations have shown that the linear proportional of the rectifier input/output is approximately true only when the rectifier input power is within a limited range that depends on the rectifier design [88–90]. Based on this observation, a simple parametric EH model that depends only on the received signal power was proposed in [17]. This model highlights an important feature of nonlinearity that arises from the saturation

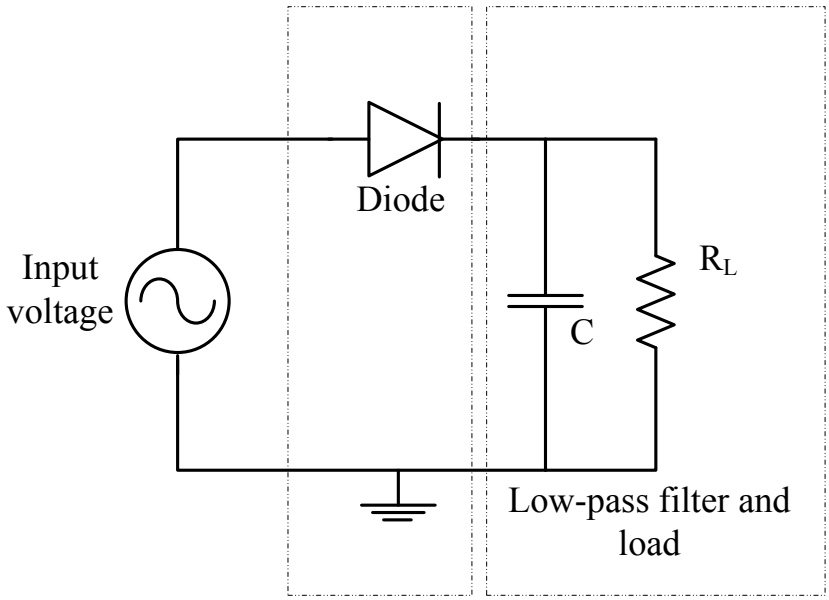

Figure 5.1: Simple representation of a rectifier [87]

.

of the converted DC power beyond a certain input RF power due to the EH circuitry [17, 87]. Due to its simplicity and ability to match the realistic EH efficiency quite well, the "saturation EH model" has been used extensively in the recent SWIPT literature. For example, the work in [91] used the saturation EH model in MIMO multiuser wireless powered communication networks (WPCN) where the problem of joint power allocation, user scheduling and beamforming was studied. The author in [92] studied the rate-energy region of PS/TS based SWIPT in point-to-point MIMO systems under the saturation EH model. In [93], the saturation EH model was adopted for multiple heterogeneous users in PS enabled SWIPT system where the optimal beamforming vectors that minimizes the transmit power at the BS and splitting ratio at each receiver were jointly obtained. The author in [94] investigated the adaptive switching mode between information decoding and energy harvesting in point-to-point SISO system where the saturation EH model is considered. The works in [95, 96] studied the resource allocation problem of SWIPT in CRN and NOMA-CRN, respectively, assuming the saturation EH model. In [97], an energy efficient SWIPT system was developed in multi-cell MISO networks where the saturation EH model is used. The research in [98] focused on maximizing the information rate of TS/PS based SWIPT system in AF relaying networks with the saturation EH

model whereas the work in [99] investigated the energy efficiency maximization of PS based SWIPT in two-way DF relaying networks consider the saturation EH model.

An alternative analytical model based on diode characteristics of the rectifier was proposed in [100]. It has been shown in this model that the harvested DC pwer is a function of the entire received signal waveform, not just the received power. Later research works [101–105] have investigated the use of this model for waveform design. Even though the diode-based model is more accurate than the EH saturation model when the rectifier input RF power is low, however, for fixed waveform and moderate-to-high input power at the rectifier, both EH models yield comparable results [87].

In the following, the saturation EH model is presented. The SS based SWIPT systems will be investigated under this model. The focus in this chapter will be on the energy harvesting maximization case.

5.2 The Saturation EH Model

In general, the energy conversion efficiency of the rectifier improves as the input RF power increases. This improvement is not infinite and the energy conversion efficiency starts diminishing when the input RF power exceeds a particular level. This occurs when the input RF is very large in which the voltage drop at the diode is larger than the reverse breakdown voltage [89].

The saturation EH model is a parametric model proposed in [17] and captures the energy conversion efficiency dependencies on the input RF power. The saturation EH model is constructed by fitting to realistic measurements of rectifier implementations based on curve fitting techniques [17]. According to [17], the harvested energy is modeled as

$$EH = M \cdot \frac{1 - e^{-up^{RF}}}{1 + e^{-up^{RF}+uv}}, \tag{5.1}$$

where p^{RF} is the RF input power at the EH circuit. Parameter M is the maximum harvested power when the rectifier is saturated due to an extremely large input RF power and constants u and v capture the effect of the EH circuit elements, such as resistance and capacitance. The set of parameters $\{M, u, v\}$ are found by curve fitting on the measurements of a given EH circuit, as illustrated in Figure 5.2. Note that now the EH efficiency

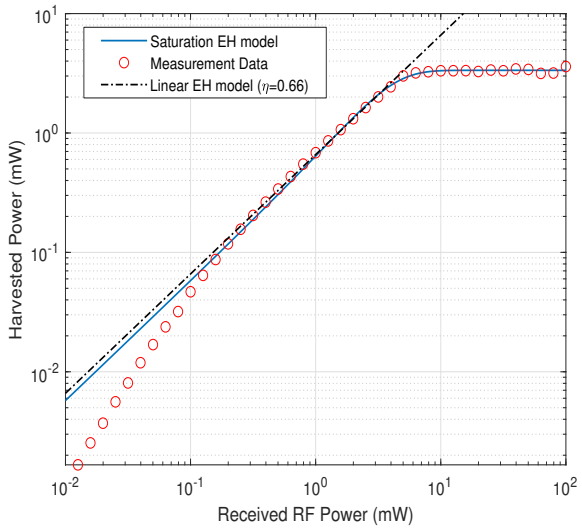

(a) $M = 3.348$, $u = 0.6152$ and $v = 1.55$. Measurement data from [106].

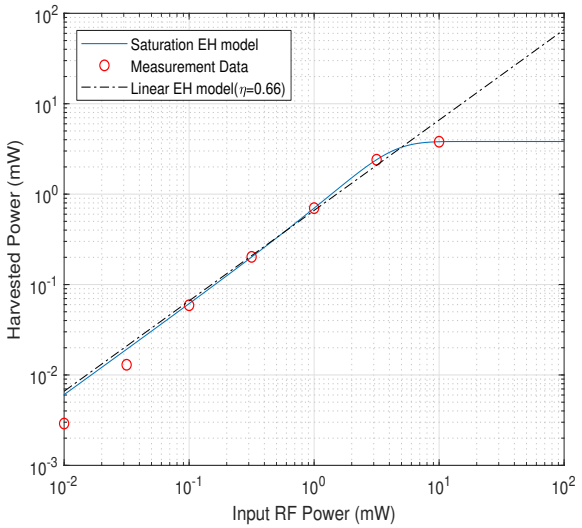

(b) $M = 3.821$, $u = 0.6606$ and $v = 1.794$. Measurement data from [107].

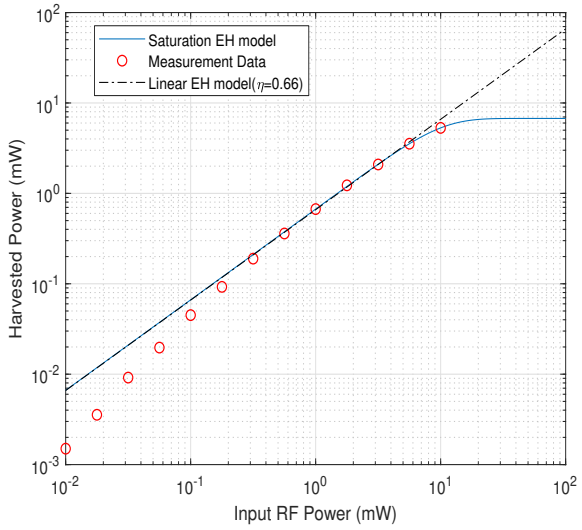

(c) $M = 6.745$, $u = 0.2231$ and $v = 1.059$. Measurement data from [108].

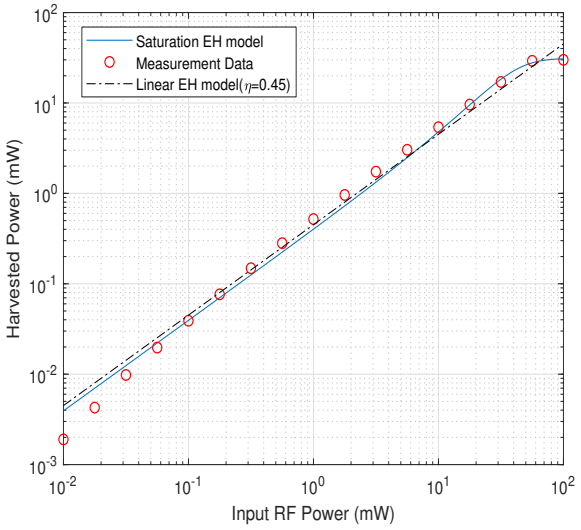

(d) $M = 30.96$, $u = 0.06897$ and $v = 21.59$. Measurement data from [109].

Figure 5.2: Comparison between the saturation EH model given by (5.1), the linear EH model, and measurements data from practical EH circuits. The parameters M, u and v in (5.1) were obtained by a standard curve fitting tool when the rectifier input power p^{RF} is in mWs.

$\eta(p^{RF}) = EH/p^{RF}$ is not a constant but a non-linear function of the rectifier input power p^{RF}.

It is clear that for each of the considered circuit there is a minimum input power above which the saturation EH model yields a good approximation to the practical implementation. This minimum power depends on the circuitry, but typically is around 0.1 mW, as was also stated in [87]. One can also observe from Figure 5.2, that the considered rectifiers operate efficiently and are approximately linear between input powers ranging from 0.1 mW to few mWs. This implies that the given rectifiers should be used in applications where the EH requirement is of the same order; otherwise RF power is wasted for operating in the inefficient or the saturation region of the rectifier. To deal with high EH requirements issue that is marginally closed to M, a reconfigurable rectifier that works efficiently in dynamic regions of input RF powers can be used [110]. Another possible solution is to split the received RF power over multiple rectifiers so each single rectifier avoids working at the saturation region [111, 112]. In this work, the multiple rectifiers solution is considered for the SS based SWIPT systems where the impact of applying this solution on the GTD and SVD based SWIPT is studied.

5.3 Transceiver Design for Energy Harvesting Maximization of SS Based MIMO SWIPT Systems With The Saturation EH Model

In general, the multiple rectifiers solution that are proposed in [111, 112] can be applied to the SS based SWIPT system by attaching multiple rectifiers to each single subchannel at the receiver, as illustrated in Figure 5.3. The following optimization problem describes the transceiver design objective.

$$\underset{\mathbf{P},\mathcal{I},\mathcal{J},\phi_{jn}}{\text{maximize}} \quad EH = \sum_{n\in\mathcal{N}} M_n \cdot \frac{1 - e^{-u_n \sum_{j\in\mathcal{J}} \phi_{jn} p_j^{RF}}}{1 + e^{-u_l \sum_{j\in\mathcal{J}} \phi_{jn} p_j^{RF} + u_n v_n}}, \tag{5.2a}$$

$$\text{s.t.} \quad \sum_{i\in\mathcal{I}} \log_2\left(1 + \rho(p_i)\right) \geqslant C, \tag{5.2b}$$

$$\sum_{n\in\mathcal{N}} \phi_{jn} = 1, \ \forall j \in \mathcal{J}, \tag{5.2c}$$

$$0 \leqslant \phi_{jn} \leqslant 1, \ \forall j \in \mathcal{J}, \ n \in \mathcal{N}, \tag{5.2d}$$

$$\sum_{k\in\mathcal{K}} p_k \leqslant P_t. \tag{5.2e}$$

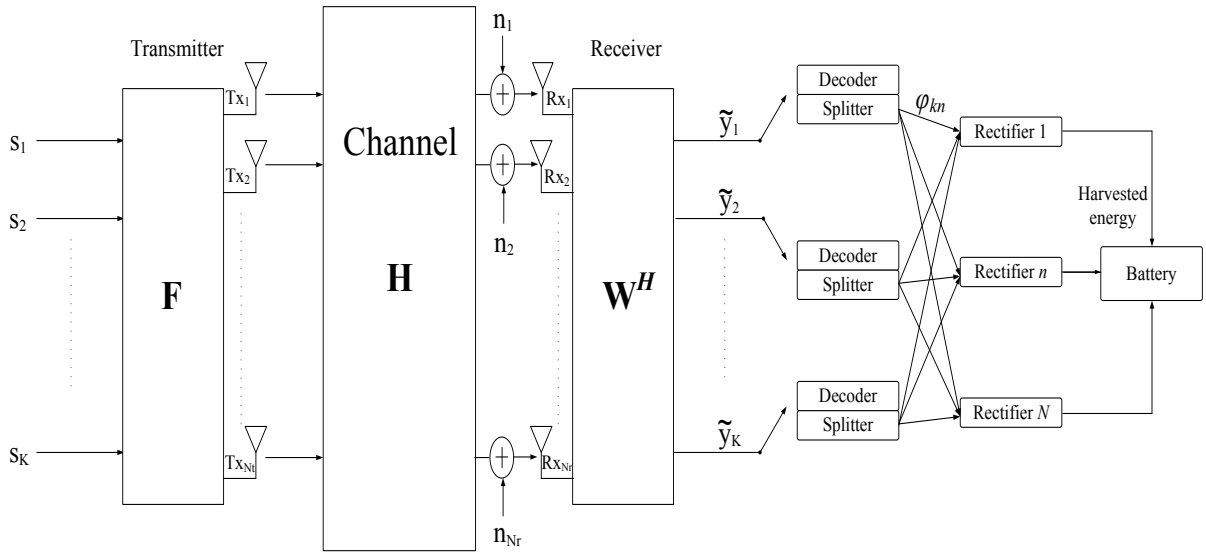

Figure 5.3: Combining the solution in [111, 112] with the SS based SWIPT system.

The sets $\mathcal{K} = \{1, 2, \ldots, K\}$ represents the total subchannels and both $\mathcal{I} \subset \mathcal{K}$ and $\mathcal{J} \subset \mathcal{K}$ denote to the sets of information bearing and energy harvesting subchannels, respectively, while $\mathcal{N} = \{1, 2, \ldots, N\}$ denotes to the number of rectifiers. The term $\rho(p_i)$ represents the signal-to-noise ratio of the i-th stream which is a function of the transmitted power p_i and ϕ_{jn} is the power splitting ratio from the j-th subchannel to the n-th rectifier.

In fact, The structure that is shown in Figure 5.3 is complex and difficult to implement from both practical and theoretical perspectives. From the practical side, implemented this structure is costly as it requires using splitters as many as the number of the available subchannel at the receiver where each splitter is connected to all rectifiers. As for the theoretical standpoint, obtaining the optimal power allocation jointly with the subchannel assignment and the splitting ratios require solving the optimization problem (5.2) which is combinatorial and non-concave. Problem (5.2) is combinatorial is due to the presence of the sets $\mathcal{I}$ and $\mathcal{J}$ as variables while the non-concavity of problem (5.2) is due to the objective function which is non-concave with respect to both p_j^{RF} and ϕ_{jn} [113, 114].

To avoid the complications mentioned above, a more simplified structure that uses only single subchannel for energy harvesting from which the received RF power is splitted over multiple rectifiers. The simplified structure leads to a reasonable realization from the practical point of view since only one splitter with multiple rectifiers are used. On the

other hand, finding the optimal power allocation and the subchannel assignment alongside the splitting ratio becomes tractable with this simplified structure as will be shown in the next sections.

5.3.1 Energy Harvesting Maximization for GTD Based SWIPT with The Saturation EH Model

Considering the simplified structure that is explained above and as illustrated in Figure 5.4, the energy harvesting maximization problem of the GTD based SWIPT is formulated as follows

$$\underset{\mathbf{P},\, \mathbf{r}\preceq\boldsymbol{\lambda},\, \mathcal{I}_{\mathrm{GTD}}\subset\mathcal{K}, j\in\mathcal{K},\, \phi_n}{\text{maximize}} \quad EH = \sum_{n\in\mathcal{N}} M_n \cdot \frac{1 - e^{-u_n\phi_n p_j^{RF}}}{1 + e^{-u_n\phi_n p_j^{RF} + u_n v_n}}, \tag{5.3a}$$

$$\text{s.t.} \quad \sum_{i\in\mathcal{I}_{\mathrm{GTD}}} \log_2\left(1 + \frac{R_{ii}^2}{\sigma^2}\right) \geqslant C, \tag{5.3b}$$

$$\sum_{n\in\mathcal{N}} \phi_n = 1, \tag{5.3c}$$

$$0 \leqslant \phi_n \leqslant 1,\ \forall n \in \mathcal{N}, \tag{5.3d}$$

$$\sum_{k\in\mathcal{K}} p_k \leqslant P_t, \tag{5.3e}$$

where $\left(p_j^{RF} = \sum_{j\in\mathcal{K}} \sum_{l=j}^{K} R_{jl}^2\right)$ represents the received RF power at the j-th subchannel. Note that there is only one subchannel assigned for energy harvesting, and hence, one splitter is used to split the received RF power over N rectifiers. Therefore, the number of the variables $\boldsymbol{\phi}$ is largely reduced from $J \times N$ in problem (5.2) to N in problem (5.3). Clearly, The reduction in the number of variables $\boldsymbol{\phi}$ makes the solution of problem (5.3) less complex.

Although problem (5.3) has a simplified form, it is still non-concave as its objective function is non-concave with respect to p_j^{RF} and ϕ_n [113, 114]. To overcome this issue, the optimal power allocation matrix $\mathbf{P}^\star$ is obtained at the first time and then optimizing the splitting ratios ϕ_n.

A. Optimal Power Allocation

To facilitate the process of finding the optimal power allocation $\mathbf{P}^\star$, the impact of p_j^{RF}

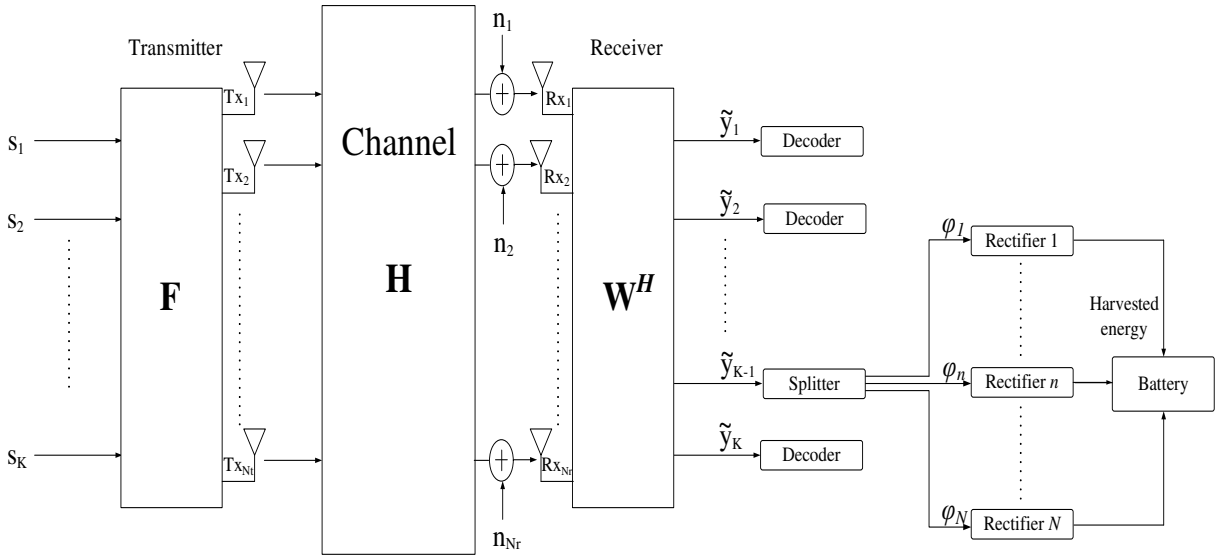

Figure 5.4: The simplified structure of the multiple rectifier solution for the GTD based SWIPT system.

on EH in (5.3) should be identified. It can be noted from Figure 5.3 that rising the value of p_j^{RF} results in an increment of EH; therefore, p_j^{RF} should be maximized in order to have EH maximized. This means the term $\left(\sum_{j\in\mathcal{K}}\sum_{l=j}^{K} R_{jl}^2\right)$ should be maximized. It is worth to be noted that, in the GTD based SWIPT, the power allocation matrix $\mathbf{P}$ is embedded in the matrix $\mathbf{R}$. Thus, obtaining the optimal power allocation $\mathbf{P}^\star$ requires solving the following optimization problem

$$\underset{\mathbf{P},\,\mathbf{r}\preceq\lambda,\mathcal{I}_{\mathrm{RX}}\subset\mathcal{K},\,j\in\mathcal{K}}{\text{maximize}} \quad \sum_{j\in\mathcal{K}}\sum_{l=j}^{K} R_{j,l}^2, \tag{5.4a}$$

$$\text{s.t.} \quad \sum_{i\in\mathcal{I}_{\mathrm{Rx}}} \log_2\left(1+\frac{R_{i,i}^2}{\sigma^2}\right) \geqslant C, \tag{5.4b}$$

$$\mathrm{tr}(\mathbf{F}\mathbf{F}^H) \leqslant P_t. \tag{5.4c}$$

Problem (5.4) is similar to problem (3.29) that is studied in section 3.5.1 ; therefore, Algorithm 5 can be applied to problem (5.4) and obtains $\mathbf{P}^\star$, $\mathbf{r}$, $\mathcal{I}_{\mathrm{RX}}$, and j. This leads to construct each of the precoder matrix $\mathbf{F}$ and the received-side matrix $\mathbf{W}$.

B. Optimal Split Ratios

After finding the optimal received RF power $p_j^{RF\star}$, the optimal split ratios can be

obtained by solving the following problem

$$\underset{\phi_n}{\text{maximize}} \quad EH = \sum_{n\in\mathcal{N}} M_n \cdot \frac{1 - e^{-u_n\phi_n p_j^{RF\star}}}{1 + e^{-u_n\phi_n p_j^{RF\star} + u_n v_n}}, \tag{5.5a}$$

$$\text{s.t.} \quad \sum_{n\in\mathcal{N}} \phi_n = 1, \tag{5.5b}$$

$$0 \leqslant \phi_n \leqslant 1. \tag{5.5c}$$

The objective function of problem (5.5) belongs to the class of fractional programming and is known in the literature as the sum-of-ratios problem that is in general non-convex optimization problem [113, 114]. The work in [114] has proposed a general solution to solve this type of problems. The solution developed in [114] is applicable to any sum-of-ratios problem if the single term of the ratios summation has a concave function in the numerator and convex function in the denominator while all the constraints are convex. By examining the objective function of (5.5), it can be easily verify that the numerator is concave function while the denominator is convex with respect to ϕ_n. Also, constraints (5.5b) and (5.5c) are convex; hence, the solution that is developed in [114] can be applied to solve problem (5.5).

According to [114],the solution of problem (5.5) is equivalent to the solution of the following problem

$$\begin{aligned} \underset{\phi_n}{\text{maximize}} \quad & \sum_{n\in\mathcal{N}} \kappa_n^\star \left[M_n \left(1 - e^{-u_n\phi_n p_j^{RF\star}}\right) - \tau_n^\star \left(1 + e^{-u_n\phi_n p_j^{RF\star} + u_n v_n}\right) \right], \\ \text{s.t.} \quad & \text{(5.5b) and (5.5b)}, \end{aligned} \tag{5.6}$$

where the parameters $\boldsymbol{\kappa} = [\kappa_1^\star, \ldots, \kappa_n^\star]$ and $\boldsymbol{\tau} = [\tau_1^\star, \ldots, \tau_n^\star]$ should satisfy the following equations:

$$\tau_n^\star \left(1 + e^{-u_n\phi_n^\star p_j^{RF\star} + u_n v_n}\right) - M_n \left(1 - e^{-u_n\phi_n^\star p_j^{RF\star}}\right) = 0, \tag{5.7a}$$

$$\kappa_n^\star \left(1 + e^{-u_n\phi_n^\star p_j^{RF\star} + u_n v_n}\right) - 1 = 0. \tag{5.7b}$$

Based on [114], problem (5.6) is solved for any given $\boldsymbol{k}$ and $\boldsymbol{\tau}$, and then optimal $\boldsymbol{k}^\star$ and $\boldsymbol{\tau}^\star$ are obtained from (5.7a) and (5.7b). Note that problem (5.6) is concave and all

the constraints are linear, and hence, it can be solved by a standard optimization solvers such as CVX package [86].

Next, a method that finds the optimal values of the parameters $\boldsymbol{\kappa}^{\star}$ and $\boldsymbol{\tau}^{\star}$ is presented. Define the following functions $\theta_n(\tau_n) = \tau_n \left(1 + e^{-u_n \phi_n p_j^{RF\star} + u_n v_n}\right) - M_n \left(1 - e^{-u_n \phi_n p_j^{RF\star}}\right)$ and $\theta_{N+l}(\kappa_l) = \kappa_l \left(1 + e^{-u_l \phi_l p_j^{RF\star} + u_l v_l}\right) - 1$, where $l \in \{1, 2, \ldots, N\}$. Based on [114], the optimal values of $\boldsymbol{\tau}^{\star}$ and $\boldsymbol{\kappa}^{\star}$ are obtained if $\boldsymbol{\theta}(\boldsymbol{\tau}, \boldsymbol{\kappa}) = [\theta_1, \theta_2, \ldots, \theta_{2N}] = \mathbf{0}$. Thus, the modified Newton method can be used to find the optimal $\boldsymbol{\tau}^{\star}$ and $\boldsymbol{\kappa}^{\star}$ iteratively as follows. In the q-th iteration, the parameters $\boldsymbol{\tau}^{(q+1)}$ and $\boldsymbol{\kappa}^{(q+1)}$ are updated, respectively, as given below

$$\boldsymbol{\tau}^{(q+1)} = \boldsymbol{\tau}^{(q)} + \zeta^{(q)} \mathbf{x}_{1:N}^{(q)}, \tag{5.8a}$$

$$\boldsymbol{\kappa}^{(q+1)} = \boldsymbol{\kappa}^{(q)} + \zeta^{(q)} \mathbf{x}_{N+1:2N}^{(q)}, \tag{5.8b}$$

where $\mathbf{x}^{(q)}$ is given as

$$\mathbf{x}^{(q)} = \frac{\boldsymbol{\theta}(\boldsymbol{\tau}^{(q)}, \boldsymbol{\kappa}^{(q)})}{\boldsymbol{\theta}^{'}(\boldsymbol{\tau}^{(q)}, \boldsymbol{\kappa}^{(q)})}, \tag{5.9}$$

and $\boldsymbol{\theta}^{'}(\boldsymbol{\tau}, \boldsymbol{\kappa})$ is the Jacobian matrix of $\boldsymbol{\theta}(\boldsymbol{\tau}, \boldsymbol{\kappa})$. $\zeta^{(q)}$ is the largest value of δ^m that satisfies

$$\left\| \boldsymbol{\theta}\left(\boldsymbol{\tau}^{(q)} + \delta^m \mathbf{x}_{1:N}^{(q)}, \boldsymbol{\kappa}^{(q)} + \delta^m \mathbf{x}_{N+1:2N}^{(q)}\right) \right\| \leqslant (1 - \nu \delta^m) \left\| \boldsymbol{\theta}(\boldsymbol{\tau}^{(q)}, \boldsymbol{\kappa}^{(q)}) \right\|, \tag{5.10}$$

where $m = \{1, 2, \ldots\}$, $\delta \in (0, 1)$, and $\nu \in (0, 1)$. According to [114], the modified Newton method converges to a unique solution $(\boldsymbol{\tau}^{\star}, \boldsymbol{\kappa}^{\star})$ that satisfy equations (5.7a) and (5.7b). Algorithm 10 summarize the solution to problem (5.5).

Algorithm 10 Solution to problem (5.5)

1: **Initialize** the maximum number of iteration Q, the maximum tolerance ϵ, $\kappa^{(q)}$, $\tau^{(q)}$, Choose $\delta \in (0, 1)$ and $\nu \in (0, 1)$.
2: **for** $q = 0$ to Q **do**
3: Using CVX, solve problem (5.6) to find $\boldsymbol{\phi}_n^{(q)}$ under given $\kappa^{(q)}$ and $\tau^{(q)}$
4: **if** $\|\boldsymbol{\theta}(\boldsymbol{\tau}, \boldsymbol{\kappa})\| \leqslant \epsilon$ **then**
5: **Set** $\boldsymbol{\phi}_n^{\star} = \boldsymbol{\phi}_n^{(q)}$ and **stop** this algorithm.
6: **else**
7: Update $\boldsymbol{\tau}^{(q+1)}$ and $\boldsymbol{\kappa}^{(q+1)}$ according to (5.8a)-(5.8b), and set $q = q + 1$.
8: **End if**
9: **End for**

C. Suboptimal Split Ratios

The optimal solution to problem (5.5) requires solving three different problems in an iterative manner as explained in the previous subsection. In this subsection, a less complex and suboptimal solution is proposed. This solution is based on dividing the total number of rectifiers into two sets; the active set and the idle set, and then the optimal received RF power $p_j^{RF\star}$ is uniformly splitted over the active set of rectifiers.

To specify the active set, we first find threshold values of power $\hat{\mathbf{p}} = [\hat{p}_1, \hat{p}_2, \ldots, \hat{p}_N]$ that satisfy the following equation

$$l \cdot \frac{1 - e^{-\frac{u\hat{p}_l}{l}}}{1 + e^{-\frac{u\hat{p}_l}{l} + uv}} = (l-1) \cdot \frac{1 - e^{-\frac{u\hat{p}_l}{l-1}}}{1 + e^{-\frac{u\hat{p}_l}{l-1} + uv}}, \forall l = \{2, 3, \ldots, N\}, \tag{5.11}$$

where $\hat{p}_1 = 0$. The active set is defined as $\hat{\mathcal{N}} = \{1, 2, \ldots, \hat{n}\}$ while $\hat{n}$ is computed as follows

$$\hat{n} = \max \left\{ l \,\middle|\, p_j^{RF\star} \geqslant \hat{p}_l \ \wedge \ l \in \{1, \ldots N\} \right\}. \tag{5.12}$$

The idle set is defined as $\overline{\mathcal{N}} = \{\hat{n} + 1, \ldots, N\}$. Hence, the split ratios are obtained as

$$\phi_n = \begin{cases} \frac{1}{\hat{n}}, & n \in \hat{\mathcal{N}}, \\ 0, & n \in \overline{\mathcal{N}}. \end{cases} \tag{5.13}$$

Note that each value of $\hat{p}_l$ is found by solving equation (5.11) using modified Newton method as explained below.

Define the following function:

$$\theta(\hat{p}_l) = \left(l \cdot \frac{1 - e^{-\frac{u\hat{p}_l}{l}}}{1 + e^{-\frac{u\hat{p}_l}{l} + uv}} - (l-1) \cdot \frac{1 - e^{-\frac{u\hat{p}_l}{l-1}}}{1 + e^{-\frac{u\hat{p}_l}{l-1} + uv}} \right). \tag{5.14}$$

We find the value of $\hat{p}_l$ that makes the function $\theta(\hat{p}_l) = 0$ in an iterative manner as follows. In q-th iteration, $\hat{p}_l^{(q+1)}$ is updated as

$$\hat{p}_l^{(q+1)} = \hat{p}_l^{(q)} + \zeta^{(q)} x^{(q)}, \tag{5.15}$$

where $x^{(q)}$ is given as

$$x^{(q)} = \frac{\theta\left(\hat{p}_l^{(q)}\right)}{\theta'\left(\hat{p}_l^{(q)}\right)}, \tag{5.16}$$

and $\theta'(\hat{p}_l)$ is first derivative of $\theta(\hat{p}_l)$. The factor $\zeta^{(q)}$ is the largest value of δ^m that satisfies

$$\left|\theta\left(\hat{p}_l^{(q)} + \delta^m x^{(q)}\right)\right| \leqslant (1 - \nu\delta^m)\left|\theta\left(\hat{p}_l^{(q)}\right)\right|, \tag{5.17}$$

where $m = \{1, 2, \ldots\}$, $\delta \in (0,1)$ and $\nu \in (0,1)$. The modified Newton method finds a unique solution $\hat{p}_l$ that satisfies equation (5.14) [115]. It is worth noting that the split ratios can be found easily after obtaining the threshold values $\hat{\mathbf{p}}$ which requires solving a single variable equation. In fact, all the threshold values $\hat{p}_l$ can be obtained only one time and used in the future transmissions to compute the split ratios. Algorithm 11 summarizes the suboptimal solution. Note that steps (1-10)in Algorithm 11 are implemented only once to specify the threshold powers $\hat{p}_l$.

Finally, using Algorithm 5 that maximizes the received RF power together with Algorithm 10 or Algorithm 11 completes the GTD based SWIPT energy harvesting maximization transceiver design.

Algorithm 11 Sub-optimal split ratios

1: **for** $l = 2$ to N **do**
2: **Initialize** the maximum number of iteration Q, the maximum tolerance ϵ, $\hat{\mathbf{p}}^{(q)}$, Choose $\delta \in (0,1)$ and $\nu \in (0,1)$.
3: **for** $q = 0$ to Q **do**
4: **if** $\theta\left(\hat{p}_l^{(q)}\right) \leqslant \epsilon$ **then**
5: **Set** $\hat{p}_l = \hat{p}_l^{(q)}$ and set $l = l + 1$.
6: **else**
7: Update $\hat{p}^{(q+1)}$ according to (5.15), and set $q = q + 1$.
8: **End if**
9: **End for**
10: **End for**
11: Find the active set $\hat{\mathcal{N}} = \{1, \ldots, \hat{n}\}$, where $\hat{n}$ is found based on (5.12).
12: Find the idle set as $\overline{\mathcal{N}} = \mathcal{N} \setminus \hat{\mathcal{N}}$.
13: Compute the split ratios ϕ_n according to (5.13).

5.3.2 Energy Harvesting Maximization for SVD Based SWIPT with The Saturation EH Model

Let consider the simplified structure that is explained earlier. The following optimization problem describes the SVD based SWIPT transceiver design objective

$$\underset{\mathbf{P},\, \mathcal{I}_{\mathrm{SVD}}\subset\mathcal{K}, e\in\mathcal{K},\, \phi_n}{\text{maximize}} \quad EH = \sum_{n\in\mathcal{N}} M_n \cdot \frac{1 - e^{-u_n\phi_n p_e^{RF}}}{1 + e^{-u_n\phi_n p_e^{RF} + u_n v_n}}, \tag{5.18a}$$

$$\text{s.t.} \quad \sum_{i\in\mathcal{I}_{\mathrm{SVD}}} \log_2\left(1 + \frac{p_i\sigma_i^2}{\sigma^2}\right) \geqslant C, \tag{5.18b}$$

$$\sum_{n\in\mathcal{N}} \phi_n = 1, \tag{5.18c}$$

$$0 \leqslant \phi_n \leqslant 1,\ \forall n \in \mathcal{N}, \tag{5.18d}$$

$$\sum_{k\in\mathcal{K}} p_k \leqslant P_t, \tag{5.18e}$$

where $p_e^{RF} = p_e\sigma_e^2$ and $e \in \mathcal{K}$ is the energy harvesting assigned subchannel. Problem (5.18) is similar to problem (5.3); thus, the approach that is used in the Subsection 5.3.1 to solve problem (5.3) is applied to obtain the optimal solution of problem (5.18). That is, the optimal power allocation $\mathbf{P}^\star$ is obtained jointly with optimal subchannel assignment $\mathcal{I}_{SVD}^\star$ and $e^\star$ in the first step, and then the optimal/sub-optimal split ratios are found secondly.

A. Optimal Power Allocation

The optimal power allocation $\mathbf{P}^\star$ should be obtained in which p_e^{RF} is maximized and the powers p_i are enough to meet the rate requirement. This requires solving the following optimization problem

$$\underset{\mathbf{P},\, \mathcal{I}_{\mathrm{SVD}}\subset\mathcal{K},\, e\in\mathcal{K}}{\text{maximize}} \quad p_e^{RF} = p_e\sigma_e^2, \tag{5.19a}$$

$$\text{s.t.} \quad \sum_{i\in\mathcal{I}_{\mathrm{SVD}}} \log_2\left(1 + \frac{p_i\sigma_i^2}{\sigma^2}\right) \geqslant C, \tag{5.19b}$$

$$\mathrm{tr}(\mathbf{F}\mathbf{F}^H) \leqslant P_t. \tag{5.19c}$$

The problem above is similar to problem (3.32) that is presented and solved by Algorithm 6 in the Subsection 3.5.2 of Chapter 3. Therefore, Algorithm 6 is applied to problem (5.18) to find jointly the power allocation $\mathbf{P}^{\star}$ and the subchannel assignment $\mathcal{I}_{SVD}^{\star}$ and $e^{\star}$.

A. Obtaining The Split Ratios

The split ratios can be obtained by solving the following optimization problem

$$\underset{\phi_n}{\text{maximize}} \quad EH = \sum_{n\in\mathcal{N}} M_n \cdot \frac{1 - e^{-u_n\phi_n p_e^{RF\star}}}{1 + e^{-u_n\phi_n p_e^{RF\star} + u_n v_n}}, \tag{5.20a}$$

$$\text{s.t.} \quad \sum_{n\in\mathcal{N}} \phi_n = 1, \tag{5.20b}$$

$$0 \leqslant \phi_n \leqslant 1. \tag{5.20c}$$

Problem (5.20) is identical to the problem of finding the split ratios of the GTD based SWIPT design. Thus, Algorithm 10 can be applied to solve problem (5.20) and find the split ratios of the SVD based design optimally or Algorithm 11 can be used to obtain sub-optimal split ratios.

5.4 Numerical Results

This section presents numerical results to evaluate the GTD and SVD approaches under the saturation EH model. A spatially uncorrelated Rayleigh MIMO channel $\mathbf{H}$ is assumed. The entries of $\mathbf{H}$ are independent ZMCSCG random variables with variance $\sigma_h^2 = ad^{-\gamma}$ where $a = 0.1$ is the path loss factor, $\gamma = 3$ is the path loss exponent and d is the distance between the transmitter and the receiver measured in meters (m). The noise power is set to -60 dBm. A symmetric antenna setup $N_t = N_r = 4$ is assumed in all simulations. For the saturation EH model, the parameters in Figure 5.2a are used in the simulations, that is, $M_n = 3.348$ mW, $u_n = 0.6152$ and $v_n = 1.55$. The power is measured in watts (W) and the information rate is measured in bits per second per hertz (bps/Hz). The results are averaged over 10^5 independent channel realizations using Monte Carlo simulations.

In all figures, the blue color refers to the GTD based SWIPT and the red color to the SVD based SWIPT. Also, the lines denote to the results related to the optimal split ratios solution while the markers represents to the suboptimal split ratios case.

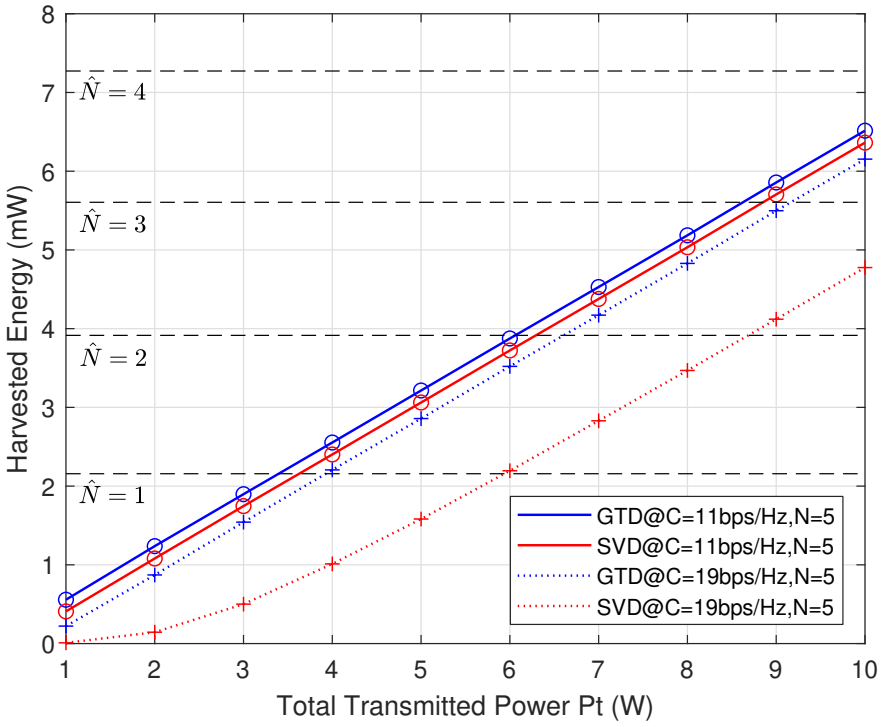

Figure 5.5: Harvested Energy vs. total transmit power constraint P_t for different rate requirements. The total number of rectifiers $N = 5$ and the distance $d = 10$ m.

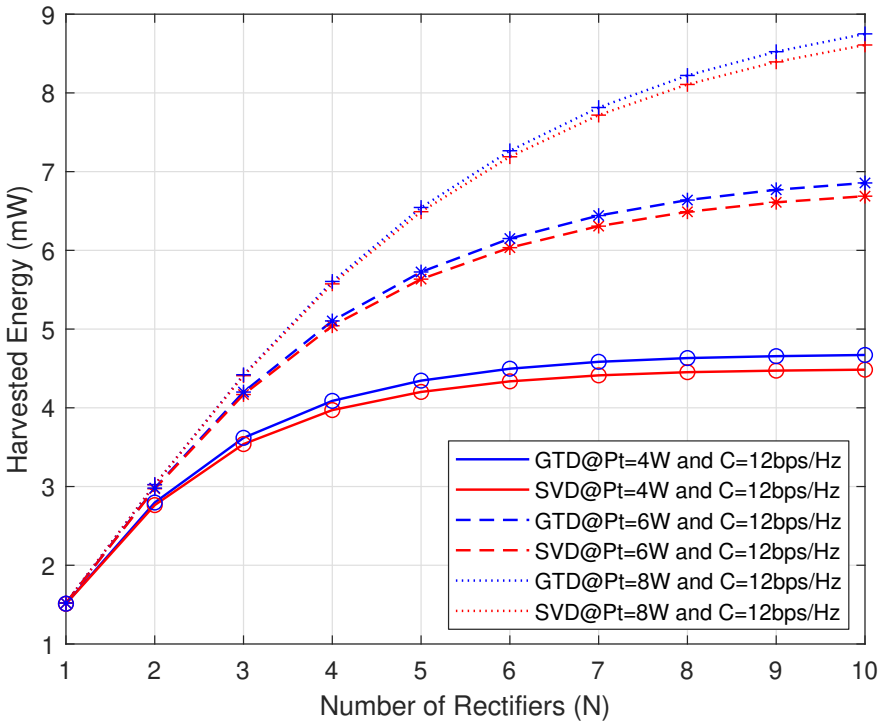

Figure 5.6: The impact of the number of rectifiers on the harvested energy for different transmit power and rate constraints with $d = 8$ m.

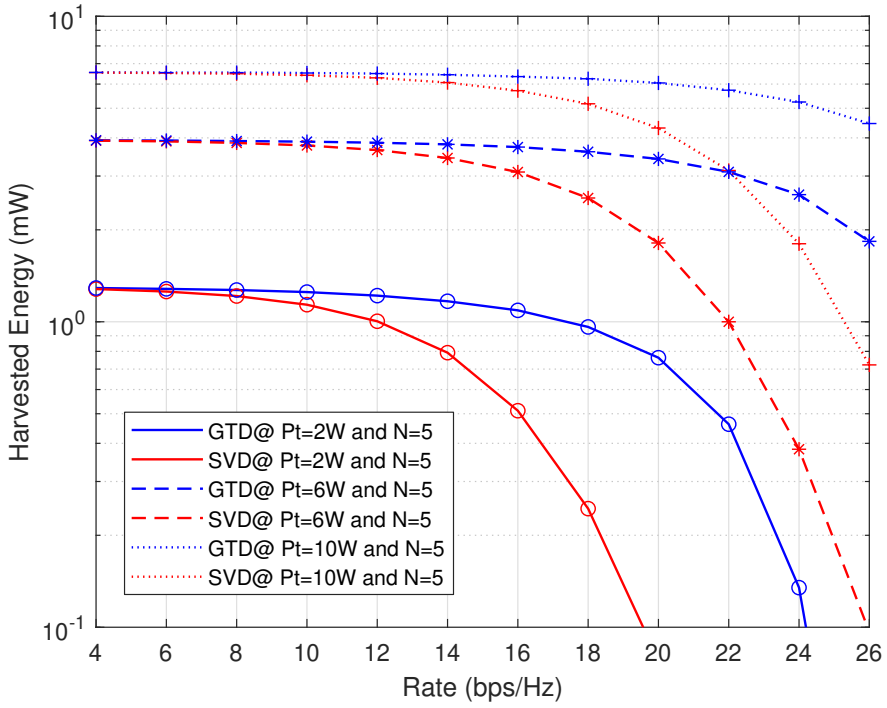

Figure 5.7: Harvested Energy vs. rate constraints C for different total transmit powers with number of rectifiers is $N = 5$ and $d = 10$ m.

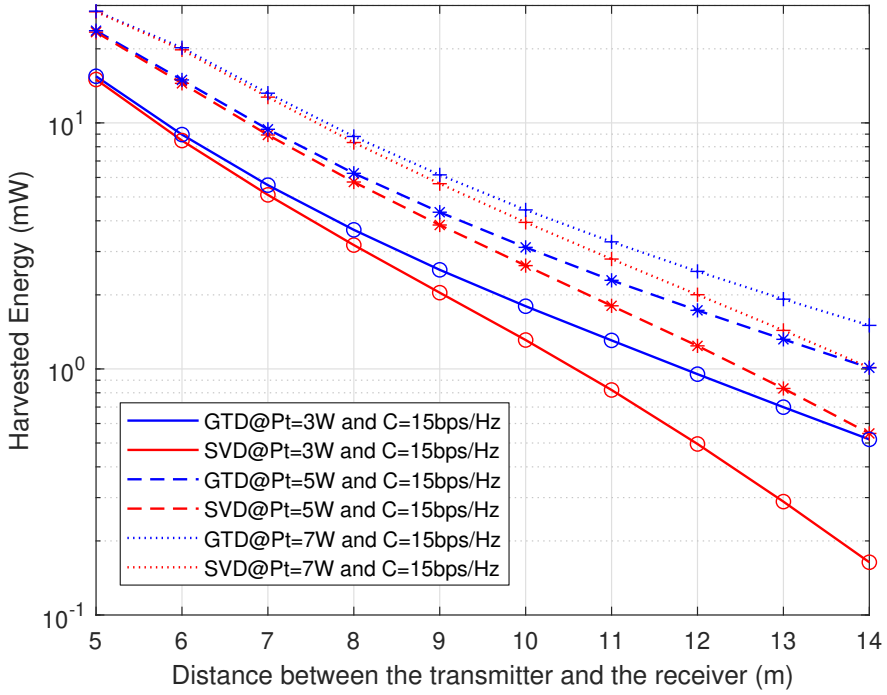

Figure 5.8: The effect of the distance between the transmitter and the receiver on the harvested energy for different total transmit power and fixed rate constraints .

Figure 5.5 plots the harvested energy using five rectifiers versus the total transmit power for different data rate requirements when the receiver is 10 m distant from the transmitter. Note that $\hat{N}$ in this figure represents the number of the active rectifiers that are used among the total available number of rectifies for energy harvesting whereas the horizontal dashed lines denote to the maximum energy that is harvested by each number of the active rectifiers. More details about specifying $\hat{N}$ can be found in Subsection 5.3.1.C.

In Figure 5.5, it can be noted that any significant increment in the data rate requirements reduces the energy harvested only marginally in the GTD approach. In contrast, the SVD approach suffers from a major loss in the harvested energy when the rate constraint is significantly increased. For example, increasing the rate constraint from $C = 11$ bps/Hz to $C = 19$ bps/Hz reduces the harvested energy only by approximately 0.35 mW in the GTD based SWIPT while the drop in the harvested energy reaches 1.4 mW in the SVD based SWIPT when the total transmitted power constraint is $P_t = 4$ W in both approaches. The difference in the performance between the approaches is due to the fact that highest gain subchannel is used for energy and information transmission simultaneously in the GTD approach while the use of any subchannel in the SVD approach is limited either for information or energy transmission.

Figure 5.6 illustrates the affect of the number of rectifiers on the harvested energy with distance $d = 8$ m. It is observed that at high transmitted power, for example $P_t = 8$ W, the harvested energy is remarkably increased when more rectifiers is used in both the GTD approach and the SVD approach.

Figure 5.7 demonstrates the harvested energy versus the rate constraint for different values of the total transmit power constraint with the number of rectifiers $N = 5$ and distance $d = 10$ m. Both approaches show comparable results at low and moderate information rate requirements, for example, both approaches harvest 1.29 mW when the information rate constraint $C = 6$ bps/Hz and the total transmit power constraint $P_t = 2$ W. This is because the data rate constraint is satisfied by applying relatively low transmit power to the low/moderate gains subchannel while the majority of the transmit power is used at the highest gain subchannel for energy transmission. However, the curves representing the SVD based SWIPT decay quickly as the information rate constraint

increases at any value of the transmit power. On the other hand, the GTD based SWIPT curves start to decay slowly as the information rate constraint increased specially when the total transmit power increases. For example, the GTD based SWIPT achieves EH = 0.96 mW while the SVD based SWIPT achieves only 0.24 mW at high information rate constraint and relatively low transmit power constraint, namely, C = 18 bps/Hz and P_t = 2 W. It can be observed when the data rate constraint is extremely high, the GTD based SWIPT harvests more energy than SVD based SWIPT in spit of using less transmitted power. For example, when the information rate constraint C = 24 bps/Hz, the GTD based SWIPT achieves EH = 2.6 mW with P_t = 6 W while the SVD based SWIPT attains EH = 1.8 W with P_t = 10 W. This remarkable improvements is due to the flexibility introduced by the GTD since it allows the use of the highest gain subchannel jointly for information transfer and energy harvesting.

Figure 5.8 shows the impact of the distance between the transmitter and the receiver on the harvested energy for different transmit power and fixed rate constraints. It is observed that both approaches show a steady drop in the harvested energy as the distance is increased. This is expected since increasing the distance reduces the subchannels gains. However, the GTD based SWIPT maintains higher energy harvesting values than its counterpart the SVD based SWIPT at any distance and total transmit power.

In all figures, the suboptimal solution of split ratios shows equivalent performance to the optimal solution that is obtained by using Algorithm 10. This is justifiable since the suboptimal solution ensures that each rectifier operates within the efficient region. This behavior is expected to be similar in the optimal solution.

5.5 Summary

This chapter studied the affect of using the saturation EH model on SS based SWIPT systems. A general transceiver design for energy harvesting maximization was presented. A more simplified design that uses single subchannel for energy harvesting with multiple rectifies was proposed to tackle the complexity introduced in the general design. The simplified design was applied for the GTD based SWIPT and the SVD based SWIPT where the optimal power allocation and subchannel assignment with the optimal/sub-

optimal split ratios were jointly obtained.

The numerical results illustrated that the use of simplified structure with multiple rectifiers provides efficient solution that avoids the saturation in each rectifier when the total number of rectifiers is relatively high. As expected, the figures in the numerical results showed that the GTD based SWIPT has a superior performance over the SVD based SWIPT. This is due to the flexibility introduced in the GTD approach where the transmitter can use the highest gain subchannel to send data and energy signals which is not possible in the SVD approach.

Chapter 6

Conclusions and Future Works

6.1 Conclusions

The work in this thesis focused on developing a novel approach for SWIPT, based on the GTD, in a point-to-point MIMO communication system. In this approach, the GTD structure is exploited to allow the transmitter to use the highest gain subchannels jointly for both energy transfer and information exchange while the receiver harvests energy and decodes information from separate received subchannels to comply with SS scheme requirements. In this study, three transceiver designs for MIMO SWIPT based on GTD were developed and tested under different circumstances. The performance of the developed designs was compared against the state-of-the-art SVD based designs.

In Chapter 2, a comprehensive overview on the techniques that enable SWIPT in different wireless networks topologies and configurations was presented. The concentration in this chapter was on defining the required tools and models to design SVD and GTD based SWIPT systems.

In Chapter 3, fundamental and key developments were introduced in Theorem 3.1, which is essentially used to construct and design different transceivers in the rest of this chapter. Based on the result derived in Theorem 3.1, three GTD based SWIPT transceivers were developed. Each transceiver targets one objective; minimizing the transmitted power, maximizing the harvested energy and maximizing the achievable rate with limited total transmit power at the transmitter. New algorithms were proposed to employ

the GTD to achieve the objective of each transceiver. In these algorithms, the optimal power allocation and the subchannel assignment that gives the optimal performance of each design were obtained. The developed algorithms have shown that the best eigenchannel in the GTD based SWIPT transceivers is adopted to carry signals used for information exchange and energy harvesting, where the information is decoded at the receiver from one stream and the energy is harvested from another particular stream at the receiver. This fact leads to two key advantages for the GTD based SWIPT transceivers over its SVD counterparts. The first advantage is that less transmitted power can be used to satisfy certain amounts of data rate and energy harvesting at the receiver, and a higher data rate can be achieved or more energy harvesting can be attained in the GTD based SWIPT transceivers. For example, to maintain an information rate equal to 14 bps/Hz and energy harvesting equal to 0.2 mW at the receiver, the proposed GTD approach uses only 48% of the average total transmitted power used by the SVD approach whenever the transmitter has sufficient power to satisfy the system rate and energy harvesting requirements. The second advantage of the GTD based transceivers is that the optimal power allocation is obtained by examining only one fixed subchannel assignment instead of examining K subchannel assignments in order to achieve the optimal power allocation in the SVD based transceivers. It is interesting to note that the transmit power minimization and the data rate maximization of SVD based SWIPT transceivers were also developed in this chapter for comparison purposes, whereas the SVD based SWIPT transceiver that maximizes the harvested energy was introduced in [76].

Chapter 4 restudied the transceivers that are developed in Chapter 3 considering a limited per subchannel transmit power constraint instead of the total transmit power constraint assumed in the designs of Chapter 3. This modification in the transmit power constraint turns the optimization problems associated with the GTD and SVD based SWIPT transceivers to be combinatorial ,and hence, the design structures such as the power allocation and the subchannel assignment are different from those designs that were developed in Chapter 3. For the GTD based SWIPT, two solutions were proposed to design a transceiver that minimizes the total transmitted power while meeting data rate and energy harvesting requirements. In the first solution, an optimal transceiver

design that has an exponential complexity was developed. In the second solution, a polynomial complexity transceiver design that achieves near optimal results (in most cases optimal) was proposed. This solution was adopted to design transceivers that maximize the harvested energy and the information rate. All the GTD based SWIPT transceivers showed that the subchannels corresponding to the highest gains are used to transmit information and energy jointly whereas these transmissions are separated at the receiver to match the requirements of the SS technique.

For comparison purposes, optimal SVD based SWIPT transceivers that maximize the harvested energy and the date rate were introduced in Chapter 4, and the transceiver that minimizes the total transmitted power was developed in [14, 16]. The numerical results demonstrated that all of the GTD based SWIPT transceivers have superior performance over the SVD based SWIPT transceivers.

In Chapter 5, the SS based SWIPT energy harvesting maximization transceiver design was studied when the saturation non-linear energy harvesting model presented in [17] is adopted. The general structure of the SS based SWIPT transceiver was described and the impact of using the saturation EH model on the transceiver design was also discussed. To overcome the complexity in the general structure of the SS based transceiver, a simplified structure that uses a single subchannel attached to multiple rectifiers for energy harvesting was proposed. Based on this simplified structure, GTD and SVD based SWIPT transceivers were developed where the optimal power allocation and subchannel assignment jointly with the optimal/suboptimal split ratios were obtained. Simulation results illustrated that the GTD approach harvests higher energy than the SVD approach.

Overall, the GTD approach exhibits better performance than the SVD approach when the system demands high data rate and works within noisy environments that involve interference such as the interference that is originated from the error in the channel estimation or the interference that is generated from other users operating within the same the frequency band. Therefore, the GTD approach would be a good option to enable SWIPT in systems that operate within the conditions mentioned above, for example, 5G systems. In general, 5G systems are expected to provide a high data rate (x1000 than the current 4G system provides) [116]. However, applying the GTD approach to 5G

systems requires more investigation. This includes testing the GTD approach assuming environments and parameters that capture 5G systems aspects such as the channel model, the distance, the number of antenna used at the transmitter and the receiver, etc[1]. Note that the numerical results presented in this thesis are not based on parameters that are used in particular applications as the aim of this study is to develop a new approach that tackle the limitations of the current state-of-the art SVD approach.

6.2 Future Works

The current GTD developments in this work can be extended to further theoretical and practical directions. Theoretically, the proposed GTD designs could be tested under the following conditions:

1. The developed transceivers can be tested assuming the case of imperfect CSI knowledge at the transmitter and receiver.

2. The work in this thesis can be evaluated considering the non-linear energy harvesting models such as the non-linear models that are proposed in [100]. In fact, considering this non-linear energy harvesting model leads to some modifications to transmit signal design in order to improve efficiency of the energy conversion [87]. Therefore, different signalling schemes that are developed in [102, 104, 117–122] could be applied to the proposed GTD approaches.

3. The GTD developments in this thesis can be examined assuming different wireless channel models that reflect more practical scenarios such using Rician fading channels or Nakagami-m fading channels.

Moreover, the proposed transceivers in this work could be extended into different network configurations, for example:

1. The GTD decomposition was used in [123, 124] as a framework to triangularize multi-user MIMO broadcasting channels, and therefore it is worth investigating the combination of the work in this thesis with the mentioned works above to generalize the proposed GTD based SWIPT for multi-user MIMO networks.

[1]This paragraph is the response to comment 1.

2. We remark that achieving the generalization in the point above could lead to other research directions, such as employing the SS technique based on GTD to enable SWIPT in AF/DF relay networks.

3. Incorporating SWIPT with physical layer security is a well-known research area, for example see the works in [125–136] and the references therein. We noted that the study in [137] has constructed an optimal coding scheme that achieves the secrecy capacity in MIMO networks that comprises two legitimate users and an eavesdropper. GTD was a fundamental tool in decomposing the MIMO wiretap channel in [137] and it would be worth incorporating the work in this thesis with the study in [137] to developed a solution for SWIPT systems based on GTD with secure connection requirements.

Another research avenue worth exploring in future is the practical implementation aspects of GTD based SWIPT. In fact, the research in [14] has addressed the main concern regarding the practical implementation of SS based SWIPT, that is, performing the required signal processing; *i.e.*, the channel matrix decomposition in the RF band. The study in [14] suggested to use analog passive electronic devices to tackle the practical limitation issue. Recently, there are works [138, 139] that have used passive electronic elements to perform analog eigenmode beamforming. According to [14], the techniques developed in [138, 139] could be used to implement the SVD based SWIPT approach. Hence, similar approaches to [138, 139] could be developed to implement the GTD based SWIPT design. In general, a practical implementation of the proposed GTD design would require efficient implementation of phase shifting, switching/multiplexing as well as implementing a complex switch-bar matrix operation in hardware including efficient control.

Appendices

Appendix A

One Subchannel is Optimal for Energy Harvesting

Let $\sigma_1 > \sigma_2 > \cdots > \sigma_K$ be the non-zero singular values of $\mathbf{H}$ and assume the energy harvesting constraint is EH. To show that one subchannel is optimal for energy harvesting, consider the following two scenarios that both satisfy the energy harvesting constraint

$$EH = p_n \sigma_n^2, \tag{A.1}$$

and

$$EH = \tilde{p}_n \sigma_n^2 + \tilde{p}_m \sigma_m^2, \tag{A.2}$$

where $n > m$ so that $\sigma_n > \sigma_m$ and $p_n, \tilde{p}_n, \tilde{p}_m > 0$ are the transmit powers required in both cases. Let $\beta > 0$ so that

$$\sigma_n^2 = \sigma_m^2 + \beta, \tag{A.3}$$

due to assumption $\sigma_n > \sigma_m$. Substituting (A.3) in (A.1) and (A.2) and equating yields

$$\left(\tilde{p}_n + \tilde{p}_m\right) \sigma_m^2 - p_n \sigma_m^2 = \beta \left(p_n - \tilde{p}_n\right), \tag{A.4}$$

where $\beta \left(p_n - \tilde{p}_n\right) > 0$ because $p_n > \tilde{p}_n$ due to (A.1) and (A.2). Therefore $p_n < \tilde{p}_n + \tilde{p}_m$.

Appendix B

Proof of Theorem 3.1

Let $\mathcal{J} = \{j\}$ so that the energy harvested at the GTD based receiver is given by

$$EH_{\text{GTD}} = \eta\big(R_{jj}^2 + R_{jj+1}^2 + \cdots + R_{jL}^2\big). \tag{B.1}$$

For simplicity, we assume that $\eta = 1$ where the proof is valid for any value of η. Substituting (2.10) in (2.13a) and following [81], it can be shown that the value of the diagonal element $R_{jj} = r_j$ is related to the off-diagonal elements on the same row as

$$R_{jj+1}^2 + \cdots + R_{jL}^2 = \frac{1}{R_{jj}^2}\big(\psi_j^2 - R_{jj}^2\big)\big(R_{jj}^2 - \omega_j^2\big), \tag{B.2}$$

where the parameters ψ_j and ω_j are set in the GTD algorithm during the j-th iteration as discussed in Section 2.3.2. From (B.1) and (B.2) the harvested energy as a function of the predefined diagonal elements $\mathbf{r}$ is thus given by

$$EH_{\text{GTD}} = r_j^2 + \frac{1}{r_j^2}\big(\psi_j^2 - r_j^2\big)\big(r_j^2 - \omega_j^2\big), \tag{B.3}$$

where the values of ψ_j and ω_j also depend on $\mathbf{r}$. Clearly (B.3) implies that for the subchannels $i \in \mathcal{I}_{\text{GTD}}$ carrying data, we must have $\psi_i = r_i$ or $\omega_i = r_i$ in the GTD algorithm at the i-th iteration to guarantee interference free information transmission.

The multiplicative majorization condition $\mathbf{r} \preceq \boldsymbol{\lambda}$ and ordering $\lambda_1 \geqslant \lambda_2 \geqslant \ldots \geqslant \lambda_L$

imply that

$$\lambda_L \leqslant r_k \leqslant \lambda_1, \quad \forall k = 1,2,\ldots,L, \tag{B.4}$$

where $\boldsymbol{\lambda}$ is a vector constructed from the diagonal elements of the matrix $\boldsymbol{\Sigma}(\mathbf{P}^\star)^{1/2}$. According to [81], the values of ψ_k and ω_k must satisfy

$$\lambda_L < \psi_k \leqslant \lambda_1, \tag{B.5a}$$

$$\lambda_L \leqslant \omega_k < \lambda_1, \tag{B.5b}$$

that together with (B.4) limit the range of C_{GTD} and EH_{GTD}. This leads to two different cases when $EH_{\mathrm{GTD}} = EH_{\mathrm{SVD}}$ is guaranteed, namely $C_{\mathrm{GTD}} = C_{\mathrm{SVD}}$ and $C_{\mathrm{GTD}} > C_{\mathrm{SVD}}$, depending on how the power and subchannels are allocated in the SVD based system as shown below.

Let us denote $e = e^\star$ for the subchannel assigned for energy harvesting by the SVD based precoder so that $\mathcal{E} = \{e\}$ and $\mathcal{I}_{\mathrm{SVD}} = \{1,\ldots,L\} \setminus \{e\}$ are the optimal subchannel assignments. The energy harvested $EH_{\mathrm{SVD}} = \lambda_e^2$ by the SVD based system satisfies $\lambda_L^2 \leqslant EH_{\mathrm{SVD}} \leqslant \lambda_1^2$. We show below that if $e \notin \{1, L\}$, the subchannels $\mathcal{J} = \{j\}$ and $\mathcal{I}_{\mathrm{GTD}} = \{1,\ldots,L\} \setminus \{j\}$ and the vector $\mathbf{r} \preceq \boldsymbol{\lambda}$ can be designed so that the energy harvested by the GTD based system (B.3) satisfies $EH_{\mathrm{GTD}} = EH_{\mathrm{SVD}}$ with $\lambda_L < r_j < \lambda_e$. Since the energy harvesting constraint is satisfied in part through interference, more power can be allocated to information transmission leading to information rate $C_{\mathrm{GTD}} > C_{\mathrm{SVD}}$. The special case $e \in \{1, L\}$, on the other hand, leads to $EH_{\mathrm{GTD}} = EH_{\mathrm{SVD}}$ and $C_{\mathrm{GTD}} = C_{\mathrm{SVD}}$.

According to (B.3), the contribution of interference to the harvested energy is highest when ψ_j is maximized and ω_j minimized. For given r_j, the constraints (B.5) imply that a maximum amount of interference is obtained when $\psi_j = \lambda_1$ and $\omega_j = \lambda_L$. However, ψ_j and ω_j are not free parameters but set during the j-th iteration of the GTD algorithm and depend in general on the first j entries $r_1, r_2, \ldots, r_j$ of $\mathbf{r}$. Based on the GTD algorithm discussed in Section 2.3.2, $\psi_j = \lambda_1$ and $\omega_j = \lambda_L$ can be obtained simultaneously if and only if energy is harvested from the subchannel $j = L - 1$ and

$$r_1 = \lambda_2;\ r_2 = \lambda_3;\ \ldots\ ;\ r_{L-2} = \lambda_{L-1}, \tag{B.6}$$

as given in (3.6). This implies that the GTD based system decodes information always from the subchannels $i = 1, 2, \ldots, L-2, L$ and there is no need for numerical optimization of subchannel assignment as in the SVD based system.

Based on the above, let us now fix the subchannel assignment for GTD as $\mathcal{J} = \{L-1\}$, $\mathcal{I}_{\text{GTD}} = \{1, \ldots, L-2, L\}$ and set $r_1, \ldots, r_{L-2}$ as in (B.6). Substitute $\psi_{L-1} = \lambda_1$, $\omega_{L-1} = \lambda_L$ and $EH_{\text{GTD}} = EH_{\text{SVD}} = \lambda_e^2$ into (B.3), so that after some algebraic manipulations we get r_{L-1} as given in (3.6). Since the interference term is maximized in (B.3), the value $r_{L-1} \leqslant \lambda_e$ is the minimum possible that satisfies the energy harvesting constraint $EH_{\text{GTD}} = EH_{\text{SVD}}$. The majorization condition, together with (B.6) provides r_L as also given in (3.6), and the only non-zero off-diagonal element in $\mathbf{R}$, R_{L-1L}, is given as (3.7) and follows from (B.3). The construction (3.6) satisfies now $\mathbf{r} \preceq \boldsymbol{\lambda}$ and yields a matrix $\mathbf{R}$ for which $EH_{\text{GTD}} = EH_{\text{SVD}} = \lambda_e^2$ given any power allocation $\mathbf{P}$ and subchannel assignment $\mathcal{E} = \{e\}$, $\mathcal{I}_{\text{SVD}} = \{1, \ldots, L\} \setminus \{e\}$ in the SVD based system.

Given $\mathbf{r}$ as described above, two cases can be identified depending on how the SVD based system allocates the energy harvesting subchannel, namely, 1) when $e \in \{1, L\}$; and 2) when $e \notin \{1, L\}$. In the first case (3.7) implies directly $r_{L-1} = \lambda_e$ and the interference term in (B.3) vanishes. Since $\mathbf{r}$ is now just a permutation of $\boldsymbol{\lambda}$, SVD and GTD based systems are equivalent so that $EH_{\text{SVD}} = EH_{\text{GTD}}$ and $C_{\text{GTD}} = C_{\text{SVD}}$. For the second case $r_{L-1} < \psi_{L-1} = \lambda_1$ and $r_{L-1} > \omega_{L-1} = \lambda_L$ so that the interference term in (B.3) is positive and $r_{L-1} < \lambda_e$. To show that this improves the rate of the GTD based system, the condition $\sum_{\mathcal{I}_{\text{GTD}}} \log_2(1 + r_i^2 \sigma^{-2}) > \sum_{i \in \mathcal{I}_{\text{SVD}}} \left(1 + \lambda_i^2 \sigma^{-2}\right)$ must hold. To check this condition is always true for the assignment discussed above, we write the achievable rate of the GTD system in term of λ's by using (B.6) and substitute the value of r_L as given in (3.6) to the above condition to obtain

$$\overbrace{\sum_{i=2}^{L-1} \log_2\left(1 + \frac{\lambda_i^2}{\sigma^2}\right) + \log_2\left(1 + \frac{\lambda_1^2 + \lambda_L^2 - \lambda_e^2}{\sigma^2}\right)}^{C_{\text{GTD}}} > \underbrace{\sum_{\substack{i=1 \\ i \neq e}}^{L} \log_2\left(1 + \frac{\lambda_i^2}{\sigma^2}\right)}_{C_{\text{SVD}}}. \tag{B.7}$$

From (B.7) the condition for $C_{\mathrm{GTD}} > C_{\mathrm{SVD}}$ can be directly written as in

$$\log_2\left(1+\frac{\lambda_e^2}{\sigma_n^2}\right)+\log_2\left(1+\frac{\lambda_1^2+\lambda_L^2-\lambda_e^2}{\sigma_n^2}\right) > \log_2\left(1+\frac{\lambda_1^2}{\sigma_n^2}\right)+\log_2\left(1+\frac{\lambda_L^2}{\sigma_n^2}\right) \tag{B.8a}$$

$$\iff \quad \log_2\left[\left(1+\frac{\lambda_1^2+\lambda_L^2}{\sigma_n^2}\right)+\frac{\lambda_1^2\lambda_e^2+\lambda_L^2\lambda_e^2-\lambda_e^4}{\sigma_n^4}\right] > \log_2\left[\left(1+\frac{\lambda_1^2+\lambda_L^2}{\sigma_n^2}\right)+\frac{\lambda_1^2\lambda_L^2}{\sigma_n^4}\right] \tag{B.8b}$$

$$\iff \quad \lambda_e^2(\lambda_1^2+\lambda_L^2-\lambda_e^2)-\lambda_1^2\lambda_L^2 > 0. \tag{B.8c}$$

To prove (B.8c) indeed holds, define $y > 0$ and $z > 0$ to be real positive numbers. Because $\lambda_L < \lambda_e < \lambda_1$, we can write $\lambda_e^2 = \lambda_L^2 + y$ and $\lambda_1^2 = \lambda_L^2 + y + z$ and substitute into (B.8c). After some simplifications we get $yz > 0$, and, thus $C_{\mathrm{GTD}} > C_{\mathrm{SVD}}$, completing the proof of Theorem 3.1.

Appendix C

Proof of Proposition 4.3

Recall (2.2) and (2.3) and let $\mathbf{r} = \mathbf{u}$, $\boldsymbol{\lambda} = \mathbf{v}$ and $L = k$. Proposition 4.3 is true if the following is satisfied

$$\prod_{l=1}^{L} r_l = \prod_{l=1}^{L} \lambda_l, \tag{C.1}$$

and their descendingly ordered elements satisfy

$$\prod_{l=1}^{n} r_l \leqslant \prod_{l=1}^{n} \lambda_l, \tag{C.2}$$

for all $1 \leqslant n < L$.

The product term (C.1) can be easily proved by substituting the corresponding elements of $\mathbf{r}$ given (4.15) and the corresponding elements of $\boldsymbol{\lambda}$ given in (4.12), (4.13) and (4.14) in (C.1).

To show (C.2) also holds, conditions (C.3a) and (C.3b) below must hold since (C.1) is true.

$$r_{\max} \leqslant \lambda_{\max}, \tag{C.3a}$$

$$r_{\min} \geqslant \lambda_{\min}, \tag{C.3b}$$

where $r_{\max}$ and $r_{\min}$ are the maximum and the minimum elements in $\mathbf{r}$ while $\lambda_{\max}$ and $\lambda_{\min}$ are the maximum and the minimum elements in $\boldsymbol{\lambda}$.

There are two cases regarding (C.3a), that is: 1) $r_{\max} = \lambda_{\max}$, and 2)$r_{\max} < \lambda_{\max}$. If $\lambda_{\max}$ is a clear subchannels ; *i.e.*, belongs to the set $\mathcal{N}$, in this case $r_{\max} = \lambda_{\max}$ according to (4.15). If $\lambda_{\max}$ is a joint subchannel ; *i.e.*, belongs to the set $\mathcal{Z}$, by construction, $\lambda_{\max} = \sqrt{\phi_1^\star + \beta_1^\star}\sigma_1^2$. Thus, any element of $\mathbf{r}$ that are defined in equation (4.15) is less than $\lambda_{\max}$. To explain this case in more details, consider $r_{\max}$ is one of the received subchannels in the set $\mathcal{D}$; equations (4.15a) and (4.13) imply that $r_{\max} < \lambda_{\max}$ is always true. On the other hand, if $r_{\max}$ is one the received subchannels in the set $\mathcal{W}$, substituting $EH_{\check{z}} = \beta_{\check{z}}^\star \sigma_{\check{z}}^2 + p_{\hat{z}}\sigma_{\hat{z}}^2$, $\lambda_{\check{z}} = \sqrt{\phi_{\check{z}}^\star + \beta_{\check{z}}^\star}\sigma_{\check{z}}^2$ and $\sqrt{p_{\hat{z}}}\sigma_{\hat{z}}$ in their corresponded $r_{\max}$ in equation (4.15c), yields $r_{\max} = \sqrt{\phi_{\check{z}}^\star}\sigma_{\check{z}}^2$ which less less than $\lambda_{\max}$. Note that the elements of $\mathbf{r}$ that are associated with the received subchannels in the set $\mathcal{E}$ cannot be $r_{\max}$ due to their definition given by equation (4.15b).

In (C.3b), only the case $r_{\min} > \lambda_{\min}$ is considered since the elements of $\mathbf{r}$ is defined assuming $\mathcal{Z} \neq \emptyset$, and hence, the set $\hat{\mathcal{Z}}$ is always existed. This means $\lambda_{\min} = \sqrt{p_{\hat{z}}}\sigma_{\hat{z}}$ as illustrated in Remark 4.1. By examining equation (4.15), $r_{\min}$ is related with the received subchannels in the set $\mathcal{E}$. Substituting $EH_{\check{z}} = \beta_{\check{z}}^\star \sigma_{\check{z}}^2 + p_{\hat{z}}\sigma_{\hat{z}}^2$, $\lambda_{\check{z}} = \sqrt{\phi_{\check{z}}^\star + \beta_{\check{z}}^\star}\sigma_{\check{z}}^2$ and $\sqrt{p_{\hat{z}}}\sigma_{\hat{z}}$ in their corresponded $r_{\min}$ in (4.15b), yields $r_{\min} = \frac{\sqrt{\phi_{\check{z}}^\star + \beta_{\check{z}}^\star}\sqrt{p_{\hat{z}}}\sigma_{\hat{z}}}{\sqrt{\phi_{\check{z}}^\star}}$ which is greater than $\lambda_{\min}$. This completes the proof of Proposition 4.3.

Appendix D

Proof of Theorem 4.1

Following the structure of the the matrix $\mathbf{R}$ that is given in equation (4.16), the received streams that are corresponded to rows $e \in \mathcal{E}$ are assigned for energy harvesting while the the received streams that are corresponded to rows rows $w \in \mathcal{W}$ are assigned for information decoding. The received streams that are corresponded to rows $d \in \mathcal{D}$ are flexible ; *i.e.*, each single received stream can be used either for energy harvesting or information decoding according to the subchannel assignment at the transmitter.

For simplicity, we assume the energy conversion process is perfect ; *i.e.*, $\eta = 1$. The energy content of received stream $e \in \mathcal{E}$ is

$$EH_e = R^2_{e,|\mathcal{N}|+1} + R^2_{e,|\mathcal{N}|+2} + \ldots, R^2_{e,L}. \tag{D.1}$$

Substituting (2.10) and (2.13a) in (D.1) and following the GTD algorithm [81], it can be shown that the value of the diagonal element $R_{e,|\mathcal{N}|+1} = r_e$ is related to the off-diagonal elements on the same row as

$$R^2_{e,|\mathcal{N}|+1} + \cdots + R^2_{e,L} = \frac{1}{R^2_{e,|\mathcal{N}|+1}} \big(\psi_e^2 - R^2_{e,|\mathcal{N}|+1}\big)\big(R^2_{e,N+1} - \omega_j^2\big), \tag{D.2}$$

where the parameters ψ_e and ω_e are set in the GTD algorithm during the e-th iteration as discussed in Section 2.3.2. Note that (D.2) implies that energy of the first off-diagonal element, which is set by the GTD algorithm at the e-th iteration, is equal to the energy of

the off-diagonal elements at row e of the matrix $\mathbf{R}$ given in equation (4.16). This is true because the elements of $\mathbf{R}$ is obtained through multiplication processes at each iteration with the unitary matrices $\mathbf{B}_1$ and $\mathbf{B_2}$ as illustrated in equation (2.12a). Thus, the energy of (2.13a) is preserved and remains intact in all the off-diagonal elements at the e-th row of the matrix $\mathbf{R}$. The energy content of the received stream $e \in \mathcal{E}$ can be written as function of the predefined diagonal element r_e as follow:

$$EH_e = r_e^2 + \frac{1}{r_e^2}\left(\psi_e^2 - r_e^2\right)\left(r_e^2 - \omega_e^2\right), \tag{D.3}$$

where the values of ψ_e and ω_e also depend on the form r_e and the values $r_1, \ldots, r_{e-1}$. According to the GTD algorithm, the values of $\mathbf{r}$; *i.e.*, $r_1, \ldots, r_e$ lead to $\psi_e = \lambda_{\check{z}}$ and $\omega_e = \lambda_{\hat{z}}$. Thus (D.2) is written as

$$EH_e = r_e^2 + \frac{1}{r_e^2}\left(\lambda_{\check{z}}^2 - r_e^2\right)\left(r_e^2 - \lambda_{\hat{z}}^2\right). \tag{D.4}$$

Substituting the corresponding $\lambda_{\check{z}}$, $\lambda_{\hat{z}}$ and r_e as given in (4.12), (4.14) and (4.15b) in (D.4), yields

$$EH_e = \beta_{\check{z}}^{\star}\sigma_{\check{z}}^2 + p_{\hat{z}}\sigma_{\hat{z}}^2 \approx \beta_{\check{z}}^{\star}\sigma_{\check{z}}^2, \tag{D.5}$$

since $p_{\hat{z}}\sigma_{\hat{z}}^2 \approx 0$. If $\sum_{e\in\mathcal{E}} EH_e = EH$, the energy harvested from the streams $\mathcal{E}$ satisfy the constraint (4.1c) and $\mathcal{J}_{Rx}^{\star} = \mathcal{E}$. On the other hand, if $\sum_{e\in\mathcal{E}} EH_e < EH$, there is a subset $\tilde{\mathcal{D}} \subseteq \mathcal{D}$ which has streams that are used for energy harvesting. Since the subchannels in $\tilde{\mathcal{D}}$ are clear subchannels, the energy harvested is

$$EH_{\tilde{d}} = r_{\tilde{d}}^2. \tag{D.6}$$

Substituting the corresponded $r_{\tilde{d}}$ from (4.15a) in (D.6) with λ_n as given (4.13), gives the energy harvested as

$$EH_{\tilde{d}} = \beta_j^{\star}\sigma_j^2. \tag{D.7}$$

Therefore, the energy is harvested from the subchannels in the set $\mathcal{J}_{Rx}^{\star} = \mathcal{E} \bigcup \mathcal{D}_e$.

According to the matrix given in (4.16), the information bearing subchannels are

interference free; thus, the rate obtained from the subchannel $w \in \mathcal{W}$ is

$$C_w = \log_2\left(1 + r_w^2\right). \tag{D.8}$$

Substituting (4.15c), (4.12) and (4.14) in (D.8), yileds

$$C_w = \log_2\left(1 + \phi_{\tilde{z}}^{\star}\sigma_{\tilde{z}}^2\right). \tag{D.9}$$

If $\sum_{w\in\mathcal{W}} C_w = C$, the achievable rate obtained by decoding the information from the stream $\mathcal{W}$ satisfies the constraint (4.1b) and $\mathcal{I}_{Rx}^{\star} = \mathcal{W}$. If $\sum_{w\in\mathcal{W}} C_w < C$, there is a subset $\mathcal{D}_w \subseteq \mathcal{D}$ which has streams that are used for information decoding. Since the subchannels in $\bar{\mathcal{D}}$ are clear subchannels, the rate can be obtained from

$$C_{\bar{d}} = \log_2\left(1 + r_{\bar{d}}^2\right). \tag{D.10}$$

Substituting the corresponded $r_{\tilde{d}}$ from (4.15a) in (D.10) with λ_n as given (4.13), gives the rate as

$$C_{\bar{d}} = \log_2\left(1 + \phi_i^{\star}\sigma_i^2\right). \tag{D.11}$$

Therefore, the information is decoded from the subchannels in the set $\mathcal{I}_{Rx}^{\star} = \mathcal{W} \bigcup \mathcal{D}_W$.

References

[1] S. Sudevalayam and P. Kulkarni, "Energy harvesting sensor nodes: Survey and implications," *IEEE Communications Surveys & Tutorials*, vol. 13, no. 3, pp. 443–461, 2011.

[2] I. Krikidis, S. Timotheou, S. Nikolaou, G. Zheng, D. W. K. Ng, and R. Schober, "Simultaneous wireless information and power transfer in modern communication systems," *IEEE Communications Magazine*, vol. 52, no. 11, pp. 104–110, 2014.

[3] R. Zhang, R. G. Maunder, and L. Hanzo, "Wireless information and power transfer: from scientific hypothesis to engineering practice," *IEEE Communications Magazine*, vol. 53, no. 8, pp. 99–105, August 2015.

[4] J. A. Hagerty, F. B. Helmbrecht, W. H. McCalpin, R. Zane, and Z. B. Popovic, "Recycling ambient microwave energy with broad-band rectenna arrays," *IEEE Transactions on Microwave Theory and Techniques*, vol. 52, no. 3, pp. 1014–1024, March 2004.

[5] P. Lu, X. Yang, J. Li, and B. Wang, "A compact frequency reconfigurable rectenna for 5.2-and 5.8-GHz wireless power transmission," *IEEE Transactions on Power Electronics*, vol. 30, no. 11, pp. 6006–6010, 2015.

[6] S. D. Assimonis, S.-N. Daskalakis, and A. Bletsas, "Sensitive and efficient RF harvesting supply for batteryless backscatter sensor networks," *IEEE Transactions on Microwave Theory and Techniques*, vol. 64, no. 4, pp. 1327–1338, 2016.

[7] Y. Chen and C. Chiu, "Maximum achievable power conversion efficiency obtained through an optimized rectenna structure for RF energy harvesting," *IEEE Transactions on Antennas and Propagation*, vol. 65, no. 5, pp. 2305–2317, 2017.

[8] C. Song, Y. Huang, J. Zhou, J. Zhang, S. Yuan, and P. Carter, "A high-efficiency broadband rectenna for ambient wireless energy harvesting," *IEEE Transactions on Antennas and Propagation*, vol. 63, no. 8, pp. 3486–3495, 2015.

[9] S. Agrawal, R. D. Gupta, M. S. Parihar, and P. N. Kondekar, "A wideband high gain dielectric resonator antenna for RF energy harvesting application," *AEU-International Journal of Electronics and Communications*, vol. 78, pp. 24–31, 2017.

[10] C. Song, Y. Huang, P. Carter, J. Zhou, S. Yuan, Q. Xu, and M. Kod, "A novel six-band dual CP rectenna using improved impedance matching technique for ambient RF energy harvesting," *IEEE Transactions on Antennas and Propagation*, vol. 64, no. 7, pp. 3160–3171, 2016.

[11] L. R. Varshney, "Transporting information and energy simultaneously," in *IEEE International Symposium on Information Theory (ISIT)*, July 2008, pp. 1612–1616.

[12] P. Grover and A. Sahai, "Shannon meets Tesla: Wireless information and power transfer," in *IEEE International Symposium on Information Theory (ISIT)*, June 2010, pp. 2363–2367.

[13] R. Zhang and C. K. Ho, "MIMO broadcasting for simultaneous wireless information and power transfer," *IEEE Transactions on Wireless Communications*, vol. 12, no. 5, pp. 1989–2001, 2013.

[14] S. Timotheou, I. Krikidis, S. Karachontzitis, and K. Berberidis, "Spatial domain simultaneous information and power transfer for MIMO channels," *IEEE Transactions on Wireless Communications*, vol. 14, no. 8, pp. 4115–4128, 2015.

[15] S. Timotheou and I. Krikidis, "Joint information and energy transfer in the spatial domain with channel estimation error," in *IEEE Online Conference on Green Communications (OnlineGreenComm)*, Oct 2013, pp. 115–120.

[16] ——, "SWIPT through eigen-decomposition of MIMO channels," in *23rd European Signal Processing Conference (EUSIPCO)*, Aug 2015, pp. 1994–1998.

[17] E. Boshkovska, D. W. K. Ng, N. Zlatanov, and R. Schober, "Practical non-linear energy

harvesting model and resource allocation for SWIPT systems," *IEEE Communications Letters*, vol. 19, no. 12, pp. 2082–2085, 2015.

[18] W. C. Brown, "The history of power transmission by radio waves," *IEEE Transactions on Microwave Theory and Techniques*, vol. 32, no. 9, pp. 1230–1242, Sep. 1984.

[19] N. Shinohara, "Power without wires," *IEEE Microwave Magazine*, vol. 12, no. 7, pp. S64–S73, Dec 2011.

[20] "Powercast PCC114 Powerharvester receiver," https://www.powercastco.com/wp-content/uploads/2018/05/PCC114-Datasheet-V1.0.pdf, accessed: 2019-05-23.

[21] X. Lu, P. Wang, D. Niyato, D. I. Kim, and Z. Han, "Wireless networks with RF energy harvesting: A contemporary survey," *IEEE Communications Surveys & Tutorials*, vol. 17, no. 2, pp. 757–789, 2015.

[22] R. J. Vyas, B. B. Cook, Y. Kawahara, and M. M. Tentzeris, "E-WEHP: A batteryless embedded sensor-platform wirelessly powered from ambient digital-TV signals," *IEEE Transactions on Microwave Theory and Techniques*, vol. 61, no. 6, pp. 2491–2505, June 2013.

[23] M. Piñuela, P. D. Mitcheson, and S. Lucyszyn, "Ambient RF energy harvesting in urban and semi-urban environments," *IEEE Transactions on Microwave Theory and Techniques*, vol. 61, no. 7, pp. 2715–2726, July 2013.

[24] L. M. Borges, R. Chávez-Santiago, N. Barroca, F. J. Velez, and I. Balasingham, "Radio-frequency energy harvesting for wearable sensors," *Healthcare Technology Letters*, vol. 2, no. 1, pp. 22–27, 2015.

[25] U. Muncuk, K. Alemdar, J. D. Sarode, and K. R. Chowdhury, "Multiband ambient RF energy harvesting circuit design for enabling batteryless sensors and IoT," *IEEE Internet of Things Journal*, vol. 5, no. 4, pp. 2700–2714, Aug 2018.

[26] A. Khemar, A. Kacha, H. Takhedmit, and G. Abib, "Design and experiments of a dual-band rectenna for ambient RF energy harvesting in urban environments," *IET Microwaves, Antennas Propagation*, vol. 12, no. 1, pp. 49–55, 2018.

[27] M. Ercoli, D. Dragomirescu, and R. Plana, "Small size high isolation Wilkinson power splitter for 60 GHz wireless sensor network applications," in *IEEE 11th Topical Meeting on Silicon Monolithic Integrated Circuits in RF Systems*, Jan 2011, pp. 85–88.

[28] A. Quddious, M. A. B. Abbasi, M. H. Tariq, M. A. Antoniades, P. Vryonides, and S. Nikolaou, "On the use of tunable power splitter for simultaneous wireless information and power transfer receivers," *International Journal of Antennas and Propagation*, vol. 2018, 2018.

[29] S.-Y. Lee and C.-C. Lai, "A 1-v wideband low-power CMOS active differential power splitter for wireless communication," *IEEE transactions on microwave theory and techniques*, vol. 55, no. 8, pp. 1593–1600, 2007.

[30] A. Safarian, L. Zhou, and P. Heydari, "CMOS distributed active power combiners and splitters for multi-antenna UWB beamforming transceivers," *IEEE Journal of Solid-State Circuits*, vol. 42, no. 7, pp. 1481–1491, 2007.

[31] A. Franc, E. Pistono, N. Corrao, D. Gloria, and P. Ferrari, "Compact high-Q, low-loss mmw transmission lines and power splitters in RF CMOS technology," in *IEEE MTT-S International Microwave Symposium*, June 2011, pp. 1–4.

[32] L. Liu, R. Zhang, and K.-C. Chua, "Wireless information transfer with opportunistic energy harvesting," *IEEE Transactions on Wireless Communications*, vol. 12, no. 1, pp. 288–300, 2013.

[33] A. A. Nasir, X. Zhou, S. Durrani, and R. A. Kennedy, "Relaying protocols for wireless energy harvesting and information processing," *IEEE Transactions on Wireless Communications*, vol. 12, no. 7, pp. 3622–3636, 2013.

[34] A. A. Nasir, X. Zhou, S. Durrani, and R. A. Kennedy, "Throughput and ergodic capacity of wireless energy harvesting based DF relaying network," in *IEEE International Conference on Communications (ICC)*, June 2014, pp. 4066–4071.

[35] M. Ju, K.-M. Kang, K.-S. Hwang, and C. Jeong, "Maximum transmission rate of PSR/TSR protocols in wireless energy harvesting DF-based relay networks." *IEEE Journal on Selected Areas in Communications*, vol. 33, no. 12, pp. 2701–2717, 2015.

[36] A. A. Al-habob, A. M. Salhab, S. A. Zummo, and M.-S. Alouini, "A modified time-switching relaying protocol for multi-destination relay networks with SWIPT," in *IEEE Wireless Communications and Networking Conference (WCNC)*, 2018, pp. 1–6.

[37] A. A. Nasir, X. Zhou, S. Durrani, and R. A. Kennedy, "Wireless-powered relays in cooperative communications: Time-switching relaying protocols and throughput analysis," *IEEE Transactions on Communications*, vol. 63, no. 5, pp. 1607–1622, 2015.

[38] Y. Dong, M. J. Hossain, and J. Cheng, "Joint power control and time switching for SWIPT systems with heterogeneous QoS requirements," *IEEE Communications Letters*, vol. 20, no. 2, pp. 328–331, 2016.

[39] J. J. Park, J. H. Moon, and D. I. Kim, "Time-switching based in-band full duplex wireless powered two-way relay," in *URSI Asia-Pacific Radio Science Conference (URSI AP-RASC)*. IEEE, 2016, pp. 438–441.

[40] F. Benkhelifa, A. S. Salem, and M. Alouini, "SWIPT in multiuser MIMO decode-and-forward relay broadcasting channel with energy harvesting relays," in *IEEE Globecom Workshops (GC Wkshps)*, Dec 2016, pp. 1–7.

[41] X. Zhou, J. Guo, S. Durrani, and I. Krikidis, "Performance of maximum ratio transmission in ad hoc networks with SWIPT," *IEEE Wireless Communications Letters*, vol. 4, no. 5, pp. 529–532, 2015.

[42] Y. Liao, J. Zhang, Y. Zhang, M. Chen, Q. Li, and T. Han, "Performance analysis of K-tier cellular networks with time-switching energy harvesting," in *IEEE 27th Annual International Symposium on Personal, Indoor, and Mobile Radio Communications (PIMRC),*, 2016, pp. 1–5.

[43] X. Zhou, R. Zhang, and C. K. Ho, "Wireless information and power transfer in multiuser OFDM systems," *IEEE Transactions on Wireless Communications*, vol. 13, no. 4, pp. 2282–2294, 2014.

[44] G. Huang, Q. Zhang, and J. Qin, "Joint time switching and power allocation for multicarrier decode-and-forward relay networks with SWIPT," *IEEE Signal Processing Letters*, vol. 22, no. 12, pp. 2284–2288, 2015.

[45] N. Janatian, I. Stupia, and L. Vandendorpe, "Joint multi-objective transmit precoding and receiver time switching design for MISO SWIPT systems," in *IEEE 17th International Workshop on Signal Processing Advances in Wireless Communications (SPAWC),*, 2016, pp. 1–5.

[46] H. H. M. Tam, H. D. Tuan, A. A. Nasir, T. Q. Duong, and H. V. Poor, "MIMO energy harvesting in full-duplex multi-user networks," *IEEE Transactions on Wireless Communications*, vol. 16, no. 5, pp. 3282–3297, 2017.

[47] H. Lee, K.-J. Lee, H. Kim, and I. Lee, "Joint transceiver optimization for MISO SWIPT systems with time switching," *IEEE Transactions on Wireless Communications*, 2018.

[48] L. Ma, Y. Wang, and Y. Xu, "Sum rate optimization for SWIPT system based on zero-forcing beamforming and time switching," in *13th International Wireless Communications and Mobile Computing Conference (IWCMC)*, 2017, pp. 351–356.

[49] J. Hu, K. Yang, G. Wen, and L. Hanzo, "Integrated data and energy communication network: A comprehensive survey," *IEEE Communications Surveys & Tutorials*, vol. 20, no. 4, pp. 3169–3219, 2018.

[50] Q. Shi, L. Liu, W. Xu, and R. Zhang, "Joint transmit beamforming and receive power splitting for MISO SWIPT systems," *IEEE Transactions on Wireless Communications*, vol. 13, no. 6, pp. 3269–3280, 2014.

[51] M. R. A. Khandaker and K. Wong, "SWIPT in MISO multicasting systems," *IEEE Wireless Communications Letters*, vol. 3, no. 3, pp. 277–280, 2014.

[52] S. Timotheou, I. Krikidis, G. Zheng, and B. Ottersten, "Beamforming for MISO interference channels with QoS and RF energy transfer," *IEEE Transactions on Wireless Communications*, vol. 13, no. 5, pp. 2646–2658, 2014.

[53] S. Timotheou, G. Zheng, C. Masouros, and I. Krikidis, "Exploiting constructive interference for simultaneous wireless information and power transfer in multiuser downlink systems," *IEEE Journal on Selected Areas in Communications*, vol. 34, no. 5, pp. 1772–1784, 2016.

[54] F. Wang, T. Peng, and Y. Huang, "Decentralized robust transceiver designs for MISO SWIPT interference channel," *IEEE Access*, vol. 6, pp. 4537–4546, 2018.

[55] Z. Zong, H. Feng, F. R. Yu, N. Zhao, T. Yang, and B. Hu, "Optimal transceiver design for SWIPT in k-user MIMO interference channels," *IEEE Transactions on Wireless Communications*, vol. 15, no. 1, pp. 430–445, 2016.

[56] C. Qin, W. Ni, H. Tian, and R. P. Liu, "Joint rate maximization of downlink and uplink in multiuser MIMO SWIPT systems," *IEEE Access*, vol. 5, pp. 3750–3762, 2017.

[57] T. Riihonen, L. Zhao, M. Vehkaperä, and X. Wang, "On the feasibility of full-duplex relaying powered by wireless energy transfer," in *IEEE 17th International Workshop on Signal Processing Advances in Wireless Communications (SPAWC)*, 2016, pp. 1–5.

[58] Z. Hu, C. Yuan, F. Zhu, and F. Gao, "Weighted sum transmit power minimization for full-duplex system with SWIPT and self-energy recycling." *IEEE Access*, vol. 4, pp. 4874–4881, 2016.

[59] A. C. Cirik, J. Xue, S. Biswas, T. Ratnarajah, and M. Sellathurai, "Transceiver design of optimum wirelessly powered full-duplex MIMO interference channel," in *IEEE 17th International Workshop on Signal Processing Advances in Wireless Communications (SPAWC)*, 2016, pp. 1–6.

[60] M.-M. Zhao, Y. Cai, Q. Shi, M. Hong, and B. Champagne, "Joint transceiver designs for full-duplex k-pair MIMO interference channel with SWIPT," *IEEE Transactions on Communications*, vol. 65, no. 2, pp. 890–905, 2017.

[61] Z. Wen, X. Liu, N. C. Beaulieu, R. Wang, and S. Wang, "Joint source and relay beamforming design for full-duplex MIMO AF relay SWIPT systems," *IEEE Communications Letters*, vol. 20, no. 2, pp. 320–323, 2016.

[62] G. Zheng, Z. K. M. Ho, E. A. Jorswieck, and B. E. Ottersten, "Information and energy cooperation in cognitive radio networks." *IEEE Trans. Signal Processing*, vol. 62, no. 9, pp. 2290–2303, 2014.

[63] J. Yan and Y. Liu, "Dynamic energy harvesting in cooperative cognitive radio networks," in *IEEE Globecom Workshops (GC Wkshps)*, Dec 2016, pp. 1–6.

[64] L. Mohjazi, I. Ahmed, S. Muhaidat, M. Dianati, and M. Al-Qutayri, "Downlink beamforming for SWIPT multi-user MISO underlay cognitive radio networks," *IEEE Communications Letters*, vol. 21, no. 2, pp. 434–437, 2017.

[65] H.-J. Chou, R. Y. Chang, and J.-M. Wu, "Multi-objective optimization of wireless information and power transfer in multiuser OFDMA systems," in *IEEE Global Communications Conference (GLOBECOM)*, 2015, pp. 1–7.

[66] Y. Xu, C. Shen, Z. Ding, X. Sun, S. Yan, G. Zhu, and Z. Zhong, "Joint beamforming and power-splitting control in downlink cooperative SWIPT NOMA systems," *IEEE Transactions on Signal Processing*, vol. 65, no. 18, pp. 4874–4886, Sep. 2017.

[67] R. Q. Hu and Z. Zhang, "Dynamic power splitting between information and power transfer in non-orthogonal multiple access (invited paper)," in *9th International Conference on Wireless Communications and Signal Processing (WCSP)*, Oct 2017, pp. 1–7.

[68] T. D. P. Perera, D. N. K. Jayakody, S. K. Sharma, S. Chatzinotas, and J. Li, "Simultaneous wireless information and power transfer (SWIPT): Recent advances and future challenges," *IEEE Communications Surveys & Tutorials*, vol. 20, no. 1, pp. 264–302, 2017.

[69] I. Krikidis, S. Sasaki, S. Timotheou, and Z. Ding, "A low complexity antenna switching for joint wireless information and energy transfer in MIMO relay channels," *IEEE Transactions on Communications*, vol. 62, no. 5, pp. 1577–1587, 2014.

[70] D. Wang, H. Yu, J. Zhang, G. Pan, H. Lei, T. Li, and Y. Chen, "On outage of dual-hop relay SWIPT system with antenna selection and GSC over nakagami-m fading channels," in *IEEE International Conference on Communication Systems (ICCS)*, 2016, pp. 1–6.

[71] C. Jeong, M. Ju, and S. H. Chae, "MIMO decode-and-forward relay systems with an energy-constrained antenna-switching relay," *IEEE Communications Letters*, vol. 21, no. 8, pp. 1851–1854, 2017.

[72] F. Benkhelifa, K. Tourki, and M.-S. Alouini, "Proactive spectrum sharing for swipt in MIMO cognitive radio systems using antenna switching technique," *IEEE Transactions on Green Communications and Networking*, vol. 1, no. 2, pp. 204–222, 2017.

[73] F. Benkhelifa and M. Alouini, "A thresholding-based antenna switching in MIMO cognitive radio networks with SWIPT-enabled secondary receiver," in *IEEE International Conference on Communications (ICC)*, May 2017, pp. 1–6.

[74] J. Tang, D. K. So, A. Shojaeifard, K.-K. Wong, and J. Wen, "Joint antenna selection and spatial switching for energy efficient MIMO SWIPT system," *IEEE Transactions on Wireless Communications*, vol. 16, no. 7, pp. 4754–4769, 2017.

[75] J. Tang, D. K. So, A. Shojaeifard, and K. Wong, "Energy efficiency optimization for spatial switching-based MIMO SWIPT system," in *IEEE 85th Vehicular Technology Conference (VTC Spring)*, 2017, pp. 1–6.

[76] D. Mishra and G. C. Alexandropoulos, "Jointly optimal spatial channel assignment and power allocation for MIMO SWIPT systems," *IEEE Wireless Communications Letters*, vol. 7, no. 2, pp. 214–217, 2018.

[77] Gurobi Optimization Inc., "Gurobi optimizer reference manual," 2015.

[78] G. H. Golub and C. F. Van Loan, *Matrix Computations*, 4th ed. The Johns Hopkins University Press, 2013.

[79] Y. Jiang, J. Li, and W. W. Hager, "Uniform channel decomposition for MIMO communications," *IEEE Transactions on Signal Processing*, vol. 53, no. 11, pp. 4283–4294, 2005.

[80] Y. Jiang, W. W. Hager, and J. Li, "Tunable channel decomposition for MIMO communications using channel state information," *IEEE Transactions on Signal Processing*, vol. 54, no. 11, pp. 4405–4418, 2006.

[81] Y. Jiang, W. Hager, and J. Li, "The generalized triangular decomposition," *Mathematics of computation*, vol. 77, no. 262, pp. 1037–1056, 2008.

[82] D. P. Palomar and Y. Jiang, "MIMO transceiver design via majorization theory," *Foundations and Trends® in Communications and Information Theory*, vol. 3, no. 4-5, pp. 331–551, 2007. [Online]. Available: http://dx.doi.org/10.1561/0100000018.

[83] E. Telatar, "Capacity of multi-antenna Gaussian channels," *European transactions on telecommunications*, vol. 10, no. 6, pp. 585–595, 1999.

[84] T. Yoo and A. Goldsmith, "Capacity and power allocation for fading MIMO channels with channel estimation error," *IEEE Transactions on Information Theory*, vol. 52, no. 5, pp. 2203–2214, 2006.

[85] A. Ben-Tal and A. Nemirovski, *Lectures on Modern Convex Optimization*. Society for Industrial and Applied Mathematics, 2001. [Online]. Available: https://epubs.siam.org/doi/abs/10.1137/1.9780898718829.

[86] M. Grant, S. Boyd, and Y. Ye, "CVX: Matlab software for disciplined convex programming," 2008.

[87] B. Clerckx, R. Zhang, R. Schober, D. W. K. Ng, D. I. Kim, and H. V. Poor, "Fundamentals of wireless information and power transfer: From RF energy harvester models to signal and system designs," *IEEE Journal on Selected Areas in Communications*, vol. 37, no. 1, pp. 4–33, 2019.

[88] C. R. Valenta and G. D. Durgin, "Harvesting wireless power: Survey of energy-harvester conversion efficiency in far-field, wireless power transfer systems," *IEEE Microwave Magazine*, vol. 15, no. 4, pp. 108–120, 2014.

[89] T. Le, K. Mayaram, and T. Fiez, "Efficient far-field radio frequency energy harvesting for passively powered sensor networks," *IEEE Journal of Solid-State Circuits*, vol. 43, no. 5, pp. 1287–1302, 2008.

[90] J. Guo and X. Zhu, "An improved analytical model for RF-DC conversion efficiency in microwave rectifiers," in *IEEE/MTT-S International Microwave Symposium Digest*, June 2012, pp. 1–3.

[91] E. Boshkovska, D. W. K. Ng, N. Zlatanov, A. Koelpin, and R. Schober, "Robust resource allocation for MIMO wireless powered communication networks based on a non-linear EH model," *IEEE Transactions on Communications*, vol. 65, no. 5, pp. 1984–1999, 2017.

[92] K. Xiong, B. Wang, and K. R. Liu, "Rate-energy region of SWIPT for MIMO broadcasting under nonlinear energy harvesting model," *IEEE Transactions on Wireless Communications*, vol. 16, no. 8, pp. 5147–5161, 2017.

[93] R. Jiang, K. Xiong, P. Fan, Y. Zhang, and Z. Zhong, "Optimal design of SWIPT systems with multiple heterogeneous users under non-linear energy harvesting model," *IEEE Access*, vol. 5, pp. 11 479–11 489, 2017.

[94] J.-M. Kang, I.-M. Kim, and D. I. Kim, "Mode switching for SWIPT over fading channel with nonlinear energy harvesting," *IEEE Wireless Communications Letters*, vol. 6, no. 5, pp. 678–681, 2017.

[95] Y. Wang, Y. Wang, F. Zhou, Y. Wu, and H. Zhou, "Resource allocation in wireless powered cognitive radio networks based on a practical non-linear energy harvesting model," *IEEE Access*, vol. 5, pp. 17 618–17 626, 2017.

[96] Y. Wang, Y. Wu, F. Zhou, Z. Chu, Y. Wu, and F. Yuan, "Multi-objective resource allocation in a NOMA cognitive radio network with a practical non-linear energy harvesting model," *IEEE Access*, vol. 6, pp. 12 973–12 982, 2018.

[97] S. Jang, H. Lee, S. Kang, T. Oh, and I. Lee, "Energy efficient SWIPT systems in multi-cell MISO networks," *IEEE Transactions on Wireless Communications*, vol. 17, no. 12, pp. 8180–8194, 2018.

[98] G. Lu, L. Shi, and Y. Ye, "Maximum throughput of TS/PS scheme in an af relaying network with non-linear energy harvester," *IEEE Access*, vol. 6, pp. 26 617–26 625, 2018.

[99] L. Shi, Y. Ye, R. Q. Hu, and H. Zhang, "Energy efficiency maximization for SWIPT enabled two-way DF relaying," *IEEE Signal Processing Letters*, vol. 26, no. 5, pp. 755–759, May 2019.

[100] B. Clerckx and E. Bayguzina, "Waveform design for wireless power transfer," *IEEE Transactions on Signal Processing*, vol. 64, no. 23, pp. 6313–6328, Dec 2016.

[101] B. Clerckx, "Waveform optimization for SWIPT with nonlinear energy harvester modeling," in *20th International ITG Workshop on Smart Antennas (WSA)*, Mar. 2016, pp. 1–5.

[102] M. Varasteh, B. Rassouli, and B. Clerckx, "Wireless information and power transfer over an AWGN channel: Nonlinearity and asymmetric Gaussian signaling," in *IEEE Information Theory Workshop (ITW)*, 2017, pp. 181–185.

[103] M. Varasteh, B. Rassouli, H. Joudeh, and B. Clerckx, "SWIPT signalling over complex AWGN channels with two nonlinear energy harvester models," *arXiv preprint arXiv:1805.03979*, 2018.

[104] R. Morsi, V. Jamali, D. W. K. Ng, and R. Schober, "On the capacity of SWIPT systems with a nonlinear energy harvesting circuit," in *IEEE International Conference on Communications (ICC)*, 2018, pp. 1–7.

[105] B. Clerckx, "Wireless information and power transfer: Nonlinearity, waveform design, and rate-energy tradeoff," *IEEE Transactions on Signal Processing*, vol. 66, no. 4, pp. 847–862, 2018.

[106] P. Nintanavongsa, U. Muncuk, D. R. Lewis, and K. R. Chowdhury, "Design optimization and implementation for RF energy harvesting circuits," *IEEE Journal on emerging and selected topics in circuits and systems*, vol. 2, no. 1, pp. 24–33, 2012.

[107] B. R. Franciscatto, V. Freitas, J. Duchamp, C. Defay, and T. P. Vuong, "High-efficiency rectifier circuit at 2.45 GHz for low-input-power RF energy harvesting," in *European Microwave Conference*, Oct 2013, pp. 507–510.

[108] U. Olgun, C. Chen, and J. L. Volakis, "Wireless power harvesting with planar rectennas for 2.45 GHz RFIDs," in *URSI International Symposium on Electromagnetic Theory*, Aug 2010, pp. 329–331.

[109] Z. Liu, Z. Zhong, and Y. Guo, "Enhanced dual-band ambient RF energy harvesting with ultra-wide power range," *IEEE Microwave and Wireless Components Letters*, vol. 25, no. 9, pp. 630–632, Sep. 2015.

[110] M. A. Abouzied, K. Ravichandran, and E. Sánchez-Sinencio, "A fully integrated reconfigurable self-startup RF energy-harvesting system with storage capability," *IEEE Journal of Solid-State Circuits*, vol. 52, no. 3, pp. 704–719, March 2017.

[111] Y. Lu, K. Xiong, P. Fan, Z. Ding, Z. Zhong, and K. B. Letaief, "Global energy efficiency in secure MISO SWIPT systems with non-linear power-splitting EH model," *IEEE Journal on Selected Areas in Communications*, vol. 37, no. 1, pp. 216–232, Jan 2019.

[112] G. Ma, J. Xu, Y. Zeng, and M. R. V. Moghadam, "A generic receiver architecture for MIMO wireless power transfer with non-linear energy harvesting," *IEEE Signal Processing Letters*, 2019.

[113] K. Shen and W. Yu, "Fractional programming for communication systems—part I: Power control and beamforming," *IEEE Transactions on Signal Processing*, vol. 66, no. 10, pp. 2616–2630, 2018.

[114] Y. Jong, "An efficient global optimization algorithm for nonlinear sum-of-ratios problem," *online: www.optimizationonline.org/DBFILE/2012/08/3586.pdf*, 2012.

[115] C. T. Kelley, *Iterative methods for linear and nonlinear equations*. Siam, 1995, vol. 16.

[116] C.-X. Wang, F. Haider, X. Gao, X.-H. You, Y. Yang, D. Yuan, H. M. Aggoune, H. Haas, S. Fletcher, and E. Hepsaydir, "Cellular architecture and key technologies for 5G wireless communication networks," *IEEE communications magazine*, vol. 52, no. 2, pp. 122–130, 2014.

[117] R. Mysore Rajashekar, M. D. Renzo, L. Yang, K. Hari, and L. Hanzo, "A finite input alphabet perspective on the rate-energy tradeoff in SWIPT over parallel gaussian channels," *IEEE Journal on Selected Areas in Communications*, 2018.

[118] Y. Kim, D. K. Shin, and W. Choi, "Rate-energy region in wireless information and power transfer: New receiver architecture and practical modulation," *IEEE Transactions on Communications*, 2018.

[119] M. Varasteh, B. Rassouli, H. Joudeh, and B. Clerckx, "SWIPT signalling over complex AWGN channels with two nonlinear energy harvester models," in *IEEE International Symposium on Information Theory (ISIT)*, June 2018, pp. 866–870.

[120] B. Clerckx and E. Bayguzina, "Low-complexity adaptive multisine waveform design for wireless power transfer," *IEEE Antennas and Wireless Propagation Letters*, vol. 16, pp. 2207–2210, 2017.

[121] Y. Zeng, B. Clerckx, and R. Zhang, "Communications and signals design for wireless power transmission," *IEEE Transactions on Communications*, vol. 65, no. 5, pp. 2264–2290, 2017.

[122] M. R. V. Moghadam, Y. Zeng, and R. Zhang, "Waveform optimization for radio-frequency wireless power transfer," in *IEEE 18th International Workshop on Signal Processing Advances in Wireless Communications (SPAWC)*, 2017, pp. 1–6.

[123] A. Khina, Y. Kochman, and U. Erez, "Joint unitary triangularization for MIMO networks," *IEEE Transactions on Signal Processing*, vol. 60, no. 1, pp. 326–336, 2012.

[124] A. Khina, I. Livni, A. Hitron, and U. Erez, "Joint unitary triangularization for Gaussian multi-user MIMO networks," *IEEE Transactions on Information Theory*, vol. 61, no. 5, pp. 2662–2692, 2015.

[125] D. W. K. Ng, E. S. Lo, and R. Schober, "Robust beamforming for secure communication in systems with wireless information and power transfer," *IEEE Transactions on Wireless Communications*, vol. 13, no. 8, pp. 4599–4615, 2014.

[126] Q. Zhang, X. Huang, Q. Li, and J. Qin, "Cooperative jamming aided robust secure transmission for wireless information and power transfer in MISO channels," *IEEE Transactions on Communications*, vol. 63, no. 3, pp. 906–915, 2015.

[127] Q. Shi, W. Xu, J. Wu, E. Song, and Y. Wang, "Secure beamforming for MIMO broadcasting with wireless information and power transfer." *IEEE Trans. Wireless Communications*, vol. 14, no. 5, pp. 2841–2853, 2015.

[128] W. Wu and B. Wang, "Efficient transmission solutions for MIMO wiretap channels with SWIPT," *IEEE Communications Letters*, vol. 19, no. 9, pp. 1548–1551, 2015.

[129] B. Fang, Z. Qian, W. Zhong, and W. Shao, "AN-aided secrecy precoding for SWIPT in cognitive MIMO broadcast channels," *IEEE Communications Letters*, vol. 19, no. 9, pp. 1632–1635, 2015.

[130] S. Wang and B. Wang, "Robust secure transmit design in MIMO channels with simultaneous wireless information and power transfer," *IEEE Signal Processing Letters*, vol. 22, no. 11, pp. 2147–2151, 2015.

[131] A. El Shafie, K. Tourki, and N. Al-Dhahir, "An artificial-noise-aided hybrid TS/PS scheme for OFDM-based SWIPT systems," *IEEE Communications Letters*, vol. 21, no. 3, pp. 632–635, 2017.

[132] X. Chen, D. W. K. Ng, and H.-H. Chen, "Secrecy wireless information and power transfer: Challenges and opportunities," *IEEE Wireless Communications*, vol. 23, no. 2, pp. 54–61, 2016.

[133] G. Pan, H. Lei, Y. Deng, L. Fan, J. Yang, Y. Chen, and Z. Ding, "On secrecy performance of MISO SWIPT systems with TAS and imperfect CSI," *IEEE Transactions on Communications*, vol. 64, no. 9, pp. 3831–3843, 2016.

[134] J. Zhang, C. Yuen, C.-K. Wen, S. Jin, K.-K. Wong, and H. Zhu, "Large system secrecy rate analysis for SWIPT MIMO wiretap channels," *IEEE Transactions on Information Forensics and Security*, vol. 11, no. 1, pp. 74–85, 2016.

[135] M. Liu and Y. Liu, "Power allocation for secure SWIPT systems with wireless-powered cooperative jamming," *IEEE Communications Letters*, 2017.

[136] M. R. Khandaker, K.-K. Wong, Y. Zhang, and Z. Zheng, "Probabilistically robust SWIPT for secrecy MISOME systems," *IEEE Transactions on Information Forensics and Security*, vol. 12, no. 1, pp. 211–226, 2017.

[137] A. Khina, Y. Kochman, and A. Khisti, "The MIMO wiretap channel decomposed," *IEEE Transactions on Information Theory*, vol. 64, no. 2, pp. 1046–1063, Feb 2018.

[138] K. Murata, N. Honma, K. Nishimori, and H. Morishita, "Analog eigenmode transmission for short-range MIMO," *IEEE Transactions on Vehicular Technology*, vol. 65, no. 1, pp. 100–109, 2016.

[139] K. Murata, N. Honma, K. Nishimori, N. Michishita, and H. Morishita, "Analog eigenmode transmission for short-range MIMO based on orbital angular momentum," *IEEE Trans. Antennas Propag*, vol. 65, no. 12, pp. 6687–6702, 2017.